Supporting Information for

Near-infrared Absorbing Ru(II) Complexes Act as Immunoprotective Photodynamic Therapy (PDT) Agents Against Aggressive Melanoma

Liubov M. Lifshits,[a,‡] John A. Roque III,[a,b,‡] Prathyusha Konda,[c,‡] Susan Monro,[d] Houston D. Cole,[a] David von Dohlen,[b] Susy Kim,[e] Gagan Deep,[e] Randolph P. Thummel,[f] Colin G. Cameron,[a*] Shashi Gujar,[c,g,h,i*] Sherri A. McFarland[a*]

[a] *Department of Chemistry and Biochemistry, The University of Texas at Arlington, Arlington, Texas, 76019-0065 United States*
[b] *Department of Chemistry and Biochemistry, The University of North Carolina at Greensboro, Greensboro, North Carolina 27402, USA*
[c] *Department of Microbiology and Immunology, Dalhousie University, Halifax, Nova Scotia B3H 1X5, Canada*
[d] *Department of Chemistry, Acadia University, Wolfville, Nova Scotia B4P 2R6, Canada*
[e] *Department of Cancer Biology, Wake Forest School of Medicine, Winston Salem, NC, 27157, USA*
[f] *Department of Chemistry, University of Houston, 112 Fleming Building, Houston, Texas, 77204-5003, USA*
[g] *Department of Pathology, Dalhousie University, Halifax, Nova Scotia B3H 1X5, Canada*
[h] *Department of Biology, Dalhousie University, Halifax, Nova Scotia B3H 1X5, Canada*
[i] *Beatrice Hunter Cancer Research Institute, Halifax, Nova Scotia B3H 4R2, Canada*

‡Coauthors contributed equally to this work.
**Corresponding authors*

1. Tables of Contents and Figures

Sections

Schemes

Chart

Figures

Tables

2. General Methods

2.1 Instrumentation and Methods

Microwave reactions were performed in a CEM Discover microwave reactor. *Purifications:* neutral aluminum oxide, activated, Brockmann Grade I (58Å, −60 Mesh Powder, S.A. 150 $m^2\,g^{-1}$) was used as a stationary phase for gravity column chromatography. Flash column chromatography was carried out on CombiFlash® EZ Prep from Teledyne ISCO (model: EZ Prep UV) using SILICYCLE SiliaSep™ Neutral Alumina cartridges. Sephadex® LH-20 was used for size-exclusion chromatography. The NMR spectra were recorded on JEOL ECA 500 NMR spectrometer, operating at 500 MHz for ^{1}H experiments (University of North Carolina at Greensboro) and on Agilent 700 MHz spectrometer (The Joint School of Nanoscience and Nanoengineering at Greensboro) operating at 700 MHz for ^{1}H experiments. The chemical shifts are reported in parts per million (ppm) and were referenced to the residual solvent peaks. ESI mass spectra were obtained using a Thermo Fisher Scientific LTQ Orbitrap XL at the Triad Mass Spectrometry Laboratory at University of North Carolina at Greensboro. HPLC analysis was carried out with 100 μM solutions in methanol using a Hypersil GOLD C18 reversed-phase column with an A–B gradient (98% → 5% A; A = 0.1% formic acid in H_2O, B = 0.1% formic acid in MeCN). Reported retention times are correct to within ±0.1 min.

2.2 Lipophilicity

Lipophilicity measurements were performed as done previously[1] but with 10 mM phosphate buffer at neutral pH (=7.4) in lieu of water. The log ($D_{o/w}$) was calculated as the log-transformed ratio of compound concentration in either phosphate buffer or 1-octanol, with each solvent saturated with the other. Compounds with observed precipitate generally only had positive absorbance readings in 1-octanol and were assigned an estimated log ($D_{o/w}$) = −3 for majority lipophilicity. Any compound with observed precipitate was not used for correlation examples nor for in-text comparisons of their relative lipophilicities.

2.3 Spectroscopy

Spectroscopic and photophysical measurements of the complexes were carried out as dilute (5–20 μM) solutions of their chloride salts in spectroscopy-grade acetonitrile that had been distilled over CaH_2. UV-vis extinction coefficients ε were determined at spectral peaks from the slope of absorbance vs. concentration at five dilutions (20 μM serially diluted four times by 25%). Emission (Φ_{em}) and singlet oxygen (Φ_{Δ}) quantum yields were determined by integrating the corresponding emission peak and applying the following equation:

$$\Phi = \Phi_s\left(\frac{I}{I_s}\right)\left(\frac{A_s}{A}\right)\left(\frac{\eta^2}{\eta_s^2}\right) \#(1)$$

where *I* is the integrated emission, *A* is the UV-vis absorbance at the excitation wavelength, and η is the index of refraction of the solvent (η^2/η_s^2 = 1 in all cases here). The subscript *s* denotes values under identical conditions from the reference compound, $Ru(bpy)_3(PF_6)_2$, for which Φ_{Δ}=0.56[2] and Φ_{em}=0.012[3] in aerated acetonitrile. Oxygen was removed from the solution by sparging with Ar in a septum-capped cuvette for emission experiments, or by five freeze-pump-thaw cycles in a custom Schlenk-style cuvette for transient absorption measurements.

UV-vis spectra were measured on a Jasco V-730 spectrometer. Steady-state emission spectra were recorded with a PTI Quantamaster emission system with a K170B PMT for measuring UV/visible spectra and a Hamamatsu R5509-42 NIR PMT for the near infrared (≲1400 nm). The emission and excitation spectra were corrected for nonlinear lamp and detector response.

Transient absorption (TA) lifetimes and spectra were determined with an Edinburgh Instruments LP-980 spectrometer equipped with a PMT-LP detector and a Continuum Minilite Nd:YAG excitation source set to 355 nm (7−9 mJ per pulse). This instrument was also used to measure emission lifetimes. An instrument response function was applied to correct short (<10 ns) signals.

2.4 Cell Culture

In general, cells were cultured using standard aseptic technique and no antibiotics.

2.4.1 A375

Female human melanoma cell line A-375 [A375] (ATCC CRL-1619) was subcultured in 75 cm^2 flasks (VWR, 10062-860) at split ratios of 1:4 to 1:8 (seeded approximately 200,00–400,000 cells mL^{-1}). A375 cells were split or fed every 2–3 days and used within 5–10 passages from receipt for reported assay results. Split steps included a rinse with 1× Dulbecco's Phosphate-Buffered Saline without Ca^{2+} or Mg^{2+} (DPBS; diluted and sterifiltered Corning 20-031-CV) and enzymatic dissociation using 0.25% w/v Trysin-EDTA. Culture media consisted of Dulbecco's Modified Eagle's Medium (DMEM; Hyclone SH30243.FS), which contained 4500 mg L^{-1} glucose, 4 mM L-glutamine, 110 mg L^{-1} sodium pyruvate, and was supplemented with 10% v/v FB essence (VWR, Avantor Seradigm, 10803-034). Cells were cultured at 10% USP-grade CO_2, ≥ 90% relative humidity, and 37°C in an air-jacketed incubator (VWR, 10810-902).

2.4.2 B16F10

The female murine melanoma cell line B16-F10 [B16F10] (ATCC CRL-6475) was subcultured using the same conditions as A375 cells. Split ratios were adjusted to approximately 1:10 after attaining confluency (200,000–300,000 cells mL^{-1}). Cells were used within 5–10 passages from receipt at UTA and 10–20 at Dalhousie for immunological work. B16F10 cells were only subcultured in DMEM due to immunological experiment requirements for no change in media. Dalhousie DMEM cell media (Gibco, 11965118) included supplementation with 10% v/v fetal bovine serum (FBS, Gibco 26140079), 1 mM sodium pyruvate (Gibco, 11360070), 1% v/v non-essential amino acids (Gibco, 11140050), and 1× antibiotic-antimycotic (Gibco, 15240096)

2.4.3 SKMEL28.

Male human melanoma cell line SK-MEL-28 [SKMEL28] (ATCC HTB-72) was subcultured as previously described at 5% USP-grade CO_2, ≥ 90% relative humidity, and 37°C in a water-jacketed incubator (ThermoFisher, Thermo Scientific 4110).[1] Split ratios were commonly performed between 1:2–1:5 (150,000–400,000 cells mL^{-1}). Cells were used within 5–10 passages from receipt at UTA and 10–15 passages at Acadia University.

2.5 Cellular Assays

There are two main categories of cellular assays, a) general dose-response screens on 384-well plate across multiple cell lines and b) specialized screens on 12- or 96-well plates. Cellular assays generally follow our previous works in 96-well plate format.[1,4] Regardless of well density, plates are only stacked 2-plates high in an incubator to facilitate temperature equilibrium. Our standard screen approach adapted to 384-well plates is described below, which had a total incubation time 1 day shorter than in 96-well plates due to observed edge effects. We describe light devices for photobiological evaluation following this procedure.

2.5.1 Ru(II) compound solutions

Stock solutions of metal compounds were prepared at 5 mM in 10% v/v DMSO:water (type 1, ≥ 18.2 MΩ·cm). Stock solutions were stored in glass vials with PTFE-lined caps, protected from light with aluminum foil, and stored at −20°C when not in use. Cellular assays involved ≤ 0.6 % v/v DMSO at the highest compound concentration (300 µM).

2.5.2 Cytotoxicity and photocytotoxicity

A miniaturized format for drug screening by hand. An electronic multichannel pipettor is strongly recommended for successful set-up by hand. Volumes of our standard assay in 96-well plates approximately decrease to 40%. Into 384-well plates (Greiner Bio-One, 781182), a DPBS perimeter of 100 µL $well^{-1}$ was installed into the outmost two wells (144 well count). After this, 10 µL $well^{-1}$ of DPBS was dispensed into all control wells (12 count). For sample and control wells (240 well count), 10 µL $well^{-1}$ of complete media was added. An additional 20 µL $well^{-1}$ media was dispensed into negative cell controls. At this point, sample wells have 10 µL $well^{-1}$ complete media, positive controls 20 µL $well^{-1}$ media and DPBS, and negative controls 40 µL $well^{-1}$ of mainly media. It is optional to pre-equilibrate plates in a humidified incubator (37°C, 5% CO_2, ≥ 90% relative humidity - RH) to aid transfer of initial aliquots.

After media is dispensed, plates are equilibrated in the incubator for a minimum 15 mins before addition of cellular slurry. If seeding multiple cell lines, 2–4 different cell lines are a suggested limit for a single researcher.

Plates were seeded 20 µL well^{-1} across five plates at a time (i.e., per cell line) for sample and positive control wells. Cells were seeded at the following densities: A375 (5500 cells well^{-1}), B16F10 (4000 cells well^{-1}), and SKMEL28 (4000 cells well^{-1}).They were mixed twice (up, down, left, right tilting) in the biosafety cabinet and before placing inside the incubator and incubated 1–3 h.

During the incubation, compound dilutions were prepared in sterile 0.8 mL 96-deep well plates (Greiner Bio-One, 780261) using DPBS as solvent. Dilutions were prepared in serial across 9 concentrations ranging from 1200–4×10^{-3} µM. Covered deep-well plates were incubated for 0.5–1 h before final dispensing (d_f = 4) at 10 µL well^{-1}. All sample and control wells total 40 µL well^{-1} at this point. Replicates are generally dispensed row-wise and spaced every 4 (triplicates) or 6 (duplicates) rows. The biosafety cabinet's lights were kept off while dispensing compound dilutions. Repeats across experiments change plate maps for compound and replicate locations. For a standard 12-channel pipettor, compounds are dispensed every other column. Therefore, it is important to plan liquid dispensing and an appropriate plate map ahead of time.

Following dark (sham) or light treatments (16–20 h drug-to-light interval, DLI), plates are further incubated overnight before final viability measurements. One day is removed from the post-PDT period of our standard 96-well plate assay to mitigate edge effects on a 384-well plate. At this point, 10 µL well^{-1} of 0.3 mM sterifiltered resazurin in 0.2 M phosphate buffer (pH = 7.4) is dispensed across all well plates. Generally, 4–6 plates are handled at a time in the biosafety cabinet. Resazurin dyed plates were incubated further for 4 h before reading fluorometrically on a Molecular Devices M2e (30 s shake, bottom-read, λ_{exc} 530 nm, long-pass 570 nm, λ_{em} 620 nm). Whereas unnecessary for a 96-well plate, it was found that assay S/N drastically improved if the reader's plate adaptor was removed prior to the read (shorter distance from well to detector).

2.5.3 Hypoxia cytotoxicity and photocytotoxicity.

Following our recent example, we probed activity of our lead compounds in hypoxia (1% O_2) for their oxygen dependence (PDT photosensitizer) relative to a compound highly oxygen-dependent for its activity [Ru(bpy)$_2$(dppn)]Cl$_2$.[1] This probe was conducted in parallel across normoxia (~18.5% O_2) and hypoxia for leads **2**, **6**, and **9** in 96-well plates and SKMEL28 cells. The results are shown in Table S7.

2.5.4 Light Devices and Protocols

For photobiological evaluation, we used various visible and NIR light sources that we list by location. Standard screens treat at a fluence of 100 J cm^{-2}. Our location at Acadia University applied a broadband visible light 190 W BenQ S 510 overhead projector (400–700 nm, 40 mW cm^{-2}) and red light (625 nm, 35–40 mW^{-2}; LED array by Photodynamic Inc., Halifax, NS). Our location at Dalhousie University applied a cool white LED panel (SOLLA-CREE, 70 W, 25–30 mW^{-2}), a 633 nm UHP-LED (Prizmatix), and 733 nm laser (2 W, CivilLaser; (9–10 mW^{-2}) coupled to a 600 µm optical fiber with a 2 mm flat-cut diffuser (Medlight, FD1). Our location at UTA applied the same SOLLA-CREE cool white LED panel (18–22 mW^{-2}), 523 and 633 nm UHP-LEDs (Prizmatix; 20 mW^{-2}), and the same 733 nm laser (8–10 mW^{-2}).

For specialized irradiation protocols at UTA we restricted our in vitro model to the single cell line SKMEL28. Dosimetry work for both irradiance and fluence dependences, was conducted using clear 96-well plates and randomized plate maps limited to a 36-well quadrant of sample wells. We further explored the scope of our lead compounds with the Modulight ML8500 platform (37°C, 5% CO_2). With the ML8500, we applied lasers centered at 445 nm (25 J cm^{-2}, 100 mW^{-2}), 525 nm (100 J cm^{-2}, 300 mW^{-2}), 630 nm (200 J cm^{-2}, 300 mW^{-2}), 753 nm (200–400 J cm^{-2}, 300 mW^{-2}), 810 nm (400–600 J cm^{-2}, 400 mW^{-2}), and 976 nm (600 J cm^{-2}, 400 mW^{-2}). Different fluences were applied with the ML8500 in an attempt to match wavelength performance at clinically relevant irradiances (e.g., short illumination periods). These conditions were confirmed to exert no light-based toxicity in the absence of compounds **1**–**9** in our model cell line SKMEL28 (Figure S50). Since the ML8500 is limited to a single well per treatment, it necessitates black well plates (96-well, Greiner Bio-One, 655090) to mitigate cross-talk between wells and randomized plate maps for studies > 1 h illumination to mitigate edge effects.

2.5.5 Quantification of cell death by flow cytometry

Cell death was assessed by Annexin V (Biolegend, 640905) and 7AAD (eBioscience, 00-6993) staining. A total of 5×10^5 cells were plated in 12-well plates and treated with the determined EC_{50} of compound **2** and 25 J cm^{-2} of 630 nm irradiation. Briefly, cells were collected, washed in PBS, pelleted, and resuspended in an incubation buffer (10 mM HEPES/NaOH (pH 7.4), 140 mm NaCl and 5 mM $CaCl_2$) at a total cell concentration of 0.5–1x10^6

cells mL^{-2}. Annexin V (5 µL) followed by 7AAD (5 µL) was added to the cell suspension, samples were kept in the dark, and incubated for 15 min at room temperature. Samples were run on a BD FACSCanto II flow cytometer, data was acquired using BD FACSDiva software, and flow cytometry data was analyzed with the FCS Express analysis program.

2.5.6 Flow cytometric analysis of calreticulin on the cell surface and cellular ROS

A total of 5×10^5 cells were plated in 12-well plates and treated with the determined EC_{50} of compound **2** and 25 J cm^{-2} of 630 nm irradiation. For Calreticulin staining, cells were collected by trypsinization 4 h post-treatment, washed twice in cold PBS, incubated for 45 min with the rabbit anti-Calreticulin primary antibody (Abcam, ab2907), diluted in cold blocking buffer (1% fetal bovine serum in PBS), followed by washing and incubation with the Alexa Fluor 647-conjugated secondary antibody (Invitrogen, A-21246) in a blocking buffer for 30 min. Cells were again washed twice with PBS and fixed in 2% paraformaldehyde in PBS for 15 min. Each sample was then analyzed on the BD FACSCanto II to identify cell surface Calreticulin. For cellular ROS analysis, trypsinized and washed cells were incubated with CM-H_2DCFDA (Molecular Probes, C6827, 1 µM) or MitoSOX (Molecular Probes, M36008) for 30 minutes at 37°C in PBS before live cell analysis on the BD FACSCanto II.

2.5.7 Detection of HMGB1 release and ATP secretion

A total of 5×10^5 cells were plated in 12-well plates and treated with the determined EC_{50} of compound **2** and 25, 50, or 100 J cm^{-2} of 630 nm irradiation as mentioned in the figures. Supernatants were collected 24 h post-treatment and immediately assessed for HMGB1 levels by enzyme-linked immunosorbent assay according to the manufacturer's instructions (IBL International, ST51011). Similarly, supernatant samples were collected 12 h post-treatment and their ATP concentrations were measured by means of an ATP Determination Kit (Invitrogen, A22066), according to the manufacturer's protocol. Readings in both cases were taken on a SpectraMax M2 well plate reader.

2.5.8 Real-time qPCR

A total of 1×10^6 B16F10 cells were plated in 6-well plates and treated with the determined EC_{50} of compound **2** and 25 J cm^{-2} of 630 nm irradiation. Cells were collected 12 h post-treatment and RNA extractions were conducted using standard TRIzol methodology as per manufacturer guideline (Invitrogen, 15596026 & 12183025). Extracted RNA was quantified, diluted to a total of 2 µg, and synthesized into cDNA using SuperScript II Reverse Transcriptase (Invitrogen, 18064014). The Bio-Rad CFX96 PCR machine was used for qPCR, using Ssoadvanced universal SYBR green supermix (Bio-Rad, 1725274) according to the manufacturer's instructions for amplification and quantification. Gene-specific primers (Table 1) for murine HSP90, HSPA1B, CXCL10, TNFα, IL6, IFNβ, IFIT1, TLR3, MHC-class I (H2D), TAP1, β2M, GAPDH were synthesized and purchased from Invitrogen. The data from the qPCR were collected and analyzed using Livak and Schmittgen's $2^{-\Delta\Delta CT}$ method. The fold change was calculated by first normalizing the cycle threshold (c^t) of the indicated gene against GAPDH, followed by comparison against the control untreated sample.

Table 1. Gene-specific primers for qPCR studies

Gene name	Forward primer	Reverse primer
CXCL10	GTTGAGATCATTGCCACGATGAAA	CTGCTGTCCATCCATCGCA
IFNβ	GTCCGAGCAGAGATCTTCAGG	GAGTCCGCCTCTGATGCTTA
HSP90	CTCCAATTCATCGGACGCTCT	AAGTCGGCCTTGGTCATTCC
HSPA1B	CAGGACCCACCATCGAGGA	ACAGTAATCGGTGCCCAAGC
TLR3	TCCTGCTGGAAAACTGGATGG	AGCCTGAAAGTGAAACTCGCT
β2M	ATGCTATCCAGAAAACCCCTCA	TTTCAATGTGAGGCGGGTGG

IL6	TCTCTGCAAGAGACTTCCATCC	TTGTGAAGTAGGGAAGGCCG
IFIT1	ACCATGGGAGAGAATGCTGATG	TTGTGCATCCCCAATGGGTT
TNFα	TGTTGCCTCCTCTTTTGCTT	TGGTCACCAAATCAGCGTTA
TAP1	CCACGAGTGTCTCGGGAAT	ATGAGACAAGGTTGCCGCT
H2D	GAGTGAGCCTGAGGAACCTG	AGCCAGACATCTGCTGGAGT
GAPDH	TGGCAAAGTGGAGATTGTTG	AAGATGGTGATGGGCTTCCC

2.5.9 Maximum tolerated dose in mice

An 8-week old litter of female C57BL/6J mice, averaging 20 g per mouse, were treated by intraperitoneal injection of **2** in accordance with protocol A20-006 (approved by WFU Animal Care and Use Committee). Mice were incrementally dosed from 25–100 mg kg−1 with 200 µL injections and 10% DMSO in 0.9% saline as the vehicle. Solutions of **2** were immediately prepared with sonication prior to injection. Female mice were dosed by slow intraperitoneal injection (IP, the lower right abdominal quadrant) only after visible confirmation of complete compound dissolution. Animals were continuously monitored for 2 h, frequently over the next 6, and periodically for up to 2 weeks before being sacrificed. Mice were accordingly euthanized if (a) a combination of moderate severity signs appeared, (b) a single severe sign appeared, or (c) the study period was complete, 2 weeks post-injection. The maximum tolerated dose (MTD) was defined as the dose that produces moderate signs of clinical toxicity in the final tested animal.

2.5.10 In vivo vaccination experiment

A total of 5×10^5 B16F10 cells per well in a 12-well plate were treated with the determined EC_{50} of compound **2** and 50 J cm^{-2} of 630 nm irradiation. For the vaccination, 4- and 16-h post-treatment cells were combined, and 5×10^5 cells in 100 µL PBS were injected subcutaneously into the left flank of 6- to 8-week old male and female C57BL/6NCrl mice (Charles River). For the challenge experiment, 5×10^4 B16F10 cells were injected into the right flank of mice 7 days post-vaccination. In vivo experimental procedures were approved by the Dalhousie University Animal Ethics Committee in accordance with the regulations/guidelines from the Canadian Council on Animal Care (CCAC; protocol number 18-151).

2.5.11 Data analysis and statistics

Data from 384-well plates was initially compiled and processed with custom R[5] scripts using the plater,[6] dplyr,[7] readxl,[8] openxlsx,[9] and tidyr[10] packages. All results from the endpoint-based resazurin assay are background subtracted with negative controls (media and DPBS) and normalized relative to positive cell controls. Any negative values are assumed to be a mismatch of background (i.e., fluorescence quenching) and assigned as zero values. Likewise, at high compound concentration, background fluorescence and/or quenching is often observed for this class of compounds. Zero values are assigned for these cases when indicated by several consecutive concentrations for a given treatment (dark or light). Additional verification is conducted via light microscopy before finalizing data corrections. Further discussion of assay limits for these compound types is provided in a recent review.[4]

Resazurin data over a wide concentration range was fit to both a three-parameter log-logistic and logistic models using GraphPad Prism 8.4.0 according to Equation S1Equation S2 (four-parameter shown) where bottom is constrained to equal zero and X is equal to concentration.

$$Y = \frac{Bottom + (Top - Bottom)}{\left(1 + (10^{Log\left(EC_{50} - X\right) * Hillslope}\right)} \qquad \text{Equation S1}$$

$$Y = \frac{Bottom + (Top - Bottom)}{\left(1 + (EC_{50}/X)^{Hillslope}\right)} \qquad \text{Equation S2}$$

Experiments are typically done in triplicate with at least one repeat staggered by several days. Replicates are always plotted ± standard deviation (SD) on a plot. Reported EC_{50} values are ± SEM for a given experiment;

these denote the effective concentration to reduce relative cell viability by 50% of the fitted curve (EC_{50}) ± standard error of the mean (SEM). Steep hill slopes with ambiguous confidence intervals are unable to determine the SEM and labelled as not determined (n.d.). Phototherapeutic indices (PI) are reported as the ratio of dark to light EC_{50} values and used as a measure of light-induced potency. Summary activity plots used for quickly comparing compound potency (Log EC_{50}, PI, and Log PI) include SEM from log-logistic fits where applicable (Log EC_{50}).

Correlation analyses for PI, lipophilicity, and Φ_{Δ} were conducted using Pearson's correlation coefficients and two-tailed t-tests for discerning significance at $\alpha = 0.05$.

Flow cytometry data was analyzed using FCS Express 6 software. Mean fluorescence intensity values (MFI) were reported after subtracting the background fluorescence of respective treatment controls. qRT-PCR analysis was done using Bio-Rad CFX Manager software. All statistical analyses at Dalhousie University were performed in GraphPad Prism 7. Hazard ratios were calculated with the , in which the ratios represent unvaccinated:vaccinated groups. One-way ANOVA coupled with Bonferroni post-test was performed and significance is listed as follows: * = $p < 0.05$, ** = $p < 0.01$, *** = $p < 0.001$, **** = $p < 0.0001$. All results represent data from a minimum of n=3 experiments for flow cytometry and immunological work.

3. Syntheses of Ru(II) complexes 1–9

3.1 Materials

All solvents were purchased from commercial sources and used without further purification. Most of the solvents were purchased from Fisher Scientific or VWR and ethanol (200 proof) was purchased from Decon Laboratories. 1,10-Phenanthroline was purchased from Oakwood Chemical and ruthenium(III) trichloride trihydrate was purchased from Ark Pharm and Acros Organics. 4-Picoline was purchased from Alfa Aesar. Silver nitrate was purchased from Sigma-Aldrich. Triethylamine was purchased from Fisher Scientific. Deuterated solvents for NMR experiments were purchased from Cambridge Isotope Laboratories.

3.2 Synthetic Procedures

Complexes **1**–**9** were synthesized using conventional heating, and synthesis of several complexes of the series was adapted for microwave reactor, which significantly shortened reaction time while provided very similar reaction yield. Purification of the complexes **1**–**9** was performed with gravity column chromatography at first and then was later replaced with flash column chromatography during synthesis optimization. The fastest way to afford the complexes **1**–**9** includes using microwave-assisted heating for synthesis and flash column chromatography for purification, but if those instrumentations are unavailable, conventional heating and gravity column chromatography could be used to afford complexes **1**–**9** in similar yields but would require longer time.

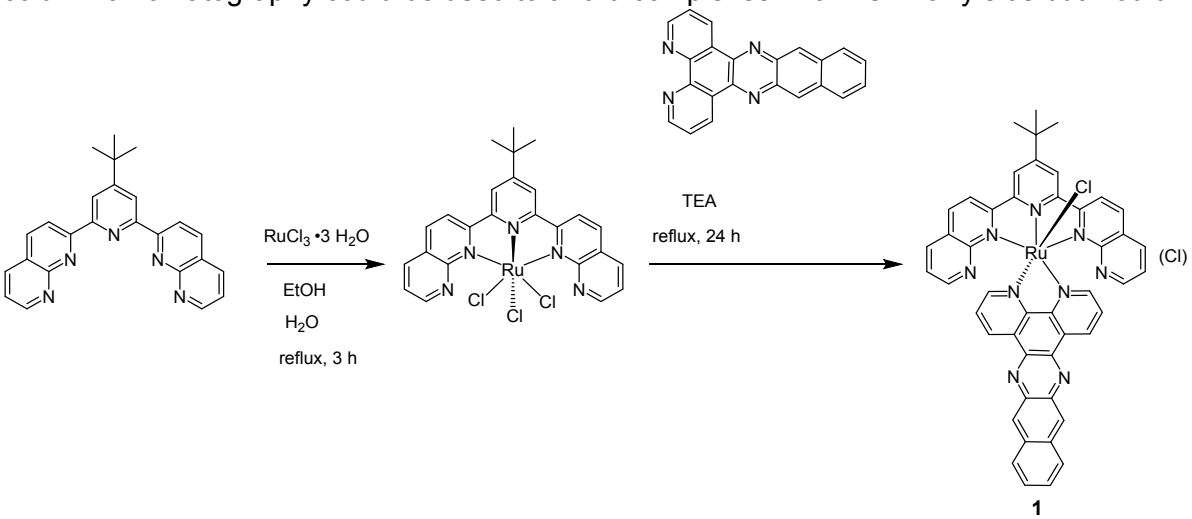

1

Scheme S1. Synthesis scheme for complex **1** [Ru(tpbn)(dppn)(Cl)]Cl (conventional heating method).

Complex 1: [Ru(tpbn)(dppn)(Cl)]Cl

Conventional heating method: A three-neck round-bottom flask, equipped with a nitrogen purge and a condenser, was charged with tpbn (0.100 g, 0.26 mmol) and EtOH (50 mL). Then, an aqueous solution of $RuCl_3$•$3H_2O$ was added (0.070 g, 0.27 mmol in 12 mL H_2O). The reaction mixture was well-stirred and refluxed for 3 h. Then, dppn (0.094 g, 0.28 mmol) and triethylamine (TEA) (1 mL) were added and the reaction mixture was refluxed for 24 h. The reaction mixture was concentrated under reduced pressure. The residue was treated with a few mL of H_2O and the precipitate was isolated by filtration. The precipitate was washed with H_2O and Et_2O and dry-loaded on a column for purification. Column chromatography was performed on neutral alumina, using gradient elution: 1) CH_2Cl_2 2) 50% CH_2Cl_2 : 50% acetone 3) acetone 4) 97% acetone : 3% MeOH. The product fraction (deep-purple band) elutes the last with 97% acetone : 3% MeOH. The product fraction was concentrated under reduced pressure and the residue was treated with a few mL of Et_2O. The precipitate was isolated by filtration, washed with Et_2O and dried. [Ru(tpbn)(dppn)(Cl)]Cl **1** was obtained as a dark-purple powder (0.095 g, 39% yield).

Microwave-assisted method: A microwave vial was filled with argon, and EtOH (2.00 mL) and H_2O (0.48 mL) were added. The solvent mixture was degassed with argon for 10 minutes, and then tpbn (0.030 g, 0.076 mmol) and $RuCl_3$•$3H_2O$ (0.021 g, 0.080 mmol) were added to the reaction vial. The vial was capped, and the reaction mixture was exposed to microwave irradiation at 140°C for 15 min. After that, dppn (0.028 g, 0.084 mmol) and TEA (20 drops) were added to the reaction mixture. The reaction mixture was exposed to microwave irradiation at 140°C for another 15 min then concentrated under reduced pressure. The residue was treated with a few mL of H_2O and the precipitate was isolated by filtration. The precipitate was washed with H_2O and Et_2O and dry-loaded on a column for purification. Column chromatography was performed on neutral alumina, using gradient elution: 1) CH_2Cl_2 2) 50% CH_2Cl_2 : 50% acetone 3) acetone 4) 97% acetone : 3% MeOH. Product fraction (deep-purple band) elutes the last with 97% acetone : 3% MeOH. Product fraction was concentrated under reduced pressure and the residue was treated with a few mL of Et_2O. The precipitate was isolated by filtration, washed with Et_2O and dried. [Ru(tpbn)(dppn)(Cl)]Cl **1** was obtained as a dark-purple powder (0.021 g, 30% yield).

R_f = 0.61 (alumina; 8% H_2O in acetonitrile).

^{1}H NMR (MeOD-d_3, 500 MHz): δ 10.73 (**d**, dd, J_1 = 5.5 Hz, J_2 = 1.5 Hz, 1H), 10.02 (**f**, dd, J_1 = 8.0 Hz, J_2 = 1.5 Hz, 1H), 9.16 (**g**, s, 1H), 9.16 (**c**, dd, J_1 = 8.0 Hz, J_2 = 1.5 Hz, 1H), 9.11 (**3**, s, 2H), 9.00 (**l**, s, 1H), 8.94 (**3′**, d, J = 8.5 Hz, 2H), 8.54 (**4′**, d, J = 8.5 Hz, 2H), 8.43 (**e**, dd, J_1 = 8.0 Hz, J_2 = 5.5 Hz, 1H), 8.30 (**h**, **k**, m, 2H), 8.27 (**5′**, dd, J_1 = 8.0 Hz, J_2 = 2.0 Hz, 2H), 7.99 (**7′**, dd, J_1 = 4.5 Hz, J_2 = 2.0 Hz, 2H), 7.89 (**a**, dd, J_1 = 5.5 Hz, J_2 = 1.5 Hz, 1H), 7.71 (**i**, **j**, m, 2H), 7.32 (**6′**, dd, J_1 = 8.0 Hz, J_2 = 4.5 Hz, 2H), 7.30 (**b**, dd, J_1 = 8.0 Hz, J_2 = 5.5 Hz, 1H), 1.80 (**4-tBu**, s, 9H).

HRMS (ESI$^+$) m/z: $[M\text{-}Cl]^+$ Calcd for $C_{47}H_{33}ClN_9Ru$ 860.1585; Found 860.1573.

HPLC retention time: 26.98 min.

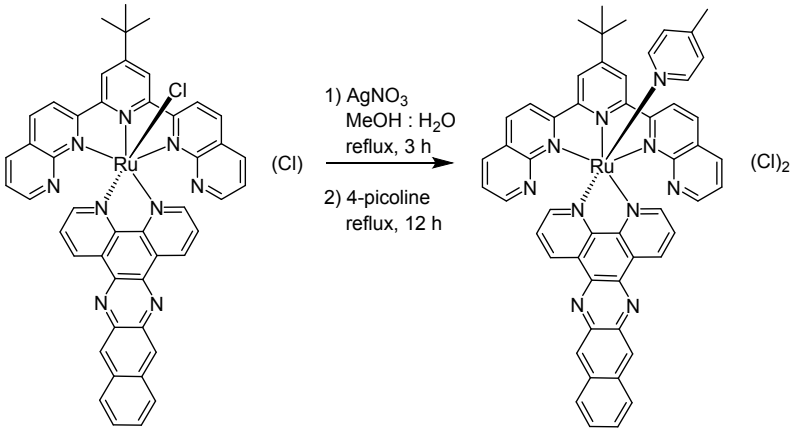

1 **2**

Scheme S2. Synthesis scheme for complex **2** [Ru(tpbn)(dppn)(4-pic)]Cl_2 (conventional heating method).

Complex 2: [Ru(tpbn)(dppn)(4-pic)]Cl_2

Conventional heating method: A round-bottom flask, equipped with a condenser, was charged with [Ru(tpbn)(dppn)(Cl)]Cl **1** (0.100 g, 0.11 mmol) and MeOH (8 mL). Then, aqueous solution of $AgNO_3$ (0.190 g, 1.10 mmol in 2 mL H_2O) was added dropwise. The reaction mixture was well-stirred and refluxed for 3 h. Then, 4-picoline (1.5 mL, 15.21 mmol) was added and the reaction mixture was refluxed for 12 h then concentrated

under reduced pressure. The residue was treated with a few mL of H_2O and the precipitate was isolated by filtration. The precipitate was washed with H_2O and Et_2O and dry-loaded on a column for purification. Column chromatography was performed on neutral alumina, using gradient elution: 1) CH_2Cl_2 2) 50% CH_2Cl_2 : 50% acetone 3) acetone 4) 95% acetone : 5% MeOH. The product fraction (maroon band) eluted last with 95% acetone : 5% MeOH. The product fraction was concentrated under reduced pressure and the residue was treated with a few mL of Et_2O. The precipitate was isolated by filtration, washed with Et_2O and dried. [Ru(tpbn)(dppn)(4-pic)]Cl_2 **2** was obtained as a maroon powder (0.088 g, 81% yield).

Microwave-assisted method: The reaction was performed in 2 batches, then combined for workup and purification. *Batch 1*: A microwave vial was charged with [Ru(tpbn)(dppn)(Cl)]Cl **1** (0.017 g, 0.02 mmol), 4-picoline (0.2 mL, 2.02 mmol) and MeOH (1.5 mL). The vial was capped, and the reaction mixture was exposed to microwave irradiation at 150°C for 15 min. After that, H_2O (0.4 mL) was added and the reaction mixture was exposed to microwave irradiation at 160°C for another 15 min. *Batch 2*: repeated procedure for batch 1. The reaction mixtures from batch 1 and batch 2 were combined and concentrated under reduced pressure. The residue was dried under high vacuum and purified with flash chromatography on alumina (eluent: gradient elution from 100% acetonitrile to 92% acetonitrile : 8% H_2O). The product fraction (maroon band, elutes with 92% acetonitrile : 8% H_2O) was concentrated under reduced pressure and further purified using size-exclusion chromatography on Sephadex LH-20 (eluent: MeOH). The main band (maroon) was collected and concentrated under reduced pressure. The residue was treated with a few mL of Et_2O, sonicated, and isolated by filtration. The precipitate was thoroughly washed with Et_2O and dried. [Ru(tpbn)(dppn)(4-pic)]Cl_2 **2** was obtained as a maroon powder (0.027 g, 77% yield).

R_f = 0.56 (alumina; 8% H_2O in acetonitrile).

^{1}H NMR (MeOD-d_3, 500 MHz): δ 10.08 (**f**, dd, J_1 = 8.5 Hz, J_2 = 1.5 Hz, 1H), 9.47 (**d**, dd, J_1 = 5.5 Hz, J_2 = 1.5 Hz, 1H), 9.32 (**c**, dd, J_1 = 8.0 Hz, J_2 = 1.0 Hz, 1H), 9.20 (**g**, s, 1H), 9.17 (**3**, s, 2H), 9.05 (**3′**, d, J = 8.5 Hz, 2H), 9.02 (**l**, s, 1H), 8.73 (**4′**, d, J = 8.5 Hz, 2H), 8.43 (**e**, dd, J_1 = 8.5 Hz, J_2 = 5.5 Hz, 1H), 8.37 (**5′**, dd, J_1 = 8.0 Hz, J_2 = 2.0 Hz, 2H), 8.36 (**h/k**, d, J = 8.0 Hz, 1H), 8.29 (**h/k**, d, J = 8.0 Hz, 1H), 8.13 (**7′**, dd, J_1 = 4.0 Hz, J_2 = 2.0 Hz, 2H), 7.80 (**a**, dd, J_1 = 5.5 Hz, J_2 = 1.0 Hz, 1H), 7.72 (**i**, **j**, m, 2H), 7.65 (**2″**, d, J = 7.0 Hz, 2H), 7.45 (**b**, dd, J_1 = 8.0 Hz, J_2 = 5.5 Hz, 1H), 7.43 (**6′**, dd, J_1 = 8.0 Hz, J_2 = 4.5 Hz, 2H), 7.00 (**3″**, d, J = 6.0 Hz, 2H), 2.25 (**4″-Me**, s, 3H), 1.77 (**4-tBu**, s, 9H).

HRMS (ESI$^+$) m/z: $[M-2Cl]^{2+}$ Calcd for $C_{53}H_{40}N_{10}Ru$ 459.1235; Found 459.1229.

HPLC retention time: 23.44 min.

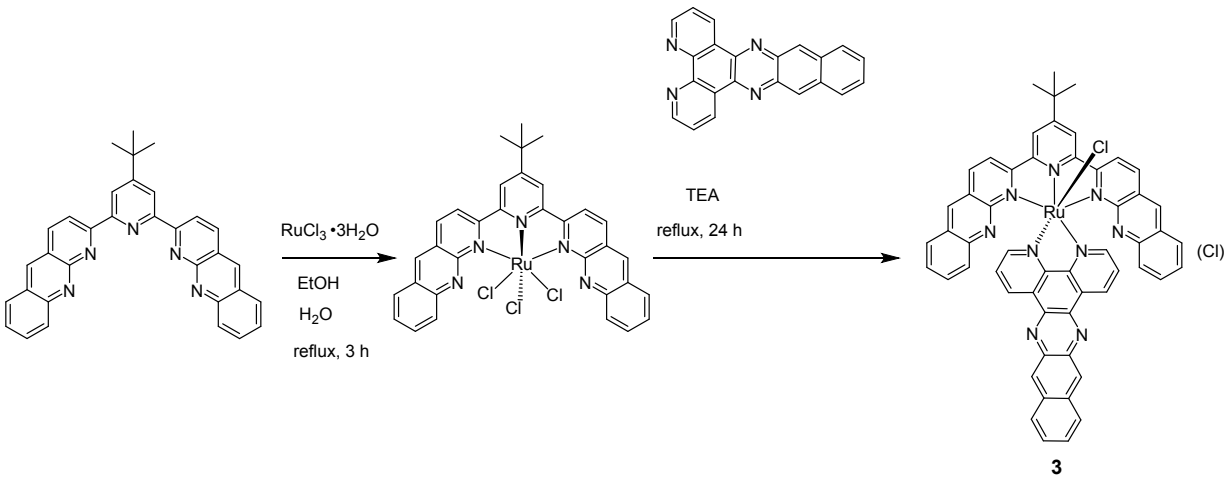

3

Scheme S3. Synthesis scheme for complex **3** [Ru(tpbbn)(dppn)(Cl)]Cl (conventional heating method).

Complex 3: [Ru(tpbbn)(dppn)(Cl)]Cl

Conventional heating method: A three-neck round-bottom flask, equipped with nitrogen purge and a condenser, was charged with tpbbn (0.200 g, 0.41 mmol) and EtOH (100 mL). Then, aqueous solution of $RuCl_3$•$3H_2O$ was added (0.112 g, 0.43 mmol in 24 mL H_2O). Reaction mixture was well-stirred and refluxed for 3 h. Then, dppn (0.150 g, 0.45 mmol) and TEA (2 mL) were added and the reaction mixture was refluxed for 24 h then concentrated under reduced pressure. The residue was treated with a few mL of H_2O and the precipitate was isolated by filtration. The precipitate was washed with H_2O and Et_2O and dry-loaded on a column for purification. Column chromatography was performed on neutral alumina, using gradient elution: 1) CH_2Cl_2 2) 50% CH_2Cl_2 : 50% acetone 3) acetone 4) 97% acetone : 3% MeOH. The product fraction (emerald-green band) eluted last with 97% acetone : 3% MeOH. The product fraction was concentrated under reduced pressure and the residue

was treated with a few mL of Et_2O. The precipitate was isolated by filtration, washed with Et_2O and dried. [Ru(tpbbn)(dppn)(Cl)]Cl **3** was obtained as a dark-green powder (0.130 g, 30% yield).
Although not tested, it is highly likely that synthesis of **3** could also be performed using microwave-assisted heating and much shorter reaction times than conventional heating.
R_f = 0.57 (alumina; 8% H_2O in acetonitrile).
^{1}H NMR (DMSO-d_6, 700 MHz): δ 10.82 (**d**, dd, J_1 = 4.9 Hz, J_2 = 0.7 Hz, 1H), 10.32 (**f**, dd, J_1 = 8.4 Hz, J_2 = 0.7 Hz, 1H), 9.38 (**g**, s, 1H), 9.34 (**3**, s, 2H), 9.22 (**2′**, d, J = 9.1 Hz, 2H), 9.17 (**9′**, s, 2H), 9.05 (**l**, s, 1H), 8.99 (**c**, dd, J_1 = 7.7 Hz, J_2 = 0.7 Hz, 1H), 8.88 (**1′**, d, J = 9.1 Hz, 2H), 8.79 (**e**, dd, J_1 = 8.4 Hz, J_2 = 4.9 Hz, 1H), 8.44 (**h/k**, d, J = 9.1 Hz, 1H), 8.35 (**h/k**, d, J = 7.7 Hz, 1H), 8.06 (**5′**, d, J = 8.4 Hz, 2H), 7.96 (**a**, dd, J_1 = 6.3 Hz, J_2 = 1.4 Hz, 1H), 7.77 (**i/j**, dd, J_1 = 8.4 Hz, J_2 = 7.0 Hz, 1H), 7.73 (**i/j**, dd, J_1 = 7.7 Hz, J_2 = 7.0 Hz, 1H), 7.69 (**7′**, dd, J_1 = 8.4 Hz, J_2 = 7.0 Hz, 2H), 7.50 (**6′**, dd, J_1 = 8.4 Hz, J_2 = 7.0 Hz, 2H), 7.39 (**b**, dd, J_1 = 7.7 Hz, J_2 = 6.3 Hz, 1H), 6.75 (**8′**, d, J = 8.4 Hz, 2H), 1.80 (**4-tBu**, s, 9H).
HRMS (ESI$^+$) m/z: $[M\text{-}Cl]^+$ Calcd for $C_{55}H_{37}ClN_9Ru$ 960.1898; Found 960.1896.
HPLC retention time: 30.23 min.

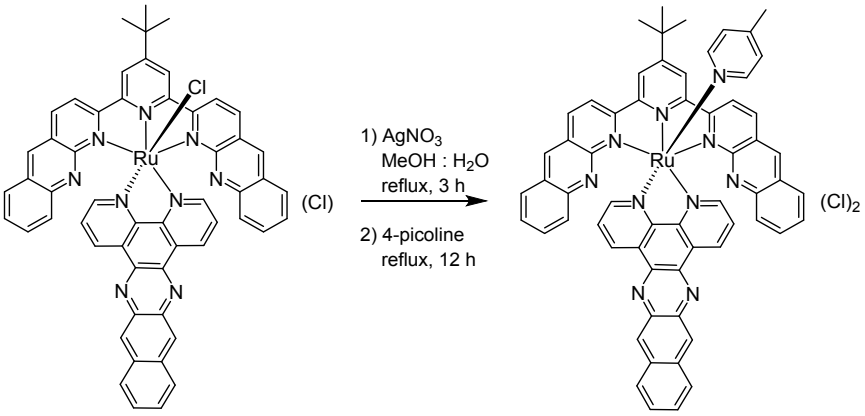

3 **4**

Scheme S4. Synthesis scheme for complex **4** [Ru(tpbbn)(dppn)(4-pic)]Cl_2 (conventional heating method).

Complex 4: [Ru(tpbbn)(dppn)(4-pic)]Cl_2
Conventional heating method: A round-bottom flask, equipped with a condenser, was charged with [Ru(tpbbn)(dppn)(Cl)]Cl **3** (0.070 g, 0.07 mmol) and MeOH (8 mL). Then, aqueous solution of $AgNO_3$ (0.120 g, 0.70 mmol in 2 mL H_2O) was added dropwise. The reaction mixture was well-stirred and refluxed for 3 h. Then, 4-picoline (1.5 mL, 15.21 mmol) was added and reaction mixture was refluxed for 12 h then concentrated under reduced pressure. The residue was treated with a few mL of H_2O and the precipitate was isolated by filtration. The precipitate was washed with H_2O and Et_2O and dry-loaded on a column for purification. Column chromatography was performed on neutral alumina, using gradient elution: 1) CH_2Cl_2 2) 50% CH_2Cl_2 : 50% acetone 3) acetone 4) 95% acetone : 5% MeOH. The product fraction (deep-purple band) eluted last with 95% acetone : 5% MeOH. The product fraction was concentrated under reduced pressure and the residue was treated with a few mL of Et_2O. The precipitate was isolated by filtration, washed with Et_2O and dried. [Ru(tpbbn)(dppn)(4-pic)]Cl_2 **4** was obtained as a dark-purple powder (0.050 g, 66% yield).
Although not tested, it is highly likely that synthesis of **4** could also be performed using microwave-assisted heating and much shorter reaction times than conventional heating.
R_f = 0.49 (alumina; 8% H_2O in acetonitrile).
^{1}H NMR (MeOD-d_3, 700 MHz): δ 10.46 (**f**, d, J = 8.4 Hz, 1H), 9.74 (**d**, d, J = 4.9 Hz, 1H), 9.28 (**3**, s, 2H), 9.21 (**c**, d, J = 7.7 Hz, 1H), 9.18 (**g**, s, 1H), 9.13 (**9′**, s, 2H), 9.05 (**2′**, d, J = 8.4 Hz, 2H), 8.93 (**1′**, d, J = 9.1 Hz, 2H), 8.91 (**l**, s, 1H), 8.83 (**e**, dd, J_1 = 8.4 Hz, J_2 = 5.6 Hz, 1H), 8.30 (**h/k**, d, J = 8.4 Hz, 1H), 8.22 (**h/k**, d, J = 7.7 Hz, 1H), 8.02 (**5′**, d, J = 7.7 Hz, 2H), 7.88 (**a**, d, J = 5.6 Hz, 1H), 7.79 (**2″**, d, J = 7.0 Hz, 2H), 7.74 (**7′**, dd, J_1 = 8.4 Hz, J_2 = 7.0 Hz, 2H), 7.67 (**i**, **j**, m, 2H), 7.53 (**6′**, dd, J_1 = 7.7 Hz, J_2 = 7.0 Hz, 2H), 7.43 (**b**, dd, J_1 = 7.7 Hz, J_2 = 5.6 Hz, 1H), 7.01 (**8′**, d, J = 8.4 Hz, 2H), 6.97 (**3″**, d, J = 6.3 Hz, 2H), 2.22 (**4″-Me**, s, 3H), 1.81 (**4-tBu**, s, 9H).
HRMS (ESI$^+$) m/z: $[M\text{-}2Cl]^{2+}$ Calcd for $C_{61}H_{44}N_{10}Ru$ 509.1391; Found 509.1389.
HPLC retention time: 25.23 min.

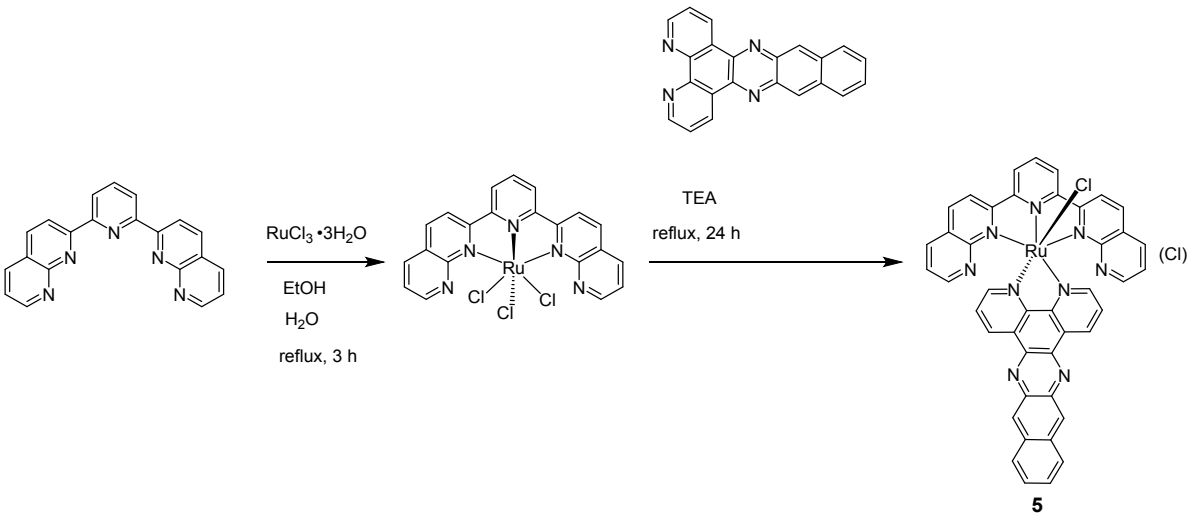

Scheme S5. Synthesis scheme for complex **5** [Ru(dnp)(dppn)(Cl)]Cl (conventional heating method).

Complex 5: [Ru(dnp)(dppn)(Cl)]Cl

Conventional heating method: A three-neck round-bottom flask, equipped with nitrogen purge and a condenser, was charged with dnp (0.100 g, 0.30 mmol) and EtOH (50 mL). Then, aqueous solution of $RuCl_3$•$3H_2O$ was added (0.082 g, 0.32 mmol in 12 mL H_2O). The reaction mixture was well-stirred and refluxed for 3 h. Then, dppn (0.111 g, 0.33 mmol) and TEA (1 mL) were added and reaction mixture was refluxed for 24 h. The reaction mixture was concentrated under reduced pressure. The residue was treated with a few mL of H_2O and the precipitate was isolated by filtration. The precipitate was washed with H_2O and Et_2O and dry-loaded on a column for purification. Column chromatography was performed on neutral alumina, using gradient elution: 1) CH_2Cl_2 2) 50% CH_2Cl_2 : 50% acetone 3) acetone 4) 97% acetone : 3% MeOH 4) 95% acetone : 5% MeOH. The product fraction (plum-purple band) eluted last with 95% acetone : 5% MeOH. The product fraction was concentrated under reduced pressure and the residue was treated with a few mL of Et_2O. The precipitate was isolated by filtration, washed with Et_2O and dried. [Ru(dnp)(dppn)(Cl)]Cl **5** was obtained as a dark-purple powder (0.080 g, 30% yield).

Microwave-assisted method: Reaction was performed in 2 batches, then combined for workup and purification. *Batch 1*: A microwave vial was filled with argon and EtOH (2.00 mL) and H_2O (0.48 mL) were added. The solvent mixture was degassed with argon for 10 minutes, and then dnp (0.028 g, 0.084 mmol) and $RuCl_3$•$3H_2O$ (0.023 g, 0.087 mmol) were added to the reaction vial. The vial was capped, and the reaction mixture was exposed to microwave irradiation at 100°C for 10 min and then at 120°C for 10 min. After that, dppn (0.030 g, 0.091 mmol) and TEA (20 drops) were added to the reaction mixture. The reaction mixture was exposed to microwave irradiation at 120°C for another 30 min. *Batch 2*: repeated procedure for batch 1. The reaction mixtures from batch 1 and batch 2 were combined and concentrated under reduced pressure. The residue was treated with a few mL of H_2O and the precipitate was isolated by filtration. The precipitate was washed with H_2O and Et_2O and dry-loaded on a gravity column for purification. Column chromatography was performed on neutral alumina, using gradient elution: 1) CH_2Cl_2 2) 50% CH_2Cl_2 : 50% acetone 3) acetone 4) 98% acetone : 2% MeOH 5) 96.5% acetone : 3.5% MeOH. The product fraction (plum-purple band) eluted last with 96.5% acetone : 3.5% MeOH. The product fraction was concentrated under reduced pressure and the residue was treated with a few mL of Et_2O. The precipitate was isolated by filtration, washed with Et_2O and dried. [Ru(dnp)(dppn)(Cl)]Cl **5** was obtained as a dark-purple powder (0.037 g, 26% yield).

R_f = 0.57 (alumina; 8% H_2O in acetonitrile).

^{1}H NMR (MeOD-d_3, 700 MHz): δ 10.74 (**d**, dd, J_1 = 4.9 Hz, J_2 = 1.4 Hz, 1H), 10.03 (**f**, dd, J_1 = 8.4 Hz, J_2 = 1.4 Hz, 1H), 9.15 (**c**, dd, J_1 = 7.7 Hz, J_2 = 0.7 Hz, 1H), 9.14 (**g**, s, 1H), 9.09 (**3**, d, J = 8.4 Hz, 2H), 8.99 (**l**, s, 1H), 8.81 (**3′**, d, J = 9.1 Hz, 2H), 8.54 (**4′**, d, J = 8.4 Hz, 2H), 8.45 (**e**, dd, J_1 = 8.4 Hz, J_2 = 4.9 Hz, 1H), 8.38 (**4**, t, J = 8.4 Hz, 1H), 8.29 (**h**,**k**, m, 2H), 8.27 (**5′**, dd, J_1 = 7.7 Hz, J_2 = 1.4 Hz, 2H), 8.01 (**7′**, dd, J_1 = 4.9 Hz, J_2 = 1.4 Hz, 2H), 7.87 (**a**, dd, J_1 = 5.6 Hz, J_2 = 0.7 Hz, 1H), 7.69 (**i**, **j**, m, 2H), 7.33 (**6′**, dd, J_1 = 7.7 Hz, J_2 = 4.9 Hz, 2H), 7.27 (**b**, dd, J_1 = 7.7 Hz, J_2 = 5.6 Hz, 1H).

HRMS (ESI$^+$) m/z: $[M\text{-}Cl]^+$ Calcd for $C_{43}H_{25}ClN_9Ru$ 804.0959; Found 804.0955.

HPLC retention time: 26.09 min.

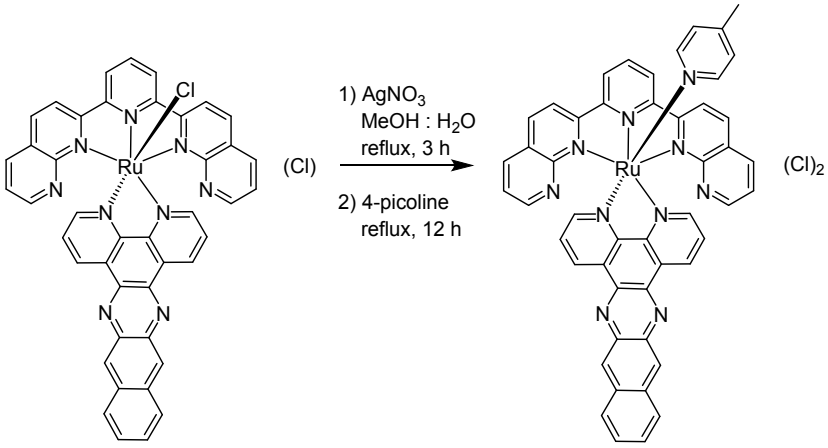

5 **6**

Scheme S6. Synthesis scheme for complex **6** [Ru(dnp)(dppn)(4-pic)]Cl_2 (conventional heating method).

Complex 6: [Ru(dnp)(dppn)(4-pic)]Cl_2

Conventional heating method: A round-bottom flask, equipped with condenser, was charged with [Ru(dnp)(dppn)(Cl)]Cl **5** (0.040 g, 0.05 mmol) and MeOH (6 mL). Then, an aqueous solution of $AgNO_3$ (0.081 g, 0.48 mmol in 1.5 mL H_2O) was added dropwise. The reaction mixture was well-stirred and refluxed for 3 h. Then, 4-picoline (1.5 mL, 15.21 mmol) was added and the reaction mixture was refluxed for 12 h, then concentrated under reduced pressure. The residue was treated with a few mL of H_2O and the precipitate was isolated by filtration. The precipitate was washed with H_2O and Et_2O and dry-loaded on a column for purification. Column chromatography was performed on neutral alumina, using gradient elution: 1) CH_2Cl_2 2) 50% CH_2Cl_2 : 50% acetone 3) acetone 4) 95% acetone : 5% MeOH. The product fraction (red band) eluted last with 95% acetone : 5% MeOH. The product fraction was concentrated under reduced pressure and the residue was treated with a few mL of Et_2O. The precipitate was isolated by filtration, washed with Et_2O and dried. [Ru(dnp)(dppn)(4-pic)]Cl_2 **6** was obtained as a maroon powder (0.035 g, 78% yield).

Microwave-assisted method: A microwave vial was charged with [Ru(dnp)(dppn)(Cl)]Cl **5** (0.037 g, 0.04 mmol), 4-picoline (0.4 mL, 4.12 mmol) and MeOH (2.8 mL). The vial was capped, and the reaction mixture was exposed to microwave irradiation at 150°C for 12 min. After that, H_2O (0.8 mL) was added and the reaction mixture was exposed to microwave irradiation at 160°C for another 15 min. The reaction mixture was concentrated under reduced pressure and dried under high vacuum. The precipitate was purified with flash chromatography on alumina (eluent: gradient elution from 100% acetonitrile to 92% acetonitrile : 8% H_2O). The product fraction (maroon band, elutes with 92% acetonitrile : 8% H_2O) was concentrated under reduced pressure and further purified using size-exclusion chromatography on Sephadex LH-20 (eluent: MeOH). The main band (maroon) was collected and concentrated under reduced pressure. The residue was treated with a few mL of Et_2O, sonicated, and isolated by filtration. The precipitate was thoroughly washed with Et_2O and dried. [Ru(dnp)(dppn)(4-pic)]Cl_2 **6** was obtained as a purple powder (0.021 g, 51% yield).

R_f = 0.43 (alumina; 8% H_2O in acetonitrile).

^{1}H NMR (MeOD-d_3, 500 MHz): δ 10.10 (**f**, dd, J_1 = 8.0 Hz, J_2 = 1.0 Hz, 1H), 9.50 (**d**, dd, J_1 = 5.5 Hz, J_2 = 1.5 Hz, 1H), 9.32 (**c**, dd, J_1 = 8.0 Hz, J_2 = 1.0 Hz, 1H), 9.19 (**g**, s, 1H), 9.18 (**3**, d, J = 8.5 Hz, 2H), 9.02 (**l**, s, 1H), 8.91 (**3′**, d, J = 8.5 Hz, 2H), 8.73 (**4′**, d, J = 8.5 Hz, 2H), 8.51 (**4**, t, J = 8.5 Hz, 1H), 8.44 (**e**, dd, J_1 = 8.5 Hz, J_2 = 5.5 Hz, 1H), 8.38 (**5′**, dd, J_1 = 8.5 Hz, J_2 = 2.0 Hz, 2H), 8.36 (**h/k**, d, J = 8.0 Hz, 1H), 8.29 (**h/k**, d, J = 8.0 Hz, 1H), 8.15 (**7′**, dd, J_1 = 4.5 Hz, J_2 = 2.0 Hz, 2H), 7.81 (**a**, dd, J_1 = 5.5 Hz, J_2 = 1.0 Hz, 1H), 7.72 (**i**, **j**, m, 2H), 7.65 (**2″**, d, J = 6.5 Hz, 2H), 7.44 (**b**, dd, J_1 = 8.0 Hz, J_2 = 5.5 Hz, 1H), 7.44 (**6′**, dd, J_1 = 8.0 Hz, J_2 = 4.0 Hz, 2H), 7.00 (**3″**, d, J = 6.0 Hz, 2H), 2.25 (**4″-Me**, s, 3H).

HRMS (ESI$^+$) m/z: $[M\text{-}2Cl]^{2+}$ Calcd for $C_{49}H_{32}N_{10}Ru$ 431.0922; Found 431.0913.

HPLC retention time: 22.91 min.

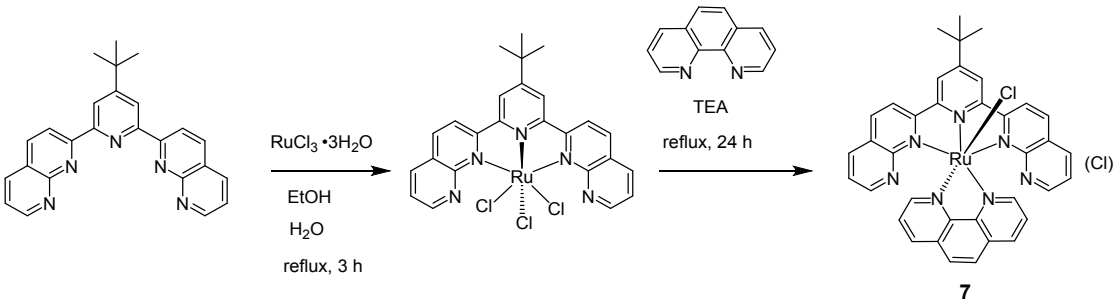

7

Scheme S7. Synthesis scheme for complex **7** [Ru(tpbn)(phen)(Cl)]Cl (conventional heating method).

Complex 7: [Ru(tpbn)(phen)(Cl)]Cl
Conventional heating method: A three-neck round-bottom flask, equipped with nitrogen purge and a condenser, was charged with tpbn (0.100 g, 0.26 mmol) and EtOH (50 mL). Then, an aqueous solution of $RuCl_3$•$3H_2O$ was added (0.070 g, 0.27 mmol in 12 mL H_2O). The reaction mixture was well-stirred and refluxed for 3 h. Then, 1,10-phenanthroline (0.051 g, 0.28 mmol) and TEA (1 mL) were added and the reaction mixture was refluxed for 24 h, then concentrated under reduced pressure. The residue was treated with a few mL of H_2O and the precipitate was isolated by filtration. The precipitate was washed with H_2O and Et_2O and dry-loaded on a column for purification. Column chromatography was performed on neutral alumina, using gradient elution: 1) CH_2Cl_2 2) 50% CH_2Cl_2 : 50% acetone 3) acetone 4) 97% acetone : 3% MeOH. Product fraction (deep-purple band) eluted last with 97% acetone : 3% MeOH. The product fraction was concentrated under reduced pressure and the residue was treated with a few mL of Et_2O. The precipitate was isolated by filtration, washed with Et_2O and dried. [Ru(tpbn)(phen)(Cl)]Cl **7** was obtained as a dark-purple powder (0.095 g, 48% yield).
Although it was not tested, it is highly likely that synthesis of **7** could also be performed using microwave-assisted heating using much shorter reaction times than conventional heating.
R_f = 0.57 (alumina; 8% H_2O in acetonitrile).
^{1}H NMR (MeOD-d_3, 500 MHz): δ 10.62 (**d**, dd, J_1 = 5.5 Hz, J_2 = 1.5 Hz, 1H), 9.08 (**3**, s, 2H), 8.90 (**3′**, d, J = 8.5 Hz, 2H), 8.89 (**f**, dd, J_1 = 8.0 Hz, J_2 = 1.5 Hz, 1H), 8.49 (**4′**, d, J = 8.5 Hz, 2H), 8.33 (**g**, d, J = 9.0 Hz, 1H), 8.29 (**e**, dd, J_1 = 8.0 Hz, J_2 = 5.5 Hz, 1H), 8.23 (**5′**, dd, J_1 = 8.0 Hz, J_2 = 2.0 Hz, 2H), 8.07 (**c**, dd, J_1 = 8.0 Hz, J_2 = 1.0 Hz, 1H), 7.90 (**h**, d, J = 9.0 Hz, 1H), 7.75 (**7′**, dd, J_1 = 4.5 Hz, J_2 = 2.0 Hz, 2H), 7.73 (**a**, dd, J_1 = 5.5 Hz, J_2 = 1.0 Hz, 1H), 7.31 (**6′**, dd, J_1 = 8.0 Hz, J_2 = 4.0 Hz, 2H), 7.15 (**b**, dd, J_1 = 8.0 Hz, J_2 = 5.5 Hz, 1H), 1.78 (**4-tBu**, s, 9H).

HRMS (ESI$^+$) m/z: $[M\text{-}Cl]^+$ Calcd for $C_{37}H_{29}ClN_7Ru$ 708.1211; Found 708.1201.
HPLC retention time: 22.74 min.

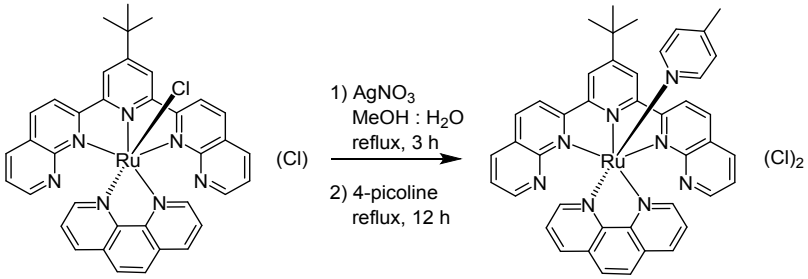

7 8

Scheme S8. Synthesis scheme for complex **8** [Ru(tpbn)(phen)(4-pic)]Cl_2 (conventional heating method).

Complex 8: [Ru(tpbn)(phen)(4-pic)]Cl_2
Conventional heating method: A round-bottom flask, equipped with a condenser, was charged with [Ru(tpbn)(phen)(Cl)]Cl **7** (0.080 g, 0.11 mmol) and MeOH (7 mL). Then, an aqueous solution of $AgNO_3$ (0.190 g, 1.10 mmol in 2 mL H_2O) was added dropwise. The reaction mixture was well-stirred and refluxed for 3 h. Then, 4-picoline (1.5 mL, 15.21 mmol) was added and the reaction mixture was refluxed for 12 h, then concentrated under reduced pressure. The residue was treated with a few mL of H_2O and the precipitate was isolated by filtration. The precipitate was washed with H_2O and Et_2O and dry-loaded on a column for purification. Column chromatography was performed on neutral alumina, using gradient elution: 1) CH_2Cl_2 2) 50% CH_2Cl_2 : 50% acetone 3) acetone 4) 95% acetone : 5% MeOH. The product fraction (deep-purple band) eluted last with 95%

acetone : 5% MeOH. The product fraction was concentrated under reduced pressure and the residue was treated with a few mL of Et_2O. The precipitate was isolated by filtration, washed with Et_2O and dried. [Ru(tpbn)(phen)(4-pic)]Cl_2 **8** was obtained as a dark-purple powder (0.070 g, 79% yield).

Microwave-assisted method: A microwave vial was charged with [Ru(tpbn)(phen)(Cl)]Cl **7** (0.044 g, 0.06 mmol), 4-picoline (0.4 mL, 4.12 mmol) and MeOH (2.8 mL). The vial was capped, and the reaction mixture was exposed to microwave irradiation at 150°C for 12 min. After that, H_2O (0.8 mL) was added and the reaction mixture was exposed to microwave irradiation at 150°C for 12 min and then at 155°C for another 12 min. The reaction mixture was concentrated under reduced pressure and dried under high vacuum. The precipitate was purified with flash chromatography on alumina (eluent: gradient elution from 100% acetonitrile to 92% acetonitrile : 8% H_2O). The product fraction (deep-purple band, elutes with 92% acetonitrile : 8% H_2O) was concentrated under reduced pressure and further purified using size-exclusion chromatography on Sephadex LH-20 (eluent: MeOH). The main band (purple) was collected and concentrated under reduced pressure. The residue was treated with a few mL of Et_2O, sonicated, and isolated by filtration. The precipitate was thoroughly washed with Et_2O and dried. [Ru(tpbn)(phen)(4-pic)]Cl_2 **8** was obtained as a dark-purple powder (0.034 g, 69% yield).

R_f = 0.45 (alumina; 8% H_2O in acetonitrile).

^{1}H NMR (MeOD-d_3, 500 MHz): δ 9.44 (**d**, dd, J_1 = 5.5 Hz, J_2 = 1.5 Hz, 1H), 9.14 (**3**, s, 2H), 9.01 (**3′**, d, J = 8.5 Hz, 2H), 8.94 (**f**, dd, J_1 = 8.5 Hz, J_2 = 1.5 Hz, 1H), 8.68 (**4′**, d, J = 8.5 Hz, 2H), 8.35 (**5′**, dd, J_1 = 8.5 Hz, J_2 = 2.0 Hz, 2H), 8.32 (**g**, d, J = 9.0 Hz, 1H), 8.29 (**e**, dd, J_1 = 8.5 Hz, J_2 = 5.5 Hz, 1H), 8.19 (**c**, dd, J_1 = 8.5 Hz, J_2 = 1.5 Hz, 1H), 7.92 (**h**, d, J = 9.0 Hz, 1H), 7.92 (**7′**, dd, J_1 = 4.5 Hz, J_2 = 2.0 Hz, 2H), 7.67 (**a**, dd, J_1 = 5.5 Hz, J_2 = 1.0 Hz, 1H), 7.66 (**2″**, d, J = 6.5 Hz, 2H), 7.42 (**6′**, dd, J_1 = 8.0 Hz, J_2 = 4.5 Hz, 2H), 7.29 (**b**, dd, J_1 = 8.0 Hz, J_2 = 5.5 Hz, 1H), 6.97 (**3″**, d, J = 6.5 Hz, 2H), 2.23 (**4″-Me**, s, 3H), 1.76 (**4-tBu**, s, 9H).

HRMS (ESI$^+$) m/z: $[M-2Cl]^{2+}$ Calcd for $C_{43}H_{36}N_8Ru$ 383.1047; Found 383.1041.

HPLC retention time: 18.39 min.

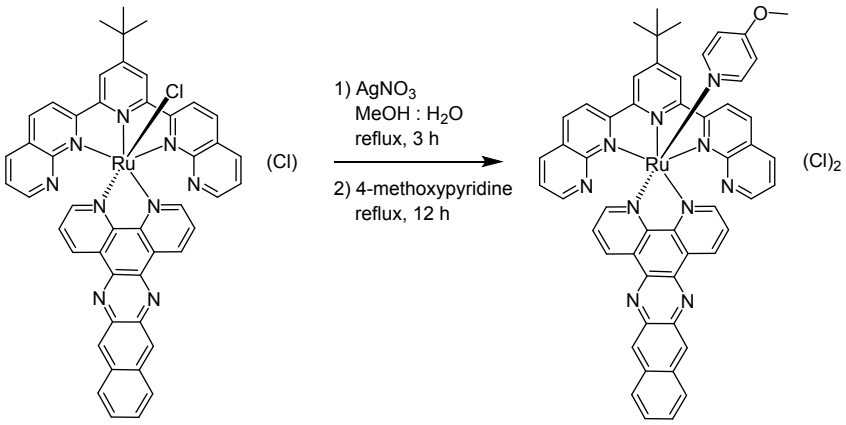

1 **9**

Scheme S9. Synthesis scheme for complex **9** [Ru(tpbn)(dppn)(4-mp)]Cl_2 (conventional heating method).

Complex 9: [Ru(tpbn)(dppn)(4-mp)]Cl_2

Conventional heating method: A round-bottom flask, equipped with condenser, was charged with [Ru(tpbn)(dppn)(Cl)]Cl **1** (0.050 g, 0.06 mmol) and MeOH (4 mL). Then, an aqueous solution of $AgNO_3$ (0.095 g, 0.56 mmol in 1 mL H_2O) was added dropwise. The reaction mixture was well-stirred and refluxed for 3 h. Then, 4-methoxypyridine (0.5 mL, 4.9 mmol) was added and reaction mixture was refluxed for 12 h, then concentrated under reduced pressure. The residue was treated with a few mL of H_2O and the precipitate was isolated by filtration. The precipitate was washed with H_2O and Et_2O and dry-loaded on a column for purification. Column chromatography was performed on neutral alumina, using gradient elution: 1) CH_2Cl_2 2) 50% CH_2Cl_2 : 50% acetone 3) acetone 4) 95% acetone : 5% MeOH. The product fraction (maroon band) eluted last with 95% acetone : 5% MeOH. The product fraction was concentrated under reduced pressure and the residue was treated with a few mL of Et_2O. The precipitate was isolated by filtration, washed with Et_2O and dried. [Ru(tpbn)(dppn)(4-mp)]Cl_2 **9** was obtained as a maroon powder (0.016 g, 29% yield).

Microwave-assisted method: The reaction was performed in 2 batches, then combined for workup and purification. *Batch 1*: A microwave vial was charged with [Ru(tpbn)(dppn)(Cl)]Cl **1** (0.020 g, 0.02 mmol), 4-methoxypyridine (0.25 mL, 2.47 mmol) and MeOH (2.0 mL). The vial was capped, and the reaction mixture was exposed to microwave irradiation at 150°C for 12 min. After that, H_2O (0.4 mL) was added and the reaction

mixture was exposed to microwave irradiation at 160°C for 12 min. *Batch 2*: repeated the procedure for batch 1. The reaction mixtures from batches 1 and 2 were combined, concentrated under reduced pressure and dried under high vacuum. The residue was treated with a few mL of Et_2O, sonicated, and isolated by filtration. The precipitate was thoroughly washed with Et_2O and dried. The precipitate was purified with flash chromatography on alumina (eluent: gradient elution from 100% acetonitrile to 92% acetonitrile : 8% H_2O). The product fraction (maroon band, elutes with 92% acetonitrile : 8% H_2O) was concentrated under reduced pressure and further purified using size-exclusion chromatography on Sephadex LH-20 (eluent: MeOH). The main band (maroon) was collected and concentrated under reduced pressure. The residue was treated with a few mL of Et_2O, sonicated, and isolated by filtration. The precipitate was thoroughly washed with Et_2O and dried. $[Ru(tpbn)(dppn)(4\text{-}mp)]Cl_2$ **9** was obtained as a maroon powder (0.029 g, 66% yield).
R_f = 0.54 (alumina; 8% H_2O in acetonitrile).
^{1}H NMR (MeOD-d_3, 500 MHz): δ 10.08 (**f**, dd, J_1 = 8.0 Hz, J_2 = 1.0 Hz, 1H), 9.49 (**d**, dd, J_1 = 5.0 Hz, J_2 = 1.0 Hz, 1H), 9.28 (**c**, dd, J_1 = 8.5 Hz, J_2 = 2.0 Hz, 1H), 9.18 (**3**, s, 2H), 9.17 (**g**, s, 1H), 9.06 (**3′**, d, J = 8.5 Hz, 2H), 9.01 (**l**, s, 1H), 8.73 (**4′**, d, J = 8.5 Hz, 2H), 8.44 (**e**, dd, J_1 = 8.0 Hz, J_2 = 5.5 Hz, 1H), 8.37 (**5′**, dd, J_1 = 8.0 Hz, J_2 = 2.0 Hz, 2H), 8.32 (**h/k**, d, J = 7.5 Hz, 1H), 8.28 (**h/k**, d, J = 8.0 Hz, 1H), 8.14 (**7′**, dd, J_1 = 4.0 Hz, J_2 = 1.5 Hz, 2H), 7.79 (**a**, dd, J_1 = 6.0 Hz, J_2 = 1.5 Hz, 1H), 7.71 (**i**, **j**, m, 2H), 7.56 (**2″**, d, J = 7.5 Hz, 2H), 7.43 (**6′**, **b**, m, 3H), 6.73 (**3″**, d, J = 7.0 Hz, 2H), 3.75 (**4″-OMe**, s, 3H), 1.78 (**4-tBu**, s, 9H).
HRMS (ESI$^+$) m/z: $[M\text{-}2Cl]^{2+}$ Calcd for $C_{53}H_{40}N_{10}ORu$ 467.1209; Found 467.1199.
HPLC retention time: 23.58 min.

4. NMR spectra of Ru(II) complexes 1–9

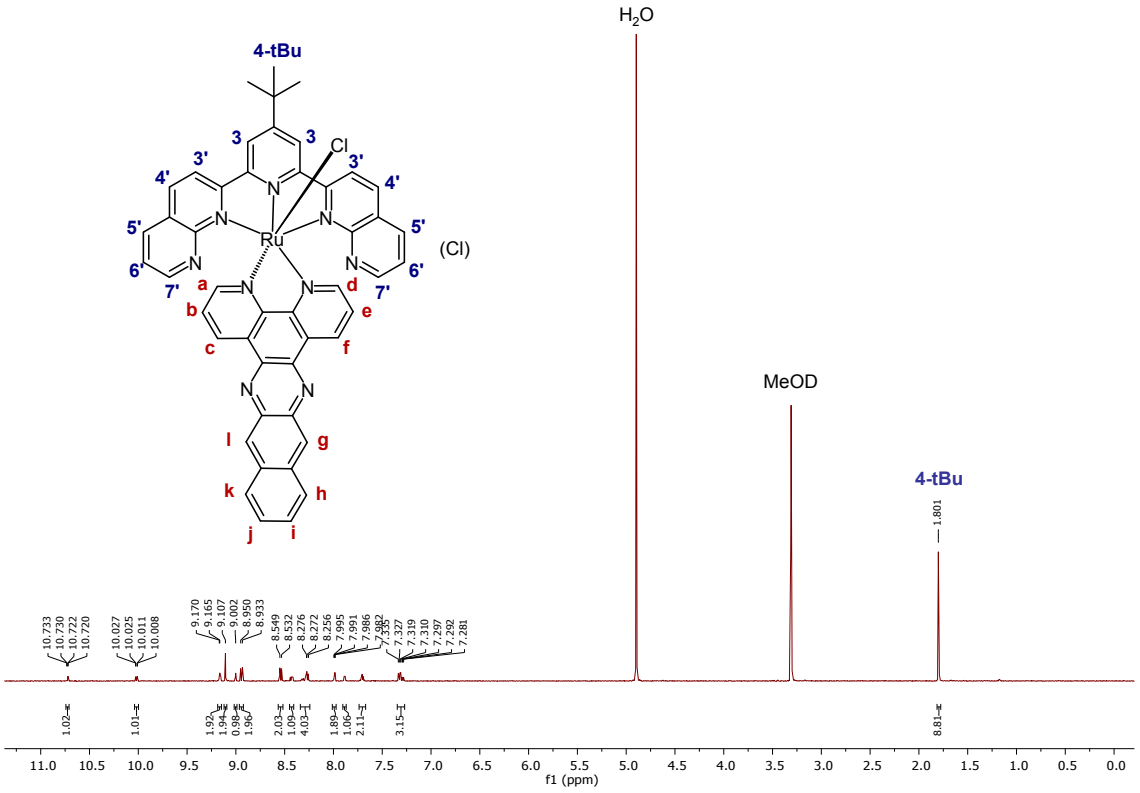

Figure S1. 500 MHz ^{1}H NMR spectrum of **1** in MeOD-d_3 at 298 K.

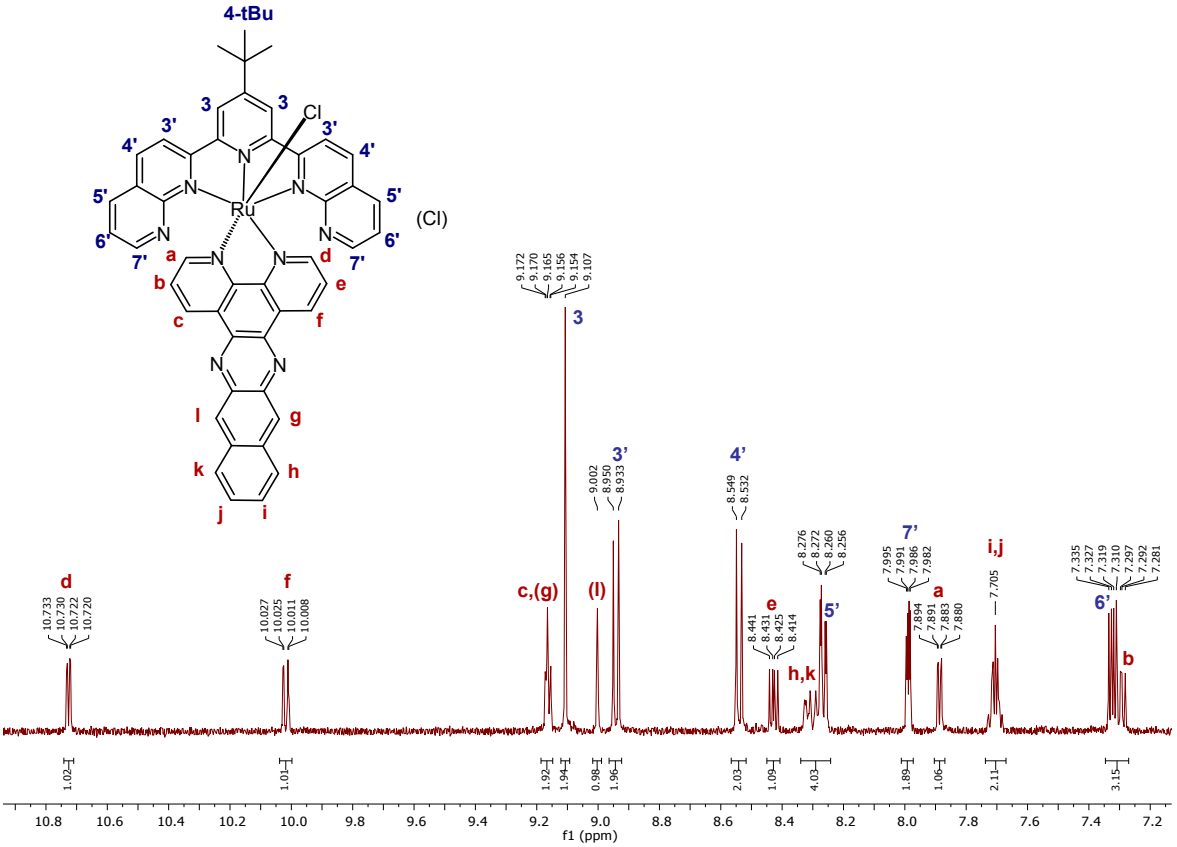

Figure S2. 500 MHz ^{1}H NMR spectrum of **1** in MeOD-d_3 at 298 K, aromatic region.

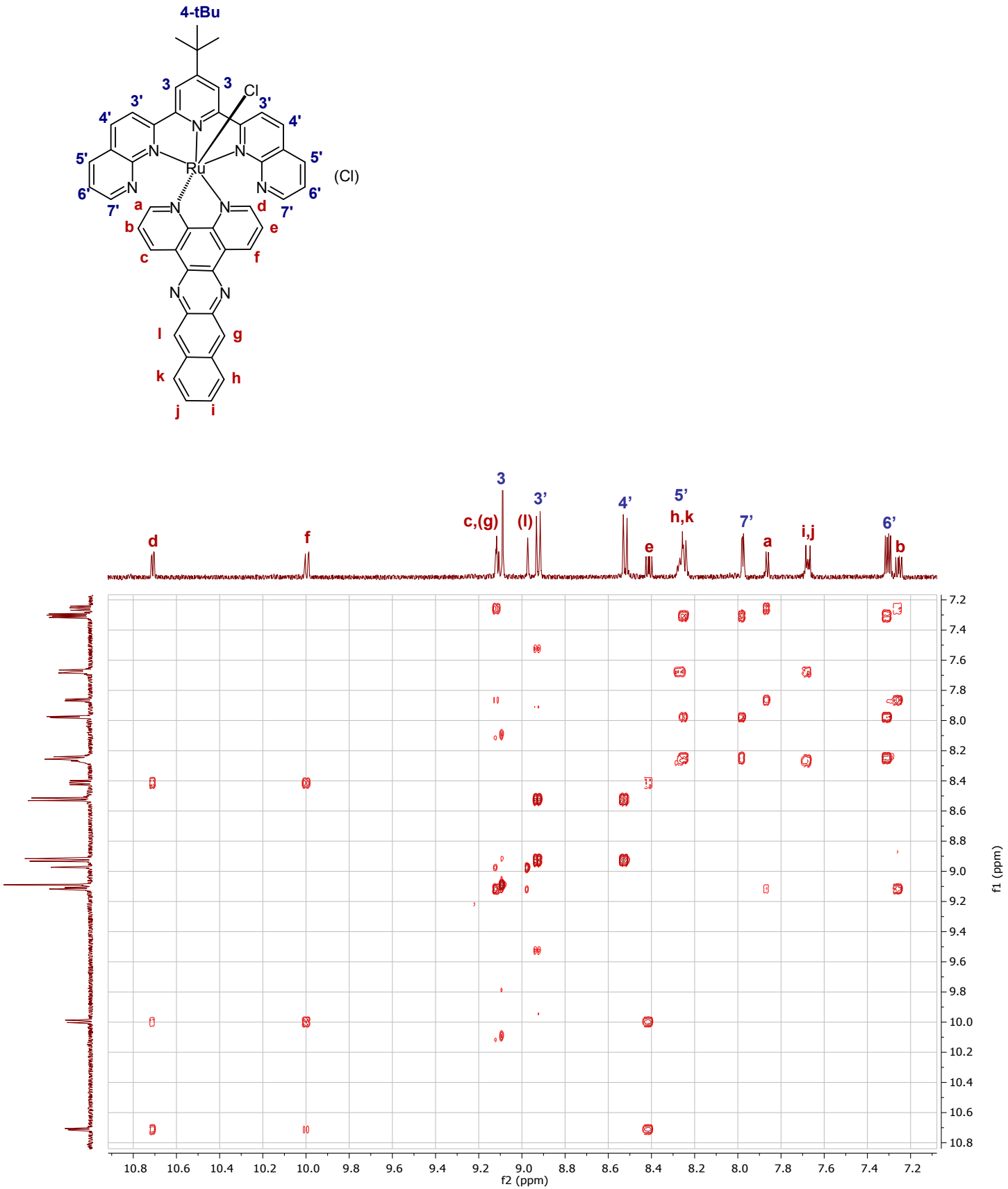

Figure S3. 500 MHz ^{1}H–^{1}H COSY NMR spectrum of **1** in MeOD-d_3 at 298 K, aromatic region.

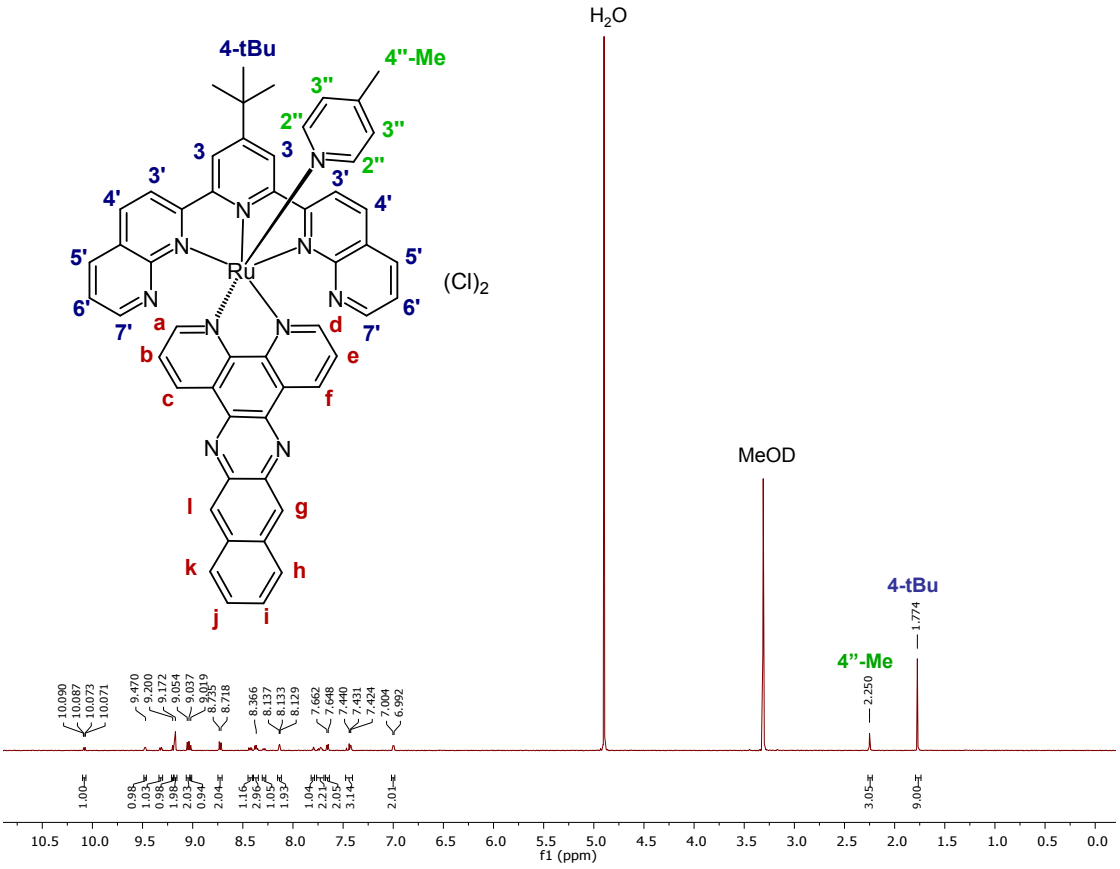

Figure S4. 500 MHz ^{1}H NMR spectrum of **2** in MeOD-d_3 at 298 K.

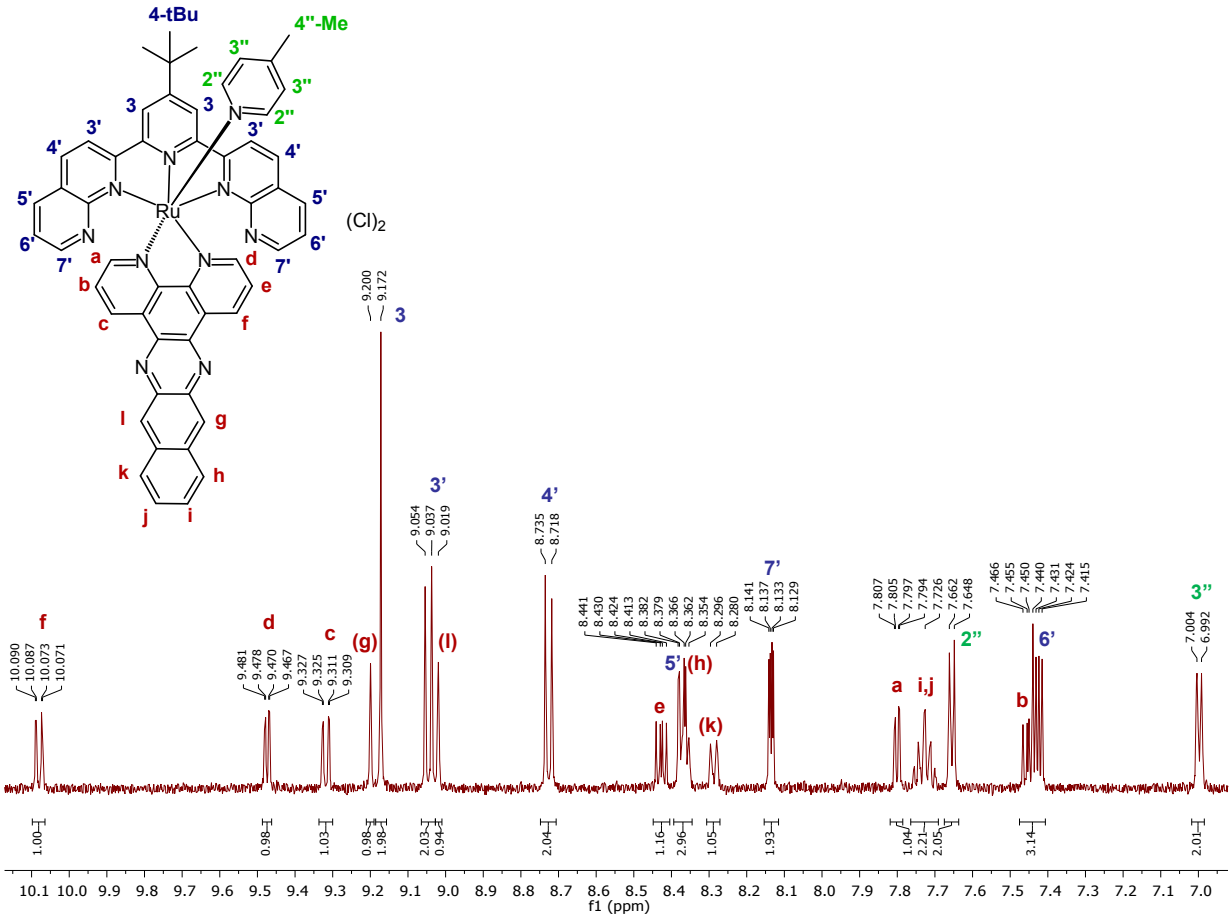

Figure S5. 500 MHz ^{1}H NMR spectrum of **2** in MeOD-d_3 at 298 K, aromatic region.

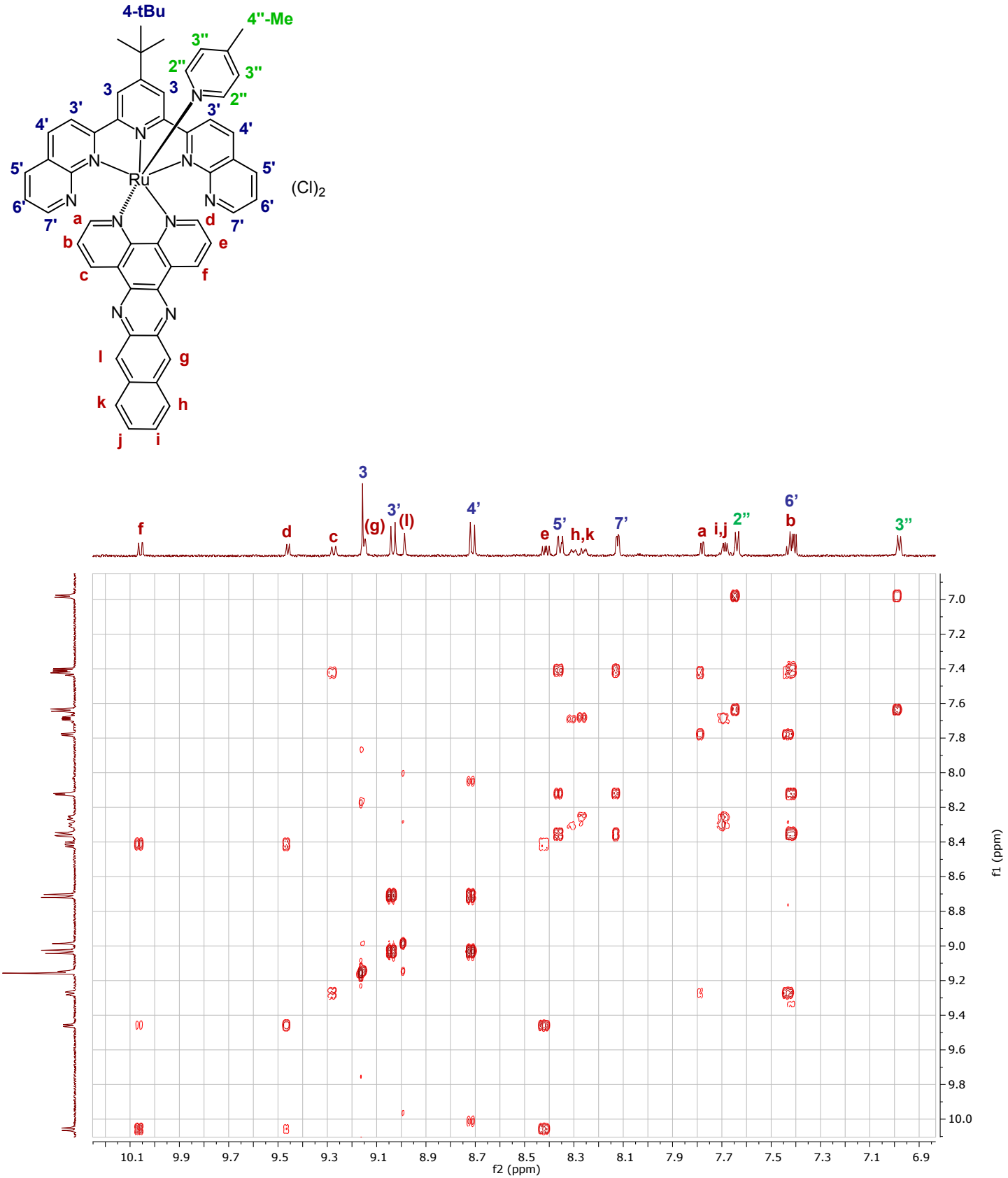

Figure S6. 500 MHz ^{1}H–^{1}H COSY NMR spectrum of **2** in MeOD-d_3 at 298 K, aromatic region.

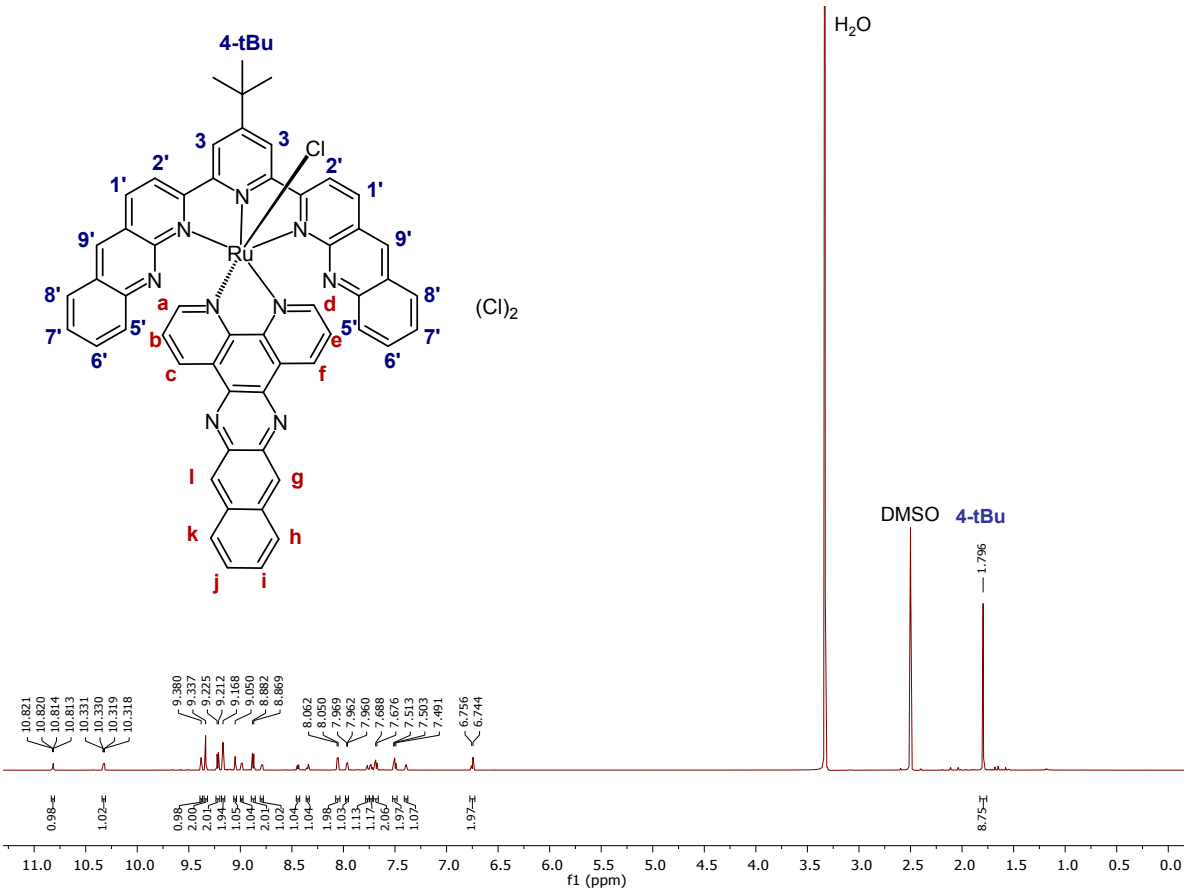

Figure S7. 700 MHz ^{1}H NMR spectrum of **3** in DMSO-d_6 at 298 K.

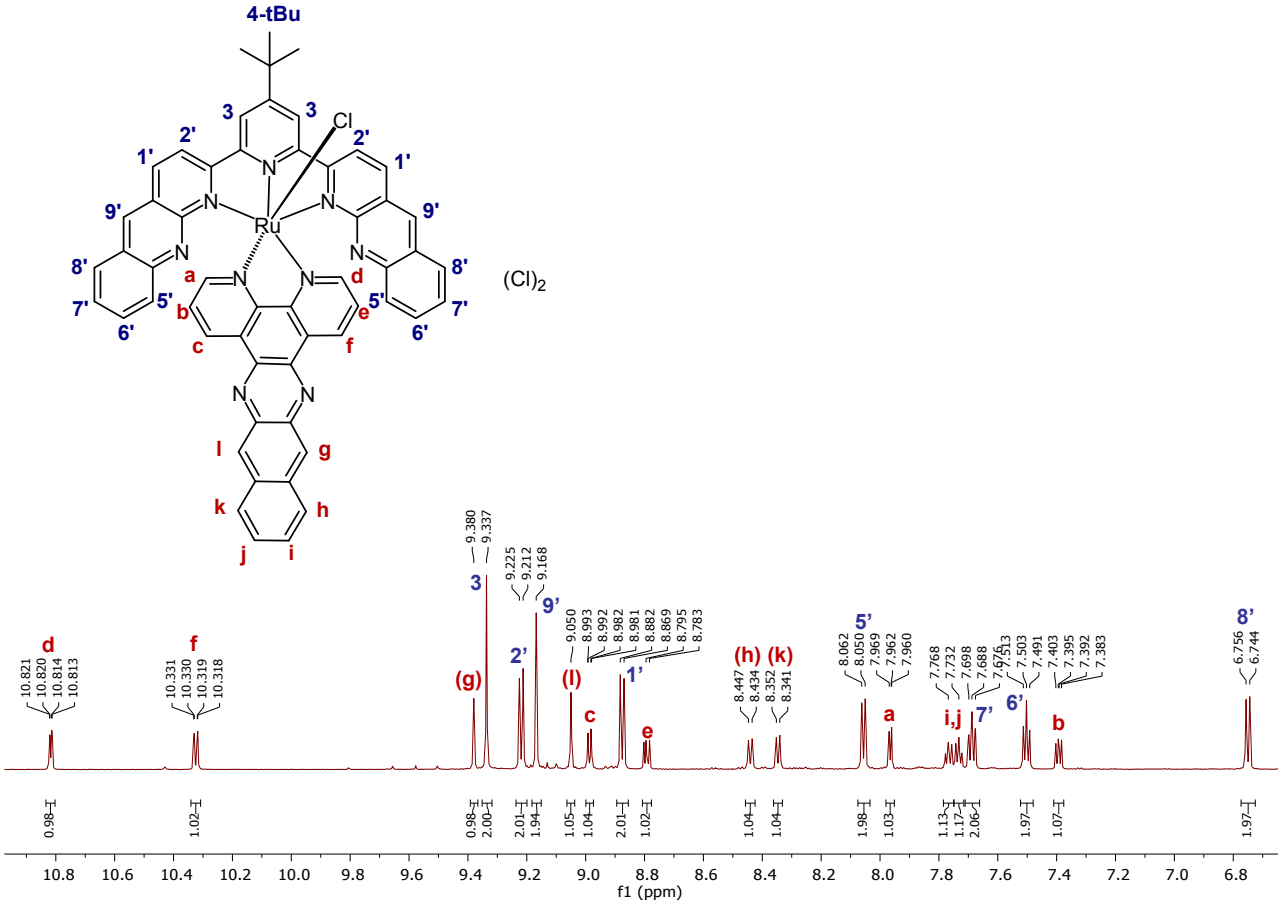

Figure S8. 700 MHz ^{1}H NMR spectrum of **3** in DMSO-d_6 at 298 K, aromatic region.

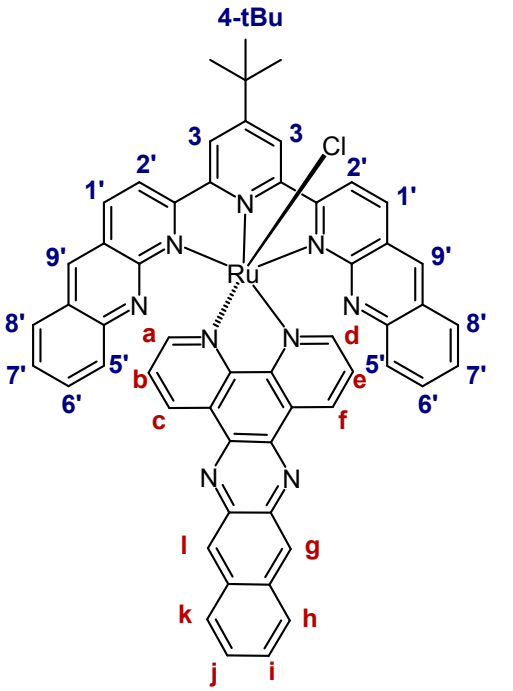

$(Cl)_2$

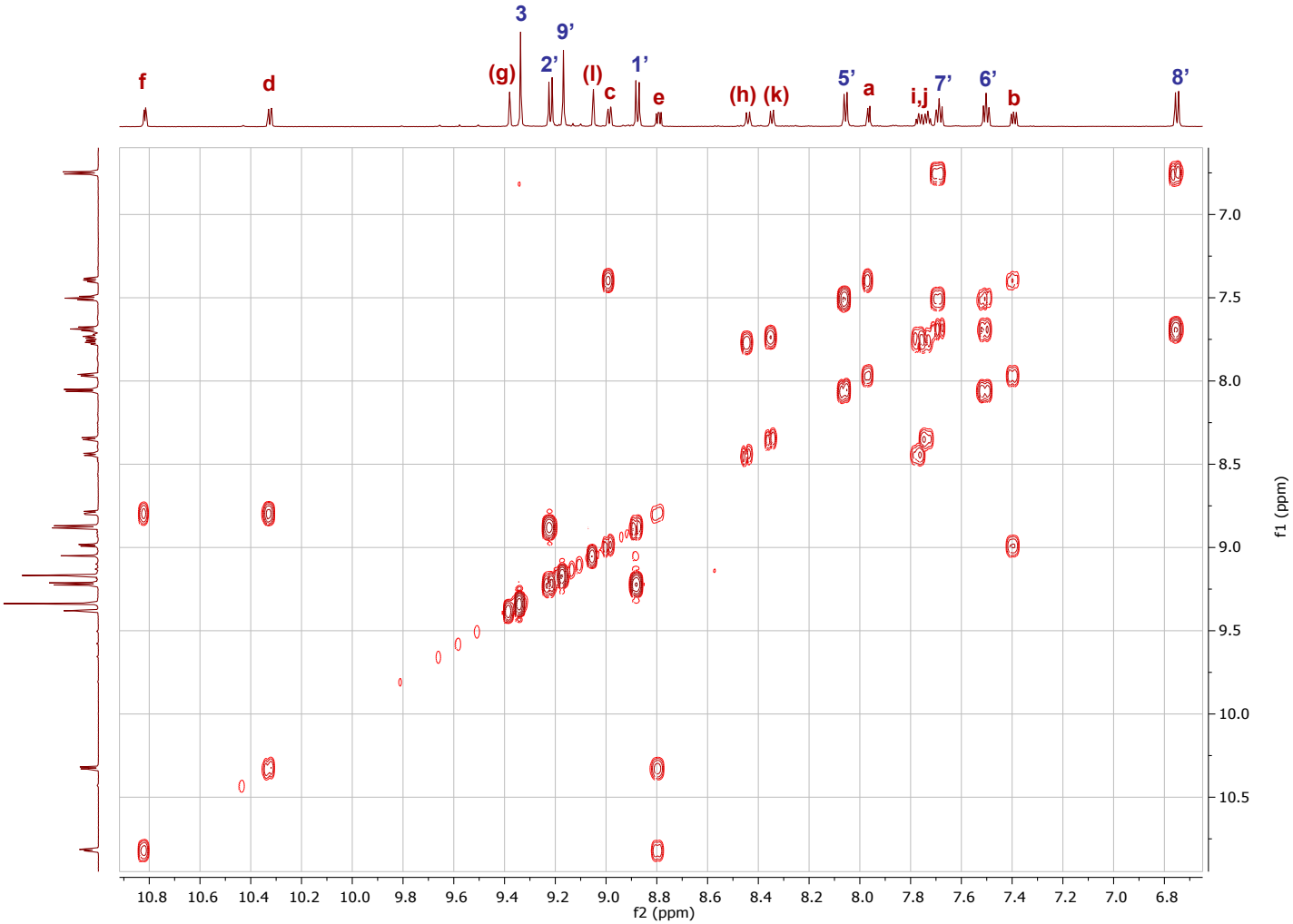

Figure S9. 700 MHz ^{1}H–^{1}H COSY NMR spectrum of **3** in DMSO-d_6 at 298 K, aromatic region.

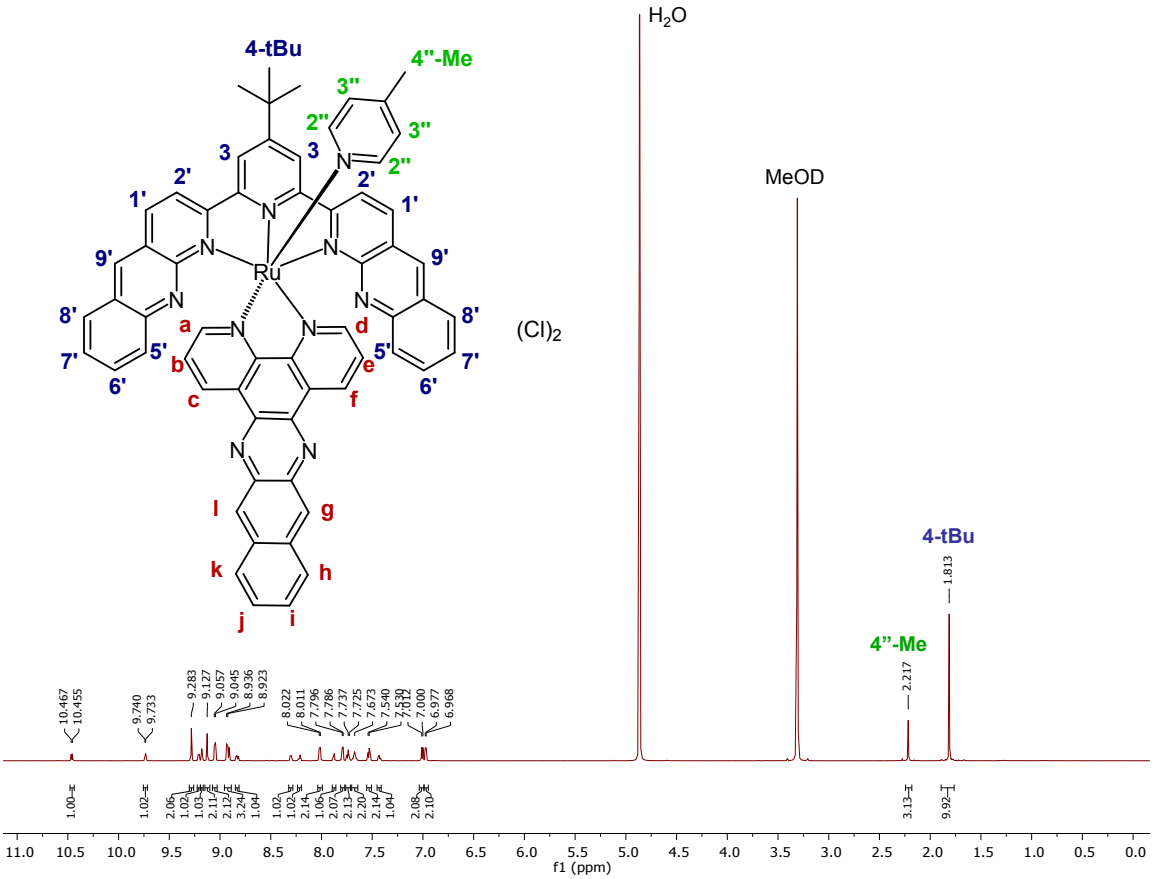

Figure S10. 700 MHz ^{1}H NMR spectrum of **4** in MeOD-d_3 at 298 K.

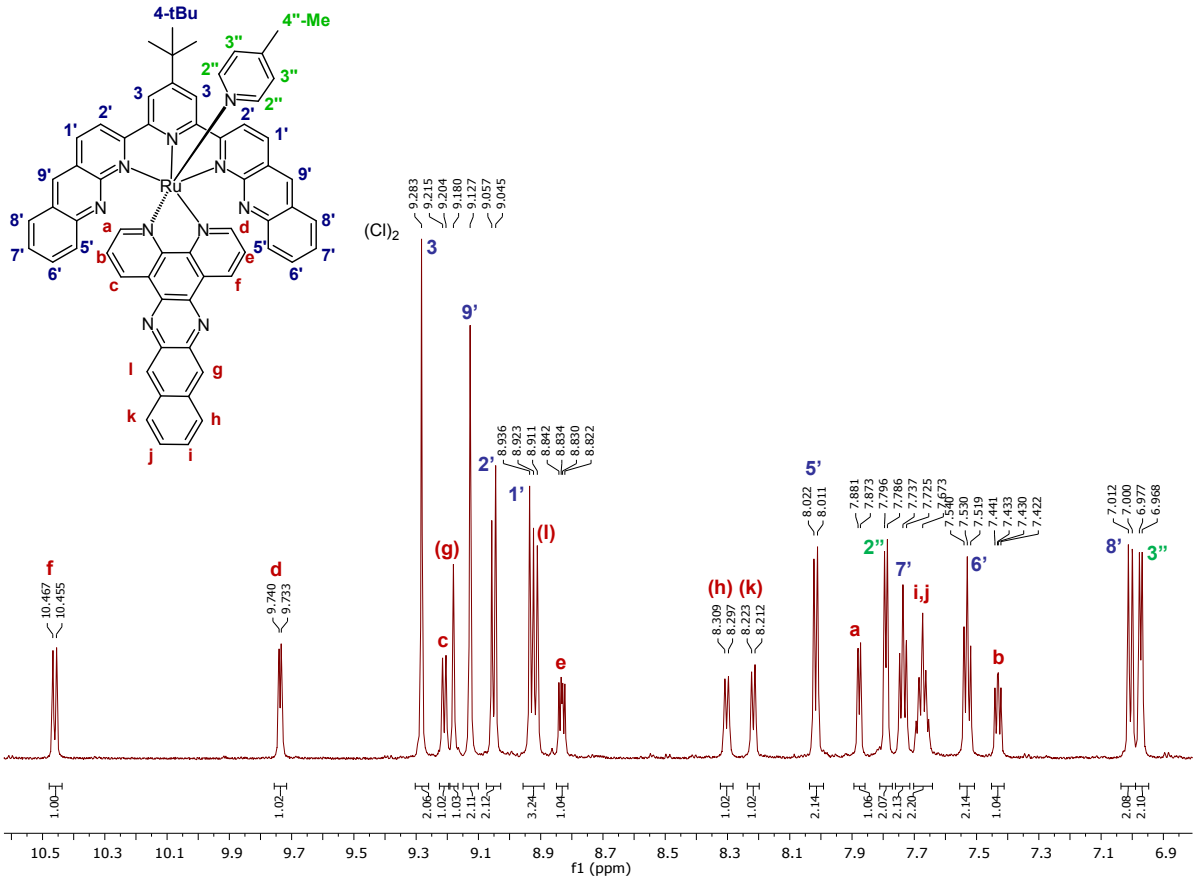

Figure S11. 700 MHz ^{1}H NMR spectrum of **4** in MeOD-d_3 at 298 K, aromatic region.

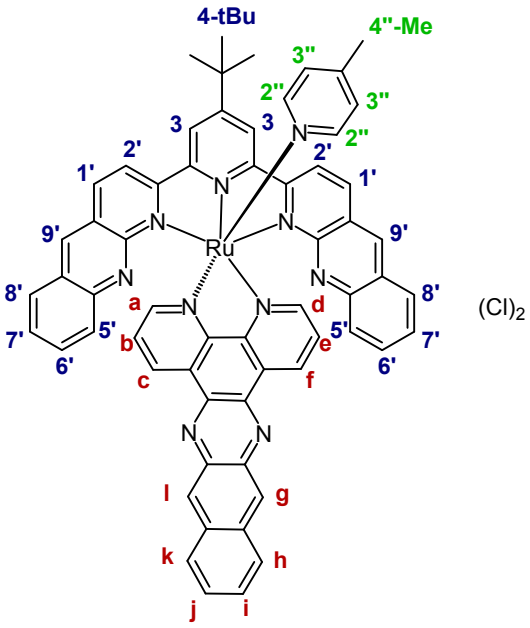

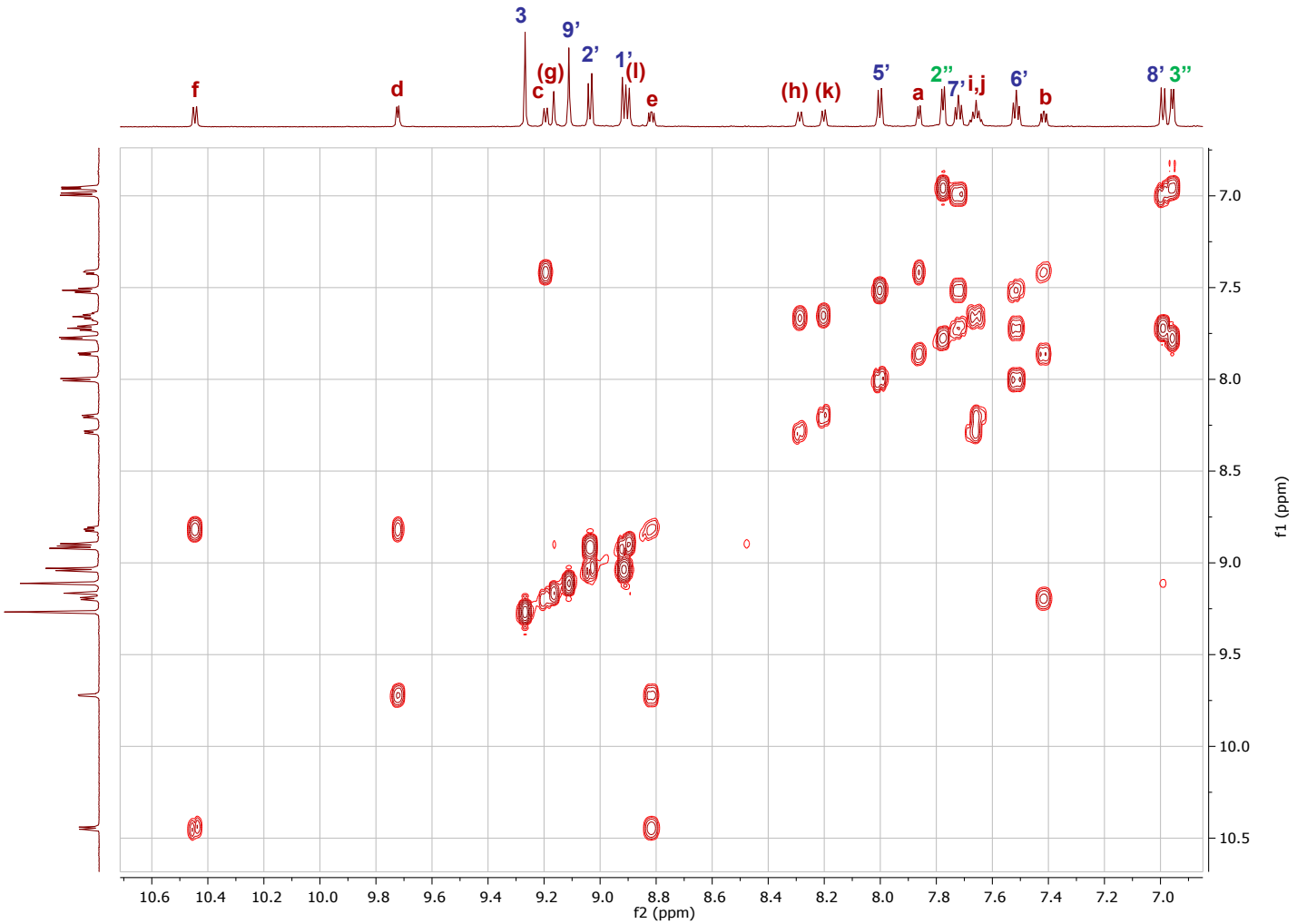

Figure S12. 700 MHz ^{1}H–^{1}H COSY NMR spectrum of **4** in MeOD-d_3 at 298 K, aromatic region.

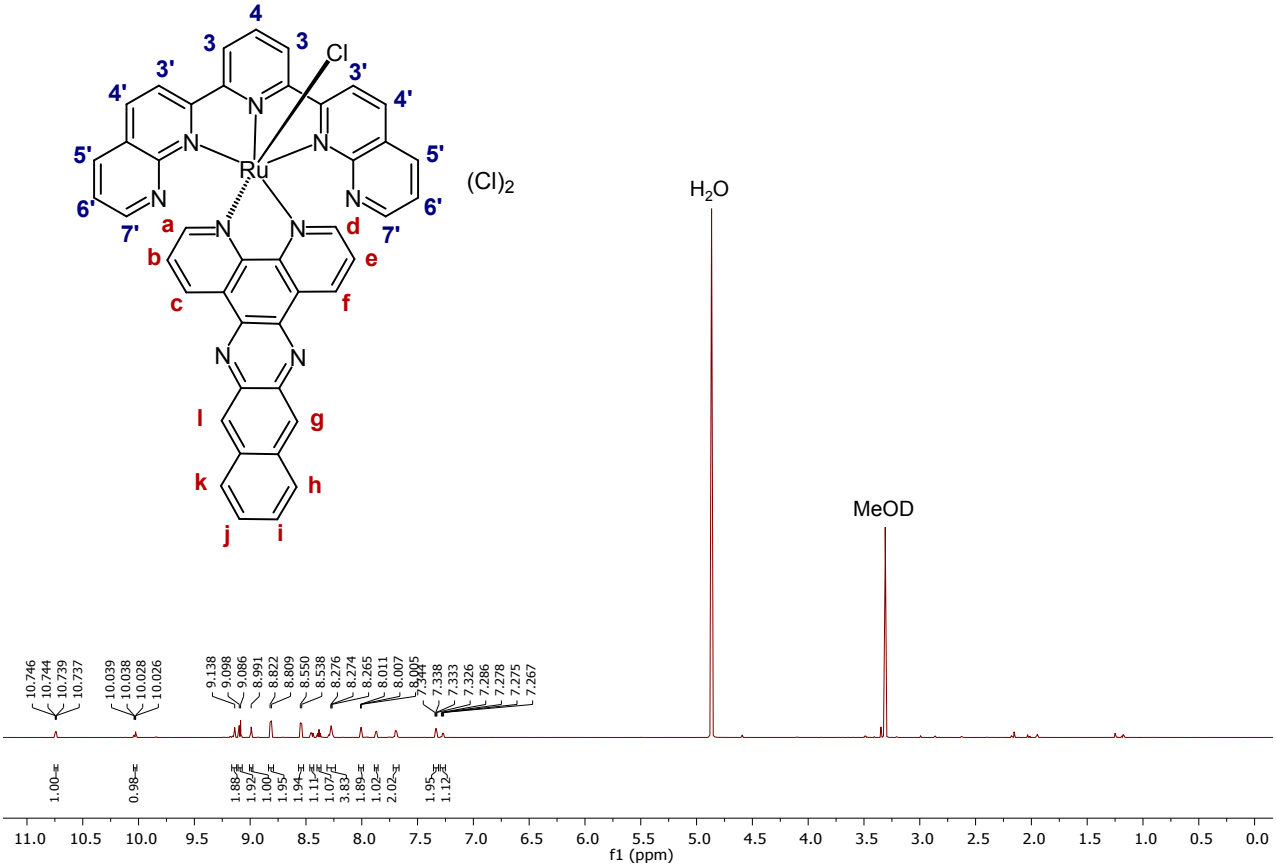

Figure S13. 700 MHz ^{1}H NMR spectrum of 5 in MeOD-d_3 at 298 K.

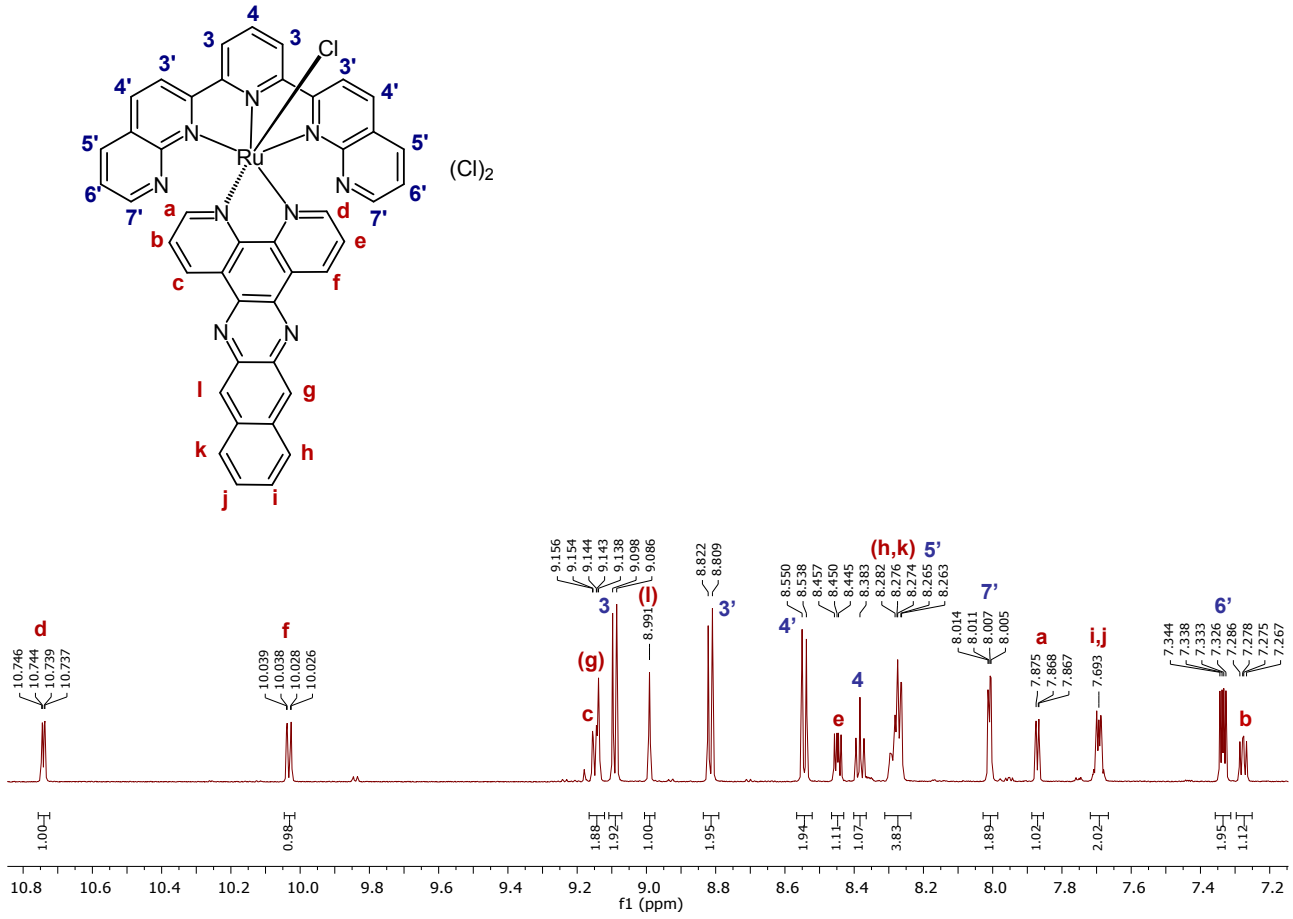

Figure S14. 700 MHz ^{1}H NMR spectrum of **5** in MeOD-d_3 at 298 K, aromatic region.

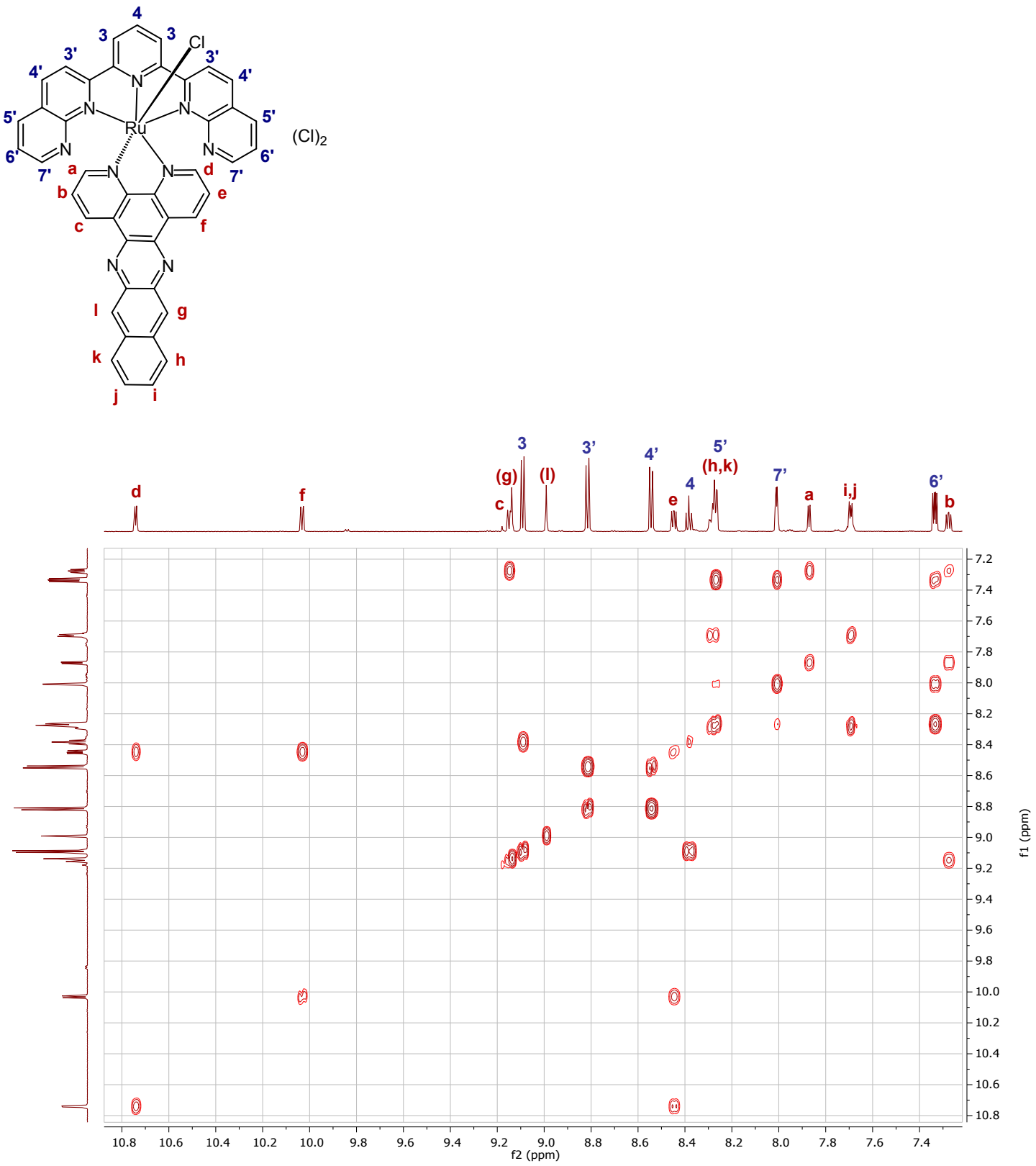

Figure S15. 700 MHz ^{1}H–^{1}H COSY NMR spectrum of **5** in MeOD-d_3 at 298 K, aromatic region.

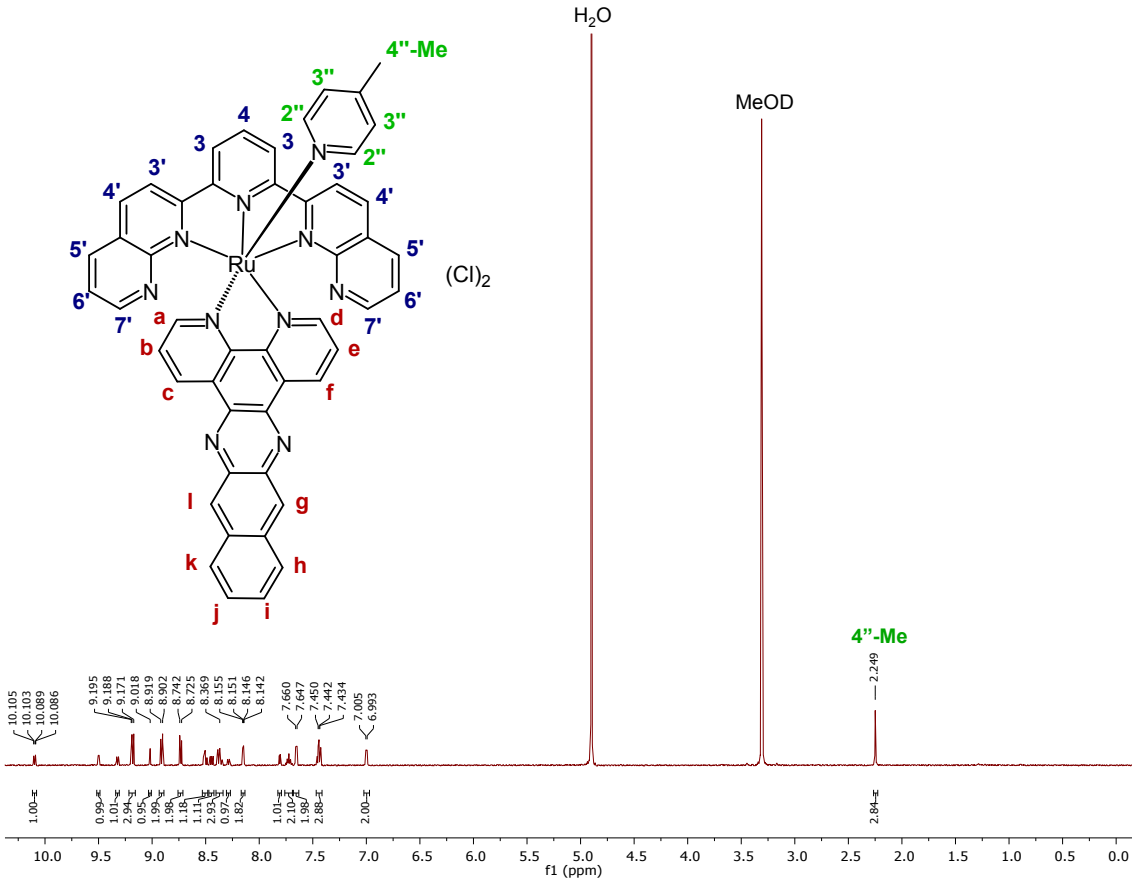

Figure S16. 500 MHz ^{1}H NMR spectrum of **6** in MeOD-d_3 at 298 K.

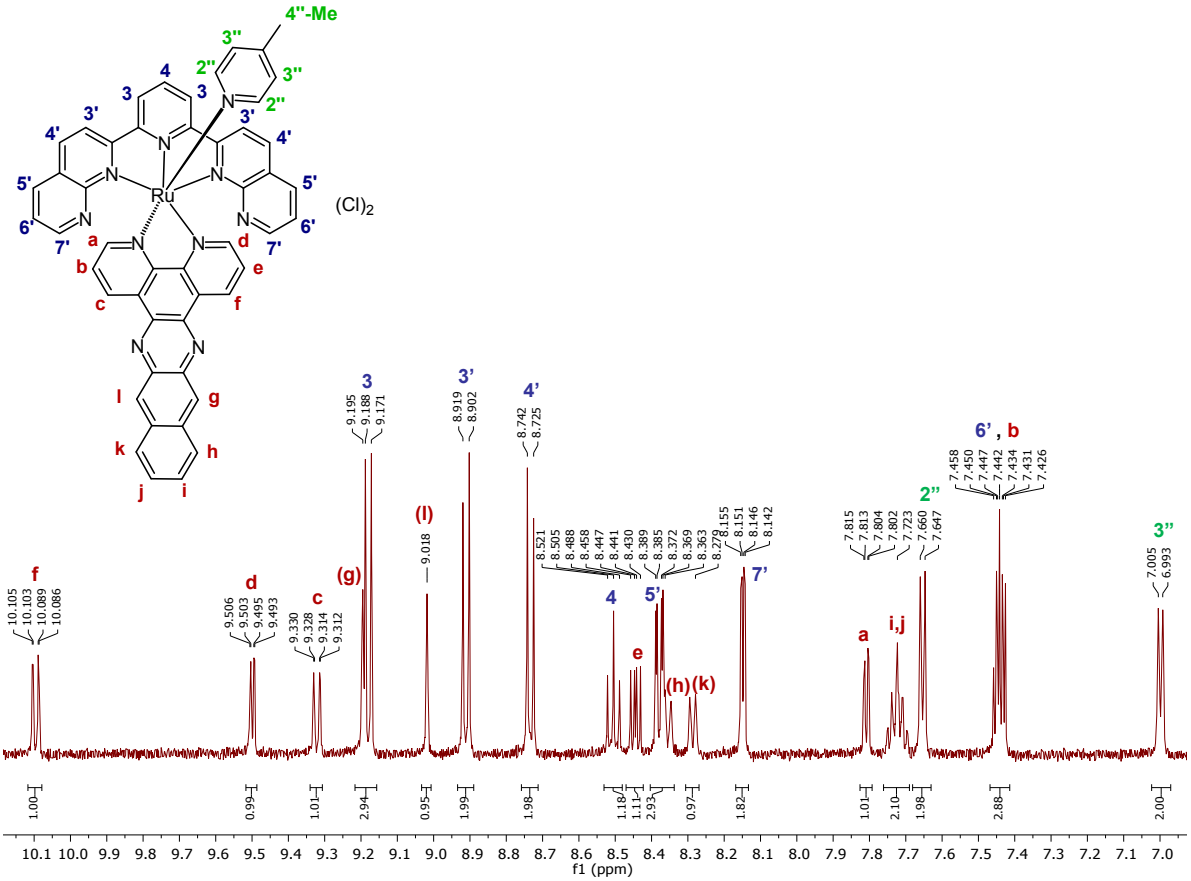

Figure S17. 500 MHz ^{1}H NMR spectrum of **6** in MeOD-d_3 at 298 K, aromatic region.

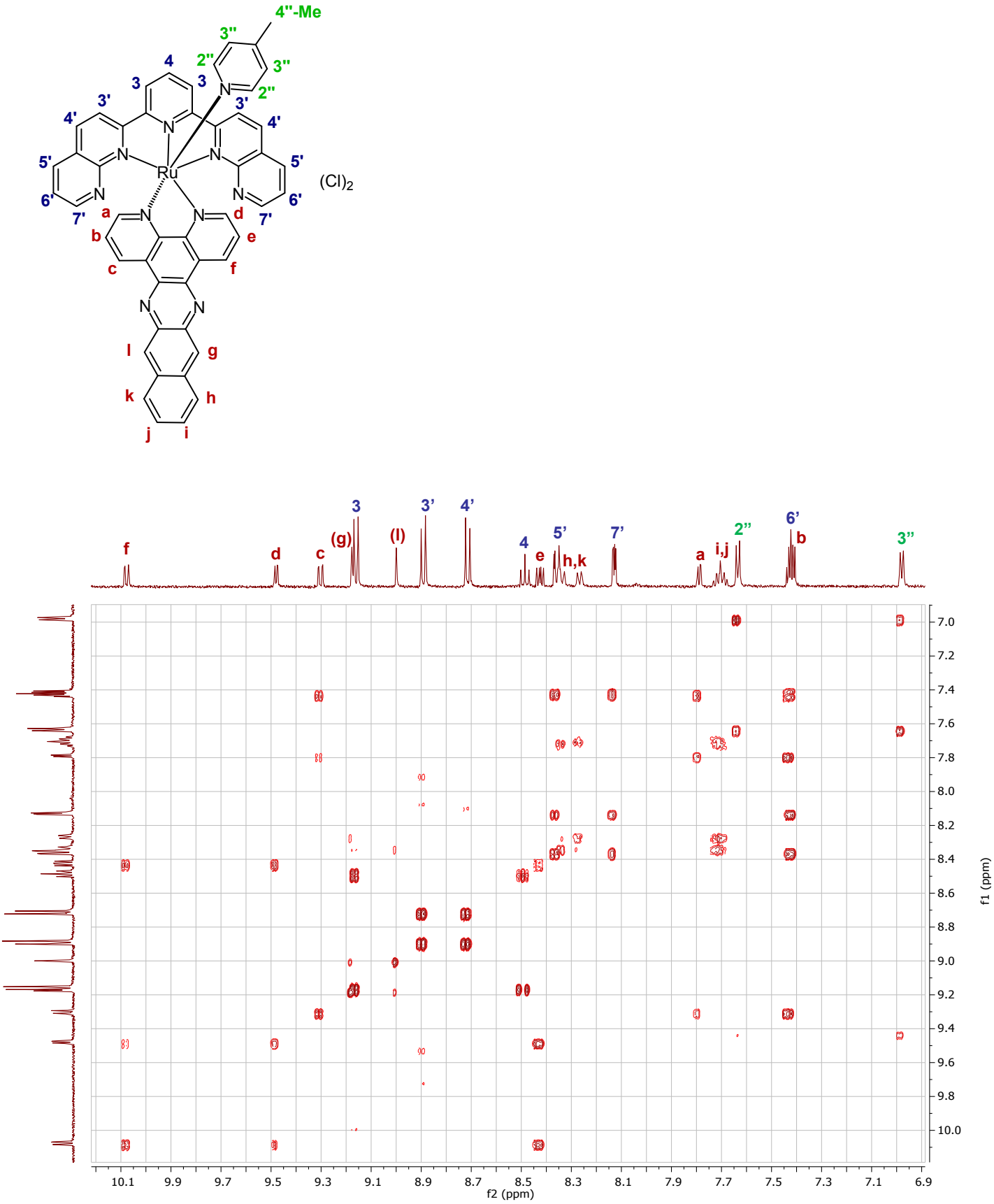

Figure S18. 500 MHz ^{1}H–^{1}H COSY NMR spectrum of **6** in MeOD-d_3 at 298 K, aromatic region.

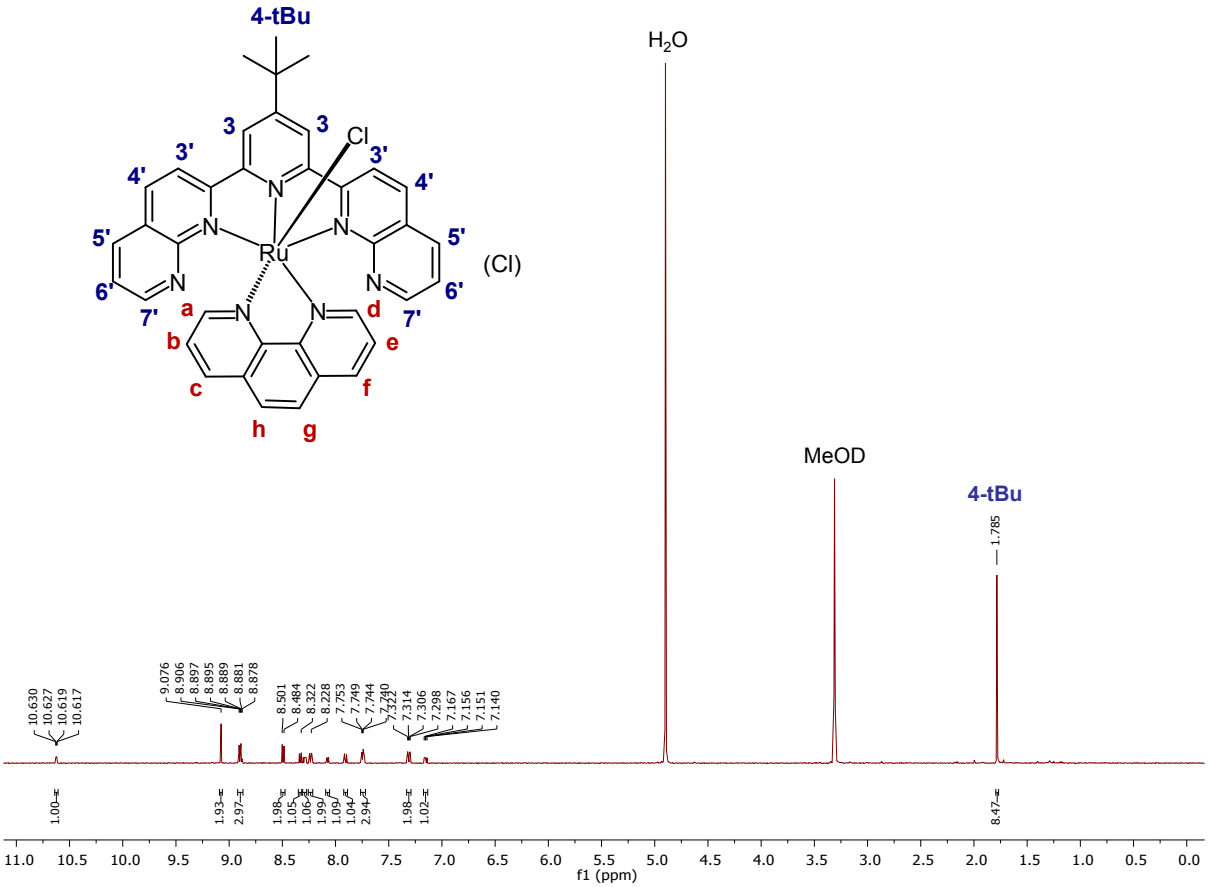

Figure S19. 500 MHz ^{1}H NMR spectrum of **7** in MeOD-d_3 at 298 K.

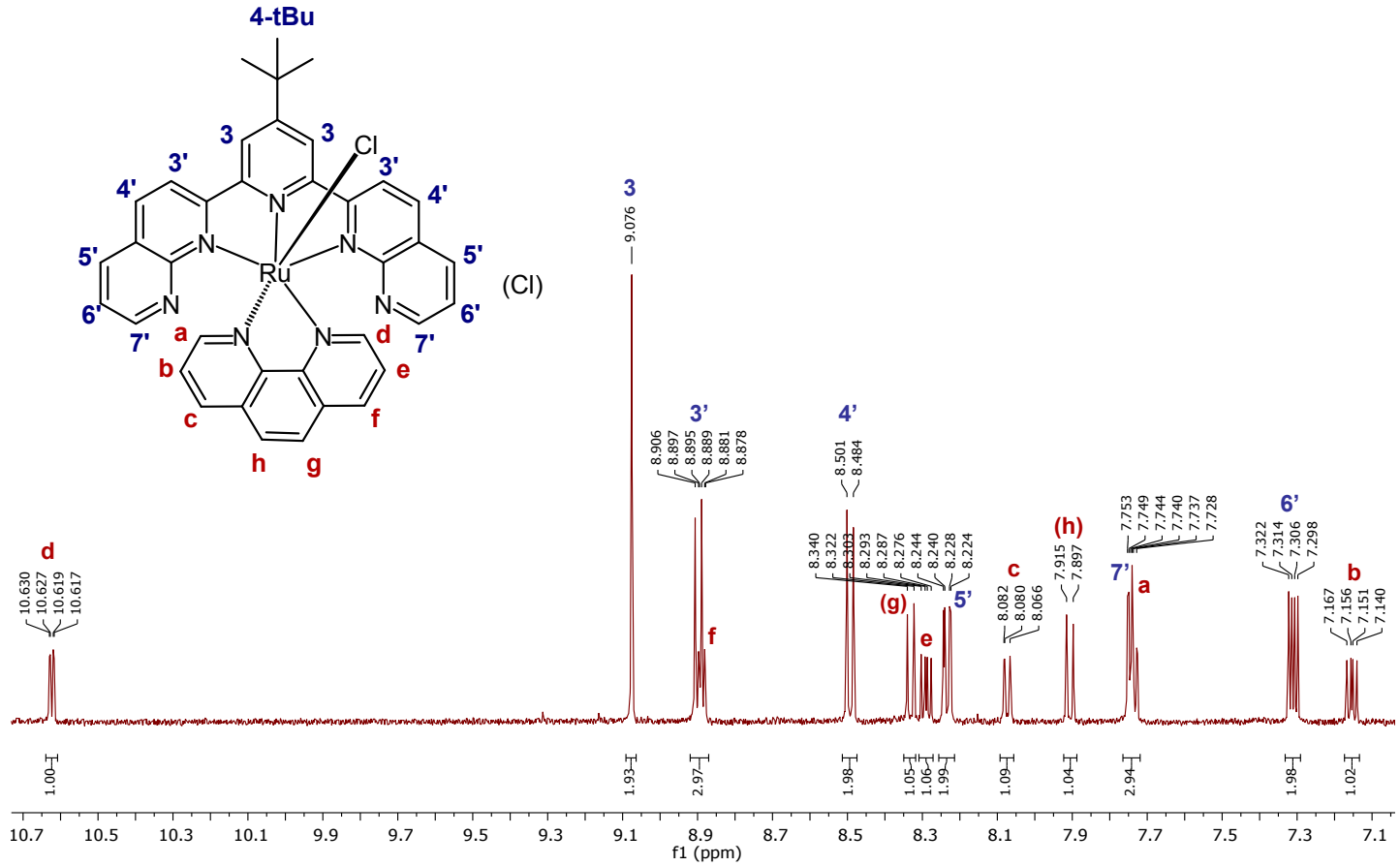

Figure S20. 500 MHz ^{1}H NMR spectrum of **7** in MeOD-d_3 at 298 K, aromatic region.

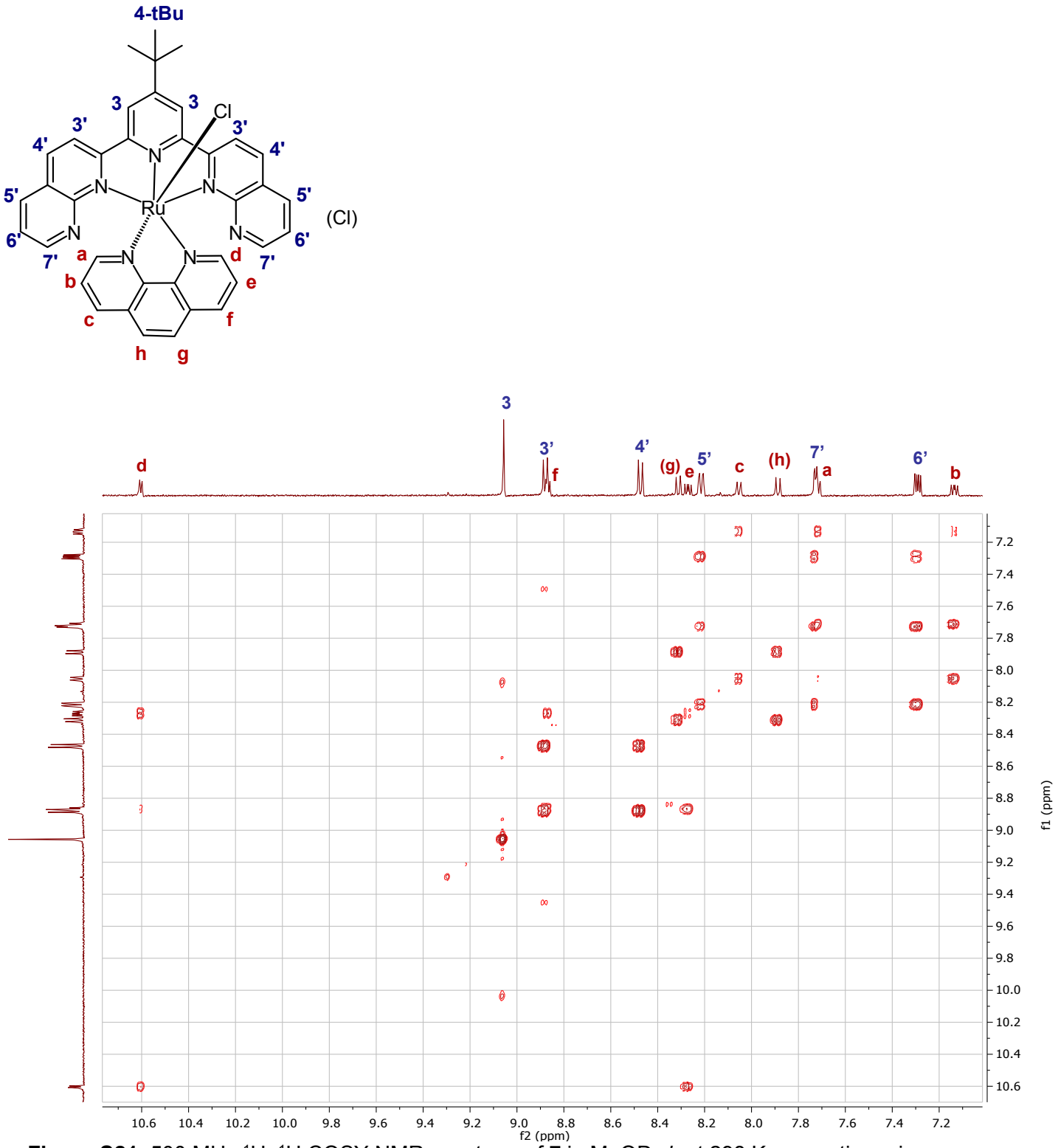

Figure S21. 500 MHz ^{1}H–^{1}H COSY NMR spectrum of **7** in MeOD-d_3 at 298 K, aromatic region.

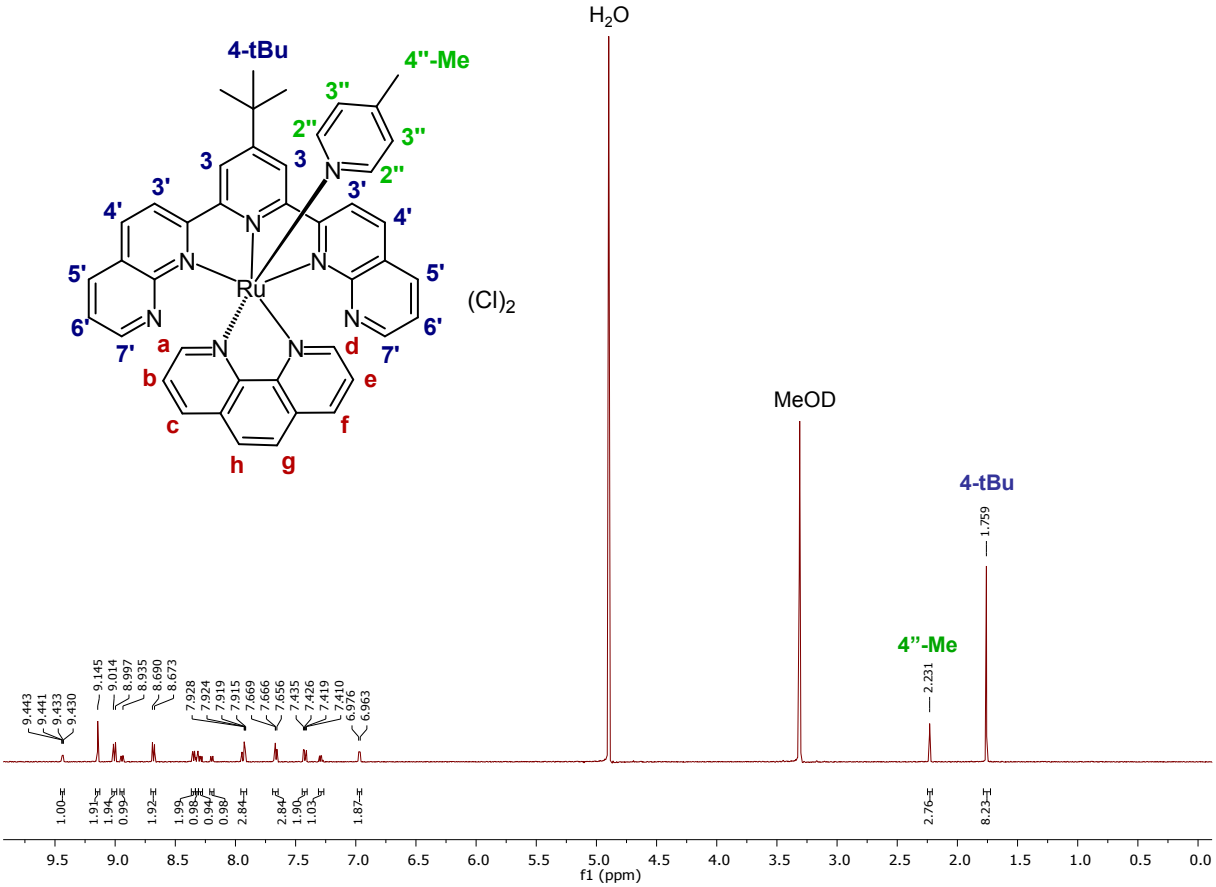

Figure S22. 500 MHz ^{1}H NMR spectrum of **8** in MeOD-d_3 at 298 K.

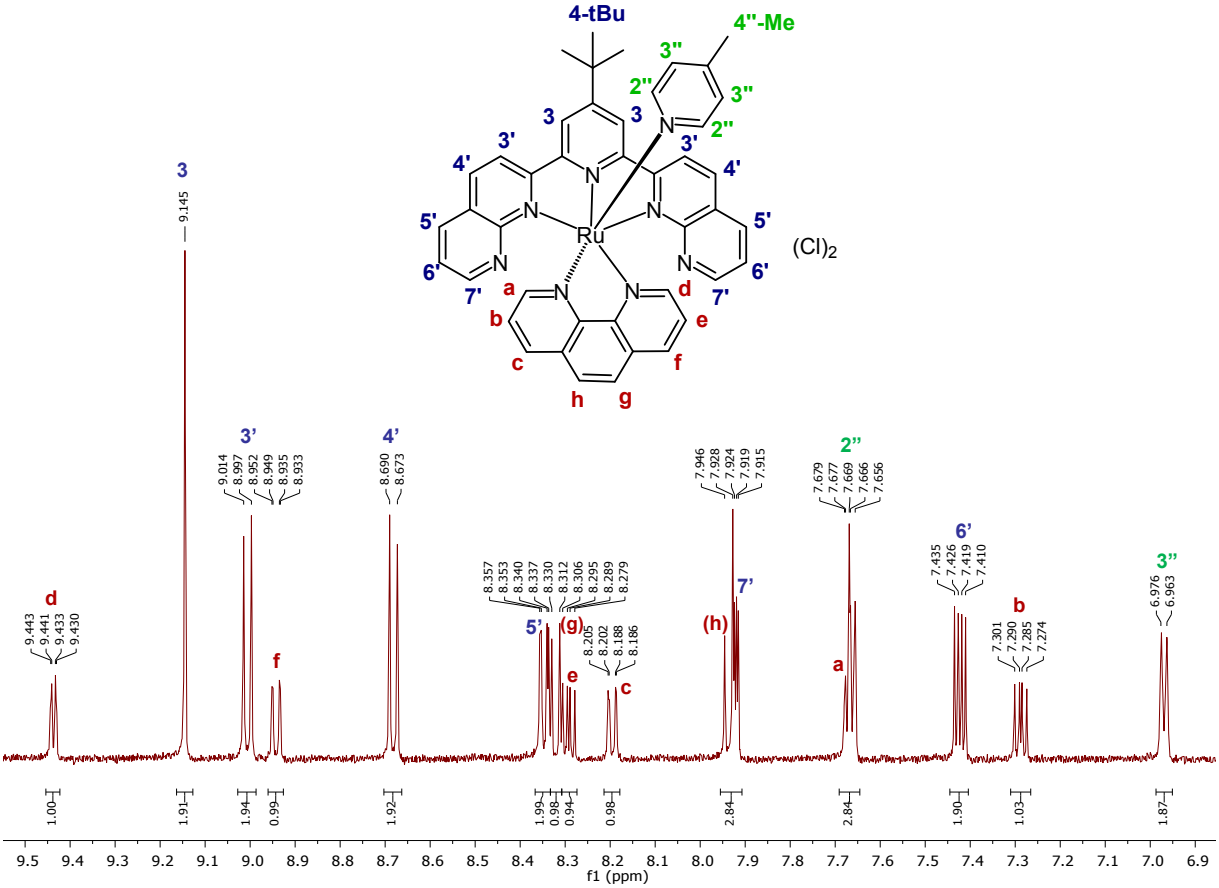

Figure S23. 500 MHz ^{1}H NMR spectrum of **8** in MeOD-d_3 at 298 K, aromatic region.

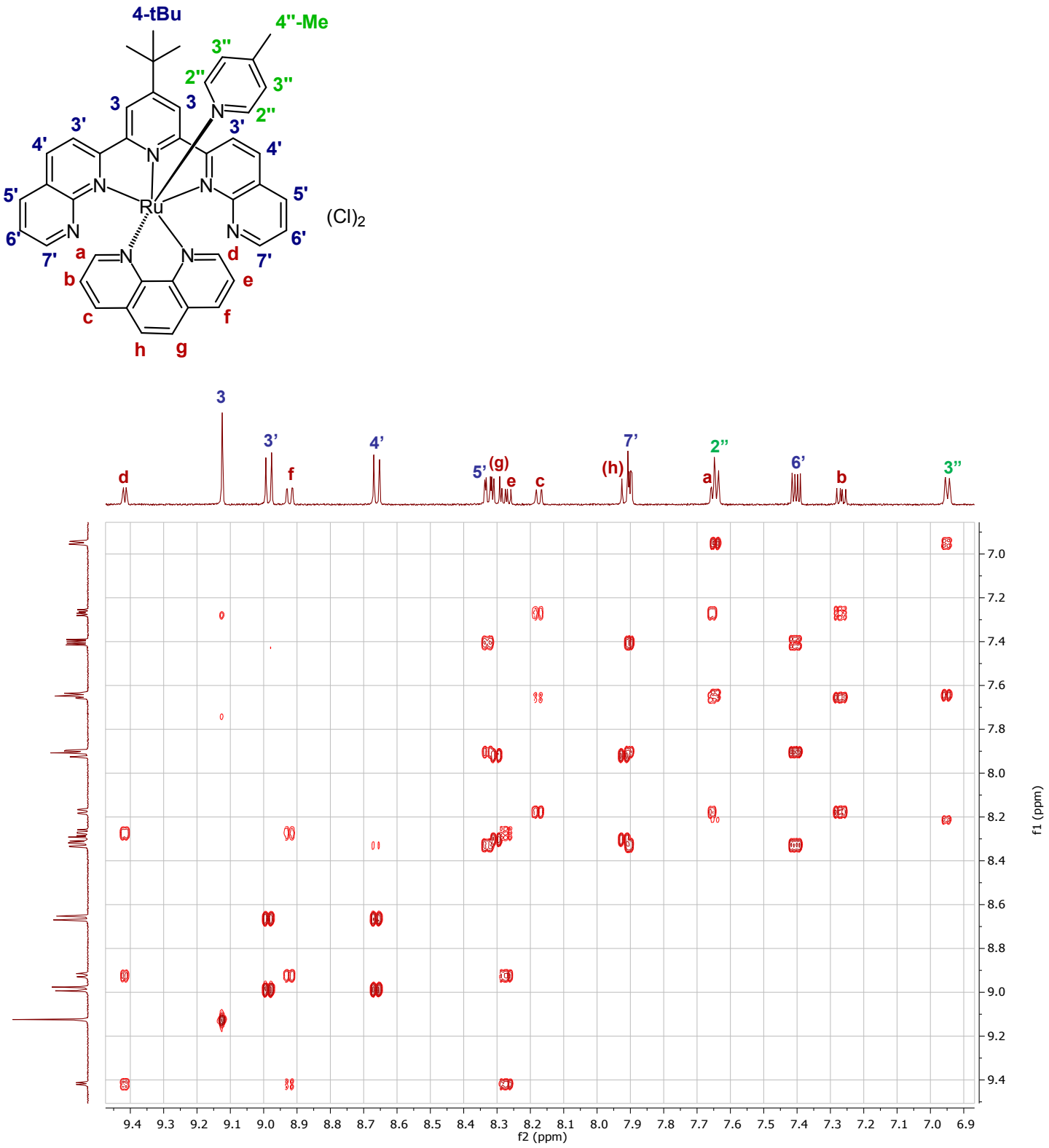

Figure S24. 500 MHz ^{1}H–^{1}H COSY NMR spectrum of **8** in MeOD-d_3 at 298 K, aromatic region.

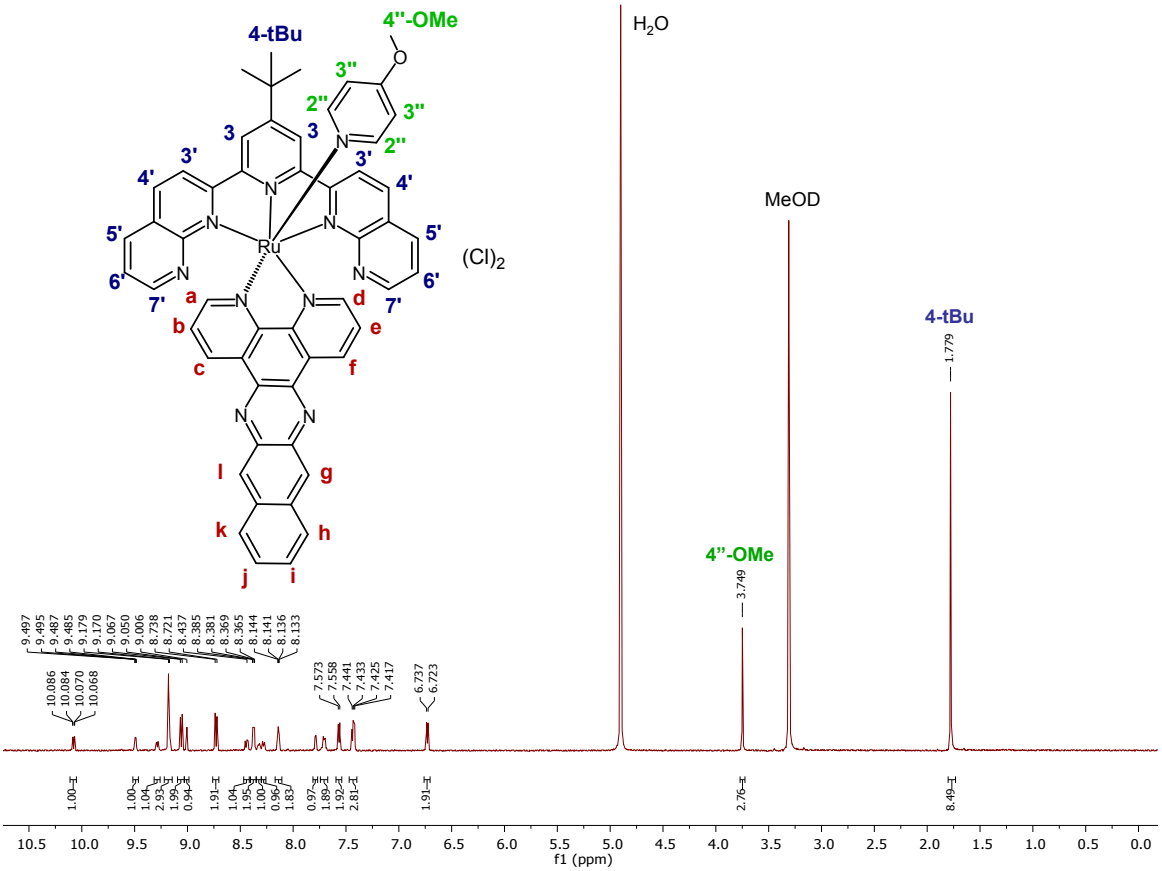

Figure S25. 500 MHz ^{1}H NMR spectrum of **9** in MeOD-d_3 at 298 K.

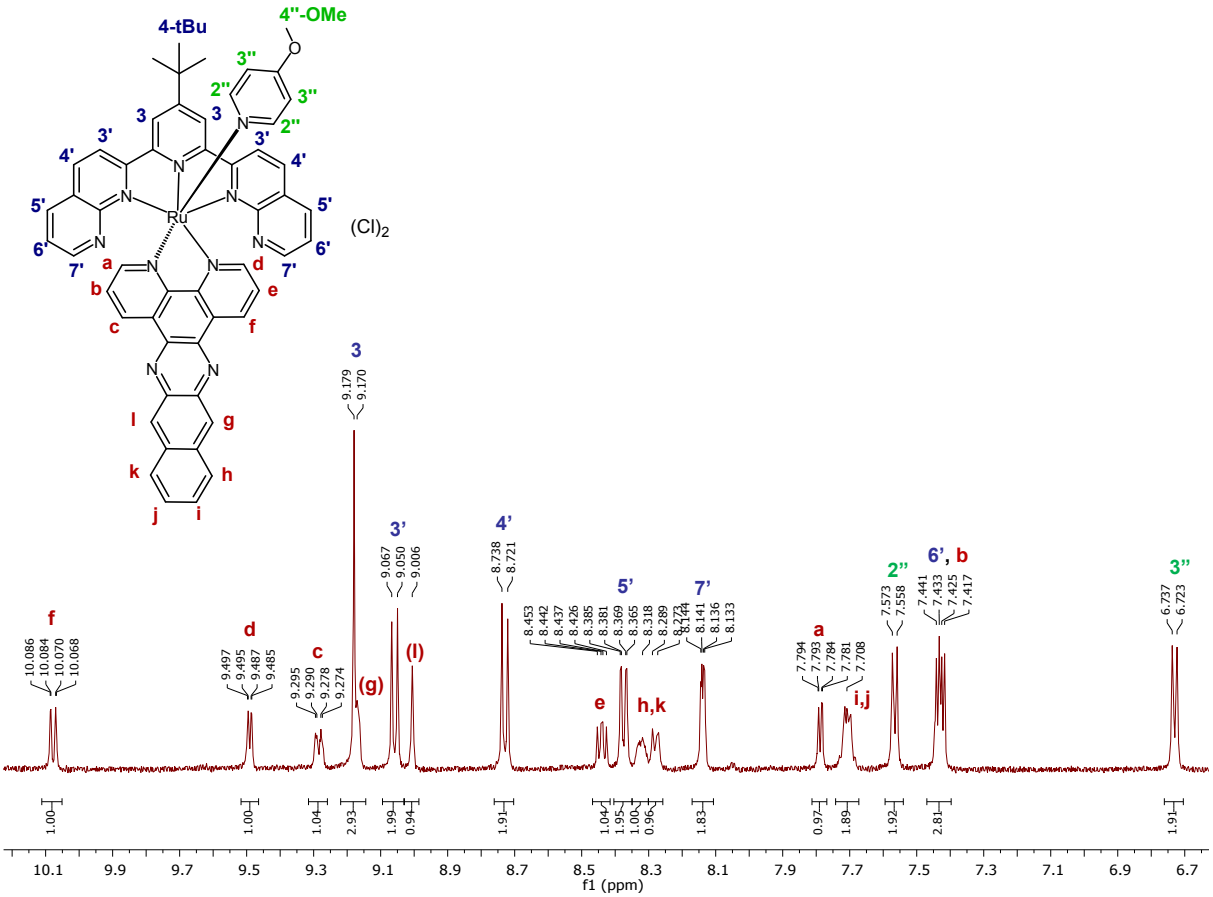

Figure S26. 500 MHz ^{1}H NMR spectrum of **9** in MeOD-d_3 at 298 K, aromatic region.

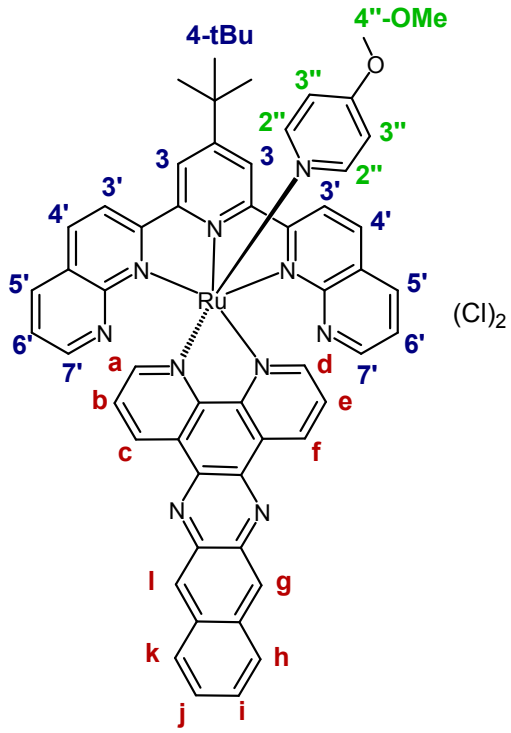

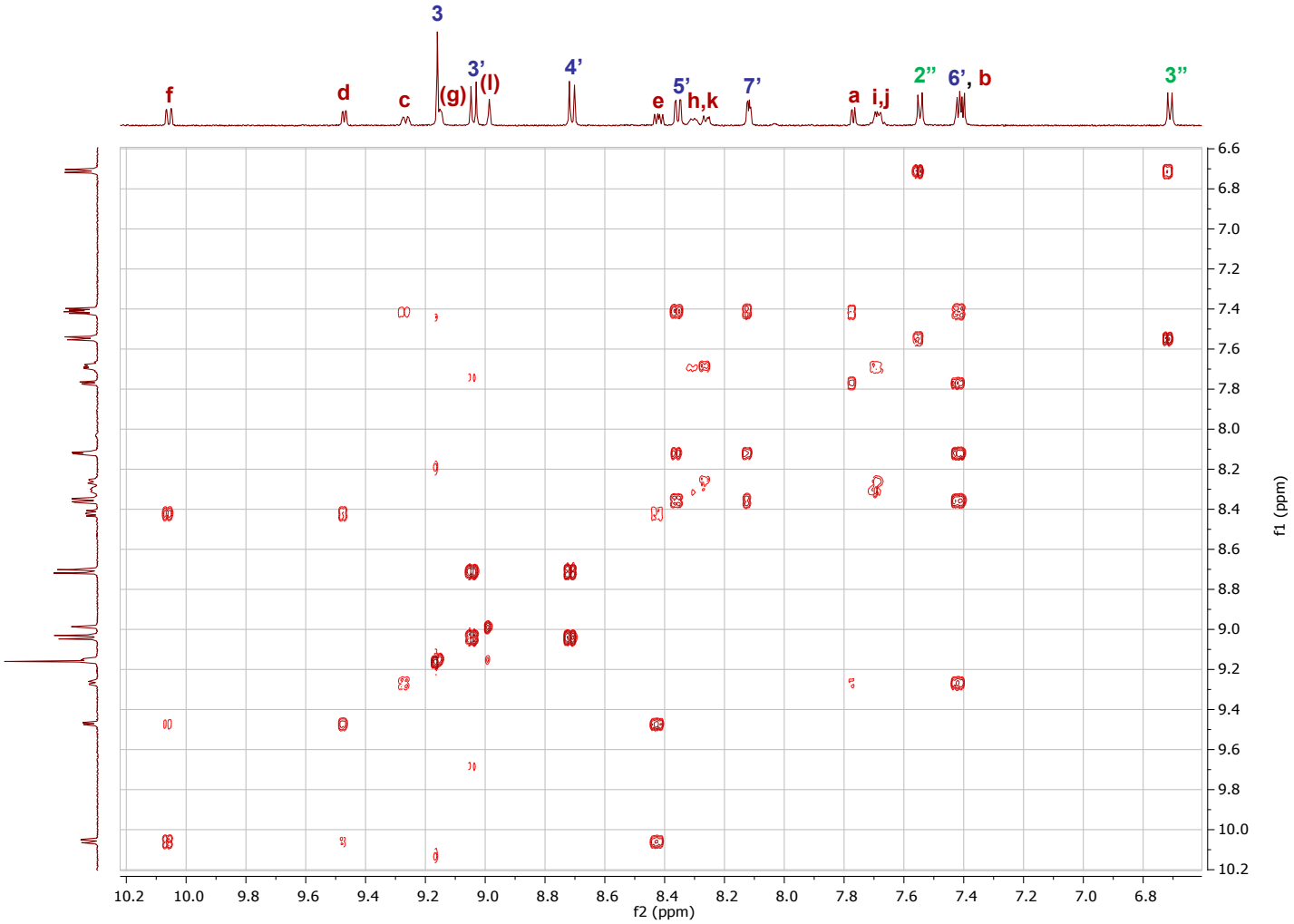

Figure S27. 500 MHz ^{1}H–^{1}H COSY NMR spectrum of **9** in MeOD-d_3 at 298 K, aromatic region.

5. Description of ^{1}H NMR assignments of Ru(II) complexes 1–9

In addition to the reasoning described below, literature sources[11,12] were used to help with the assignments. When two nonequivalent hydrogens are forming a single overlapping signal, they were denoted with a comma in between, for example: 7.43 (**6′**, **b**, m, 3H). When two nonequivalent, but very similar hydrogens, could be assigned to either of two signals, the two possible assignments were listed with a slash in between, for example: 8.36 (**h**/**k**, d, *J* = 8.0 Hz, 1H), 8.29 (**h**/**k**, d, *J* = 8.0 Hz, 1H). When two nonequivalent hydrogens in very similar electronic environments could be assigned to either of two signals but we have an assumption for which assignment is which, they were listed in parentheses, for example: see signals **(g)** and **(l)** at Figure S2.

Chart S1. Molecular Structures of Ru(II) Complexes 1–9 with labeling used for hydrogen assignments

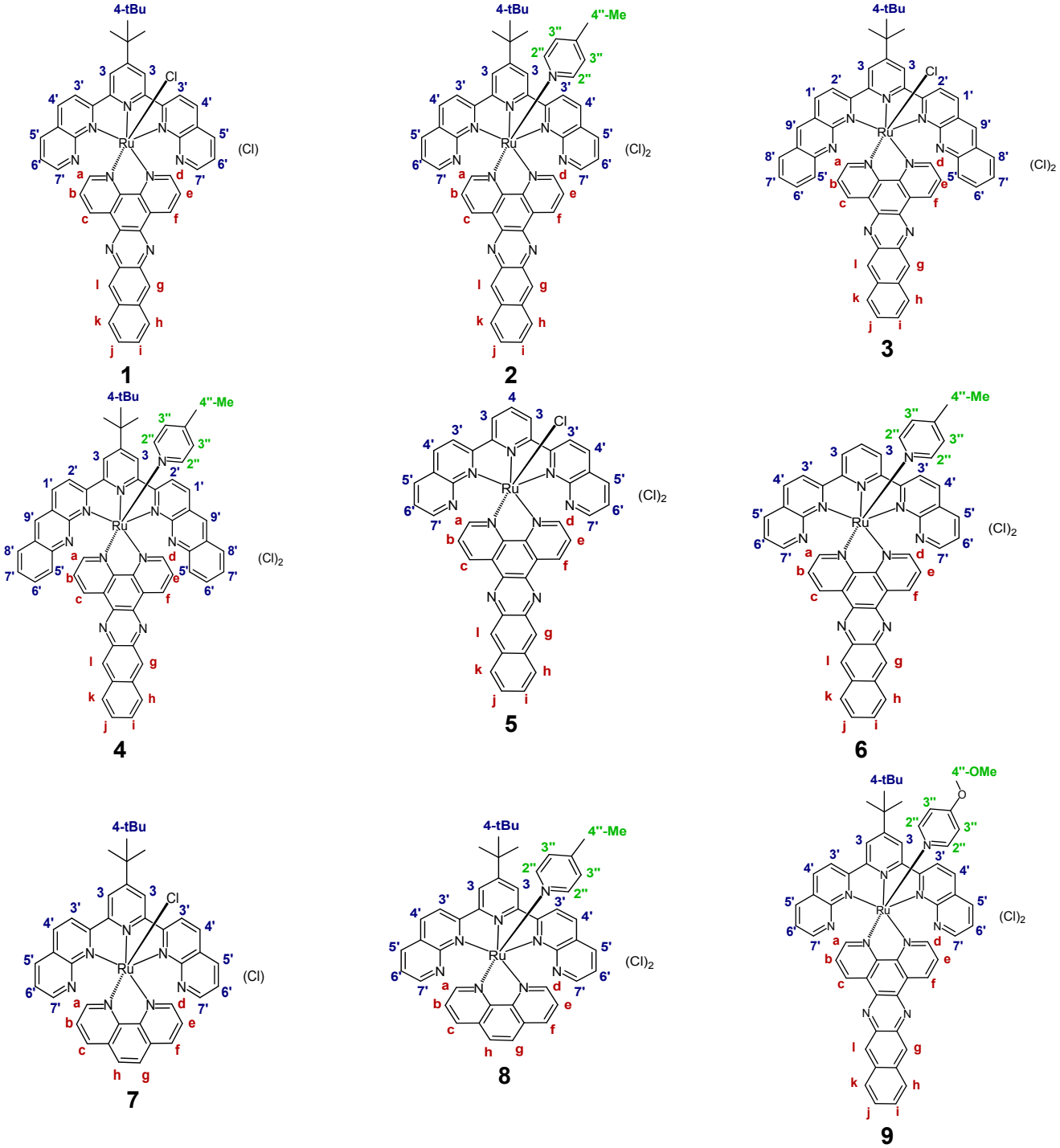

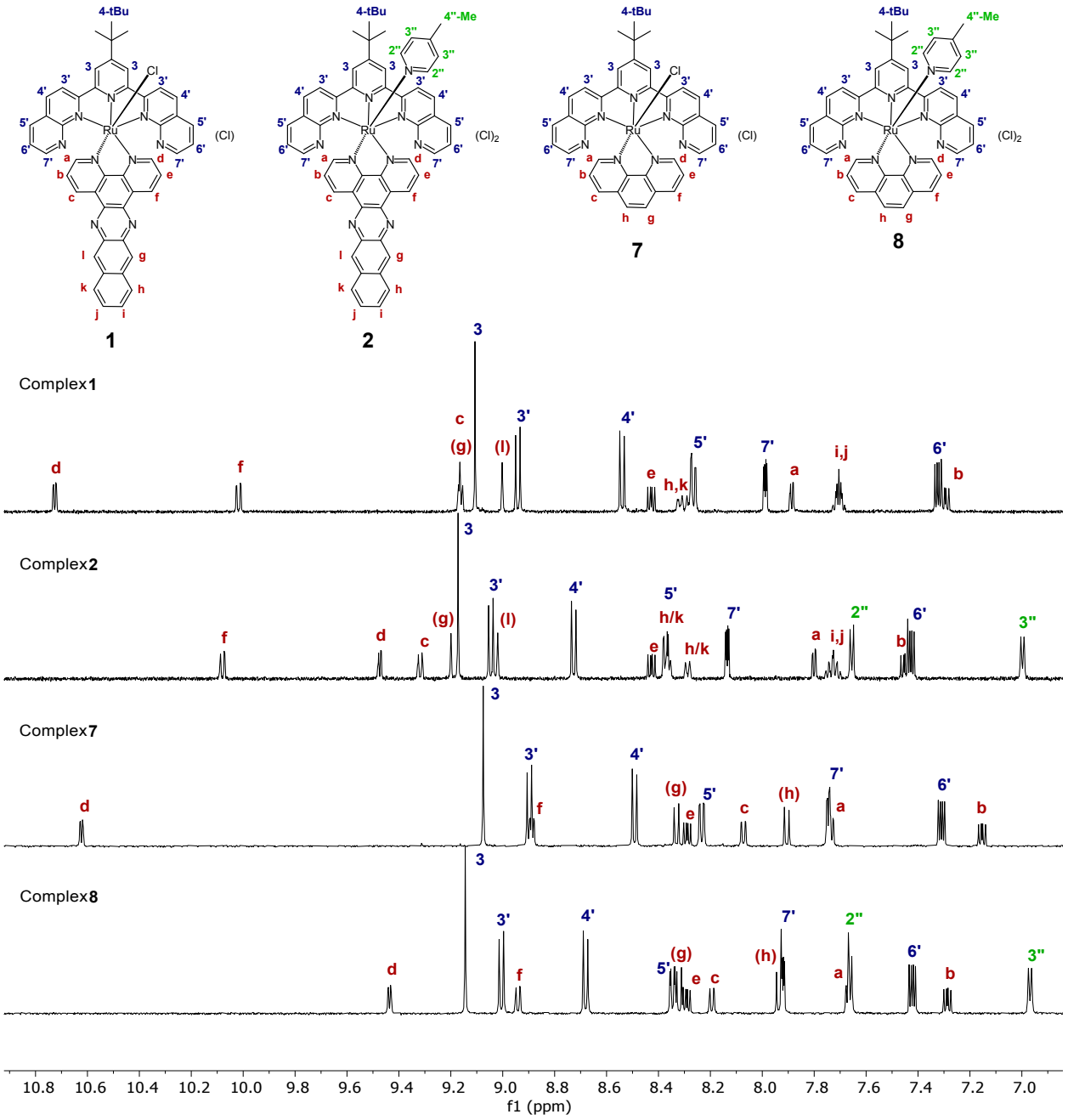

Figure S28. ^{1}H NMR spectra of Ru(II) complexes **1**, **2**, **7**, and **8** in MeOD-d_3, aromatic region.

5.1 General trends

Several general trends could be derived from the assignments of ^{1}H NMR signals from complexes **1**–**9**. All ^{1}H signals from the chromophoric ligands (tpbn, tpbbn, dnp) integrated as 2 hydrogens each, which indicates that the chromophoric ligands were symmetrical relative to the other parts of the complex. The observed chemical shifts of the hydrogens were strongly influenced by the presence of both bonding and nonbonding electronegative nitrogens present in the ligand. The magnitude of the nitrogen's deshielding effect was based on its relative positioning to each hydrogen. For complexes with naphthyridine-based chromophoric ligands tpbn and dnp (complexes **1**, **2**, **5**–**9**), the relative chemical shifts for hydrogens followed the same pattern in each complex: **3** > **3′** > **4′** > **4** > **5′** > **7′** > **6′** in MeOD-d_3; hydrogen in position **4** was only present in complexes **5** and **6**, while for all other complexes this position was occupied by a ***t*-Bu** group. The most downfield hydrogen of all chromophoric ligand hydrogens was **3** (chemical shift ranging 9.08–9.18 ppm), which is positioned on the central

pyridine ring of the ligand and appeared as a characteristic singlet (*s*) in complexes **1**, **2**, and **9**, or as a doublet (*d*) that coupled with **4** in complexes **5** and **6**. Hydrogens **3′** and **4′** were the next most downfield and occurred as doublets (*d*) that only coupled with each other. Based on the assumption that proton **3** (9.08–9.18 ppm) and **3′** have similar environments and would be closer in chemical shift than **3** and **4′**, hydrogen **3′** was assigned as the more downfield *d* of the two (8.81–9.06 ppm) and **4′** as the more upfield *d* of the two (8.49–8.73 ppm). When hydrogen **4** was present, it appeared as a characteristic triplet (*t*) at chemical shifts 8.38–8.51 ppm, upfield from **3**, **3′** and **4′** and downfield from **5′**, **6′**, and **7′**. The rest of the hydrogens from the chromophoric ligand (**5′**, **6′**, **7′**) appeared as doublets of doublets (*dd*) that coupled with each other. Hydrogen **6′** appeared as the most upfield *dd* in this spin system (7.31–7.44 ppm) and the most upfield of the ligands. It was clearly distinguished from *dd* **5′** and **7′** as the one with the largest second *J*-value. Hydrogen **5′** was assigned as the most downfield *dd* of the **5′**-**6′**-**7′** spin system (8.23–8.37 ppm), and **7′** was assigned as a *dd* (7.75–8.15 ppm) in between **5′** and **6′**, based on the observed *J*-values and the assumption that $J_{5'6'} > J_{7'6'}$.

For complexes with the benzonaphthyridine-based chromophoric ligand tpbbn (complexes **3** and **4**), the relative chemical shifts for hydrogens of the tpbbn followed similar patterns: **3** > **2′** > **9′** > **1′** > **5′** > **7′** > **6′** > **8′** for **3** in DMSO-d_6 (relatively poor solubility in methanol) and **3** > **9′** > **2′** > **1′** > **5′** > **7′** > **6′** > **8′** for **4** in MeOD-d_3. As for the complexes with naphthyridine-based chromophoric ligands, the most downfield hydrogen was **3** (9.28–9.34 ppm), which is positioned on the central pyridine ring of the ligand. The most upfield hydrogens were **6′** (7.50–7.53 ppm) and **8′** (6.75–7.01 ppm), which are located on the distal phenyl ring of tpbbn (Figures S7–S12).

The monodentate ligand (L) that occupies the axial position in complexes **1**–**9** (Cl^-, 4-pic, or 4-mp) made all hydrogens from the NN ligand (dppn, phen) magnetically inequivalent, with one side of the bidentate ligand (NN) facing the same side as L and another pointing away from L. In all complexes (**1**–**9**) it was observed that hydrogens on the NN ligand that were facing the same side as L were typically positioned more downfield (deshielded by L) than similarly-positioned hydrogens on the side that was pointing away from L.

For all dppn-containing complexes (**1**–**6**, **9**), all ^{1}H signals from the NN ligand dppn (**a**, **b**, **c**, **d**, **e**, **f**, **g**, **h**, **i**, **j**, **k**, **l**) were magnetically inequivalent due to the presence of L, with one side of dppn facing the same side as L (**d**, **e**, **f**, **g**, **h**, **i**) and the other pointing away from L (**a**, **b**, **c**, **l**, **k**, **j**). For all dppn-containing complexes (**1**–**6**, **9**), the relative chemical shifts for hydrogens on dppn followed very similar patterns: **d**, **f** > **c**, **g**, **l** > **e** > **h**, **k** > **a** > **i**, **j** > **b**. Hydrogens **d**–**f**, which are spatially the closest to L, were affected the most by deshielding due to L. At closest proximity, the observed deshielding effect caused by L was strongest with Cl^- (which is to be expected due to its electronegativity) and was attenuated, but still apparent, for 4-pic and 4-mp. Due to its close proximity to L, the chemical shift of hydrogen **d** was most strongly affected by the presence of L, ranging from 9.47-10.82 ppm across the **1**–**6**, **9** series. Hydrogen **d** was deshielded relative to **a** by almost 3 ppm when L was Cl^-, and by ~1.7–1.9 ppm when L was 4-pic or 4-mp. Hydrogens **e** and **f** are still relatively close to L and were deshielded by L as well, but less significantly than **d**; due their increased distance from L, the strength of the deshielding effect was approximately equal for Cl^-, 4-pic, or 4-mp. Hydrogen **e** was deshielded relative to **b** by ~1.1–1.4 ppm when L is Cl^-, and by ~1.0–1.4 ppm when L is 4-pic or 4-mp. Hydrogen **f** was deshielded relative to **c** by ~0.9–1.3 ppm when L is Cl^-, and by a similar ~0.8–1.2 ppm when L is 4-pic or 4-mp. As a result, in the complexes with Cl^- in the axial position (**1**, **3**, **5**), hydrogen **d** appeared the most downfield (10.73–10.82) followed by hydrogen **f** (10.02–10.32). In the complexes with 4-pic (**2**, **4**, **6**) or 4-mp (**9**) in the axial position, hydrogen **f** appeared the most downfield (10.08–10.46), followed by hydrogen **d** (9.47–9.74).

Hydrogen **f** appeared more downfield than **e** due to it being in the *para*- position relative to the nitrogen coordinated to Ru and due to the spatial proximity of the non-coordinated nitrogen on dppn. Hydrogen **b**'s signal appeared very similar to that of proton **e** in terms of multiplicity and *J*-values (both are *dd* with J_1 = ~8 Hz and J_2 = ~5 Hz), but **b** (7.27–7.45 ppm) was much more upfield than **e** (8.43–8.83 ppm) due to the absence of deshielding effect from L. The assignments for hydrogens **a** and **c** were derived from their coupling to **b**, observed by ^{1}H–^{1}H COSY NMR. Hydrogens **b** and **e**, which are in the *meta*-position relative to the Ru-coordinated nitrogen, were the most upfield among **a**-**b**-**c** and **d**-**e**-**f**, with **c** and **d** being the most downfield signals in their respective spin systems. In the absence of L's influence, proton **a** (7.79–7.96 ppm), which is in the *ortho*-position, was shielded by Ru[11] and appeared more upfield than **c** (8.99–9.32 ppm), which is in the *para*-position relative to the Ru-coordinated nitrogen and was consequently not shielded by Ru. While **d** was shielded by Ru as much as **a**, spatial proximity to L affected its chemical shift so that it appeared more downfield than **f** when L is Cl^-. However, once L is 4-pic or 4-mp, the chemical shift of **d** shifted less downfield than those by Cl^-. With the shielding effect of Ru on proton **d** still in place, proton **f** (*para*-position) appeared more downfield than proton **d** (*ortho*-position)

just like proton **c** (*para*-position) appeared more downfield than proton **a** (*ortho*-position). Another factor influencing the chemical shift of **f** and **c** was spatial proximity to the non-coordinated nitrogen from dppn, which strongly exacerbated the deshielding effect. Hydrogens **g** and **l** appeared as singlets that integrated as 1 proton each. Because it is assumed that hydrogens on the side of dppn that are facing L (**d**–**i**) would be deshielded, **g** was assigned as being slightly more downfield (9.14–9.38 ppm) than **l** (8.91–9.05 ppm). Hydrogens on different sides of dppn that are more distant from L became more and more similar by chemical shifts, with **h** and **k** signals observed to be very close to each other around ~8.3 ppm and **i** & **j** overlapping to form one multiplet at ~7.7 ppm.

In the phen-containing complexes (**7**, **8**), all ^{1}H signals from the phen ligand (**a**–**g**) were magnetically inequivalent, as observed for the ^{1}H signals from the dppn ligand in the dppn-containing complexes (**1**–**6**, **9**). The chemical shifts for hydrogens of the phen ligand followed the same pattern in both complexes **7** (L = Cl) and **8** (L = 4-pic): **d** > **f** > **g** > **e** > **c** > **h** > **a** > **b**. Hydrogen **d** appeared the most downfield in complexes **7** (L = Cl^{-}) and **8** (L = 4-pic). Chemical shifts of hydrogen **d** in complex **7** (10.62 ppm) *vs* in complex **8** (9.44 ppm) were significantly different due to a stronger deshielding of **d** in **7** by Cl^{-} than **d** in **8** by 4-pic — similar to what was observed for dppn-containing complexes **1–6**, **9**. While hydrogen **d** appeared the most downfield in dppn-containing complexes with Cl^{-} (**1**, **3**, **5**), hydrogen **f** is the one that appeared the most downfield in dppn-containing complexes with 4-pic or 4-mp (**2**, **4**, **6**, **9**). Hydrogen **f** appeared at ~8.9 ppm in complexes **7** and **8** (phen, L = Cl^{-}), which was significantly more upfield from 10.02–10.46 ppm where it appeared in dppn-containing complexes **1, 3, 5** (L = Cl^{-}) and **2**, **4**, **6**, **9** (L = 4-pic or 4-mp). This difference outlines the effect of spatial proximity of the non-coordinated nitrogen from dppn on hydrogen **f**, as the proximity to this nitrogen significantly deshielded **f**. Since phen does not have a non-coordinated nitrogen analogous to that of dppn, the chemical shift for **f** was moved upfield in phen-containing complexes **7** and **8** when compared to that of **f** in dppn-containing complexes **1–6**, **9**. The same effect was responsible for proton **c** appearing more upfield in complexes **7** and **8** (~8.1 ppm) than in complexes **1–6**, **9** (8.99–9.32 ppm). Protons **h** and **g** in complexes **7** and **8** formed a two-spin system, which was identified by correlations observed with ^{1}H–^{1}H COSY NMR, with **g** assigned as the more downfield of the two (~8.3 ppm) and **h** assigned as the more upfield of the two (~7.9 ppm) based on the assumption that protons from the side of phen facing L appear more downfield.

In the complexes with 4-pic or 4-mp (**2**, **4**, **6**, **8**, **9**), aromatic ^{1}H signals **2″** and **3″** from 4-pic or 4-mp were present. Both **2″** and **3″** integrated as 2 hydrogens each (due to the symmetry of the complex) and were picked out as a *d* that only coupled with each other. **2″** was assigned as the more downfield *d* of the two (7.56–7.79 ppm) and **3″** as the more upfield *d* of the two (6.73–7.00 ppm) based on the assumption that the one in *ortho*-position to nitrogen (**2″**) would appear more downfield. Overall, the spin system of **2″**-**3″** resembles the spin system **3′**-**4′**, as each appeared as a pair of doublets. However, it is characteristic of 4-pic protons such as **2″** and especially **3″** to appear upfield relative to other polypyridyl protons, such as that of tpbn, tppbn, dnp and dppn, which makes **2″**-**3″** and **3′**-**4′** spin systems easy to distinguish.

The ***t*-Bu** group from tpbn and tpbbn (~1.8 ppm), the methyl group from 4-pic (~2.2 ppm) and the methoxy group from 4-mp (3.75 ppm) all gave rise to characteristic singlets (*s*) that are clearly observed in the aliphatic region of the spectra and are easily assigned (see Figures S1–S27).

A 2D ^{1}H–^{1}H ROESY experiment was carried out for the related **4-pic**- and **tpbn**-containing Ru(II) complex, which revealed characteristic through-space couplings for the following hydrogens: **3** with **3′** ; **4’** with **5’** ; **3** with **4-tBu** ; **3″** with **4″-Me** ; and equivalent position of **d** with **2″**, and confirmed our assumptions for the assignments of **3′** *vs* **4’**, **5′** *vs* **7’**, and **2″** *vs* **3″**.[13]

Complex **1**

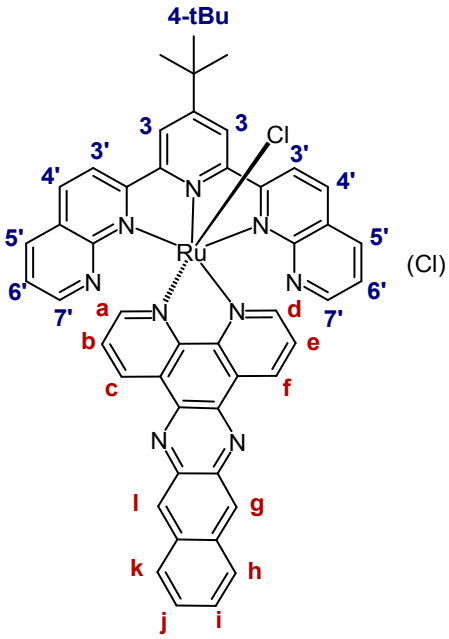

^{1}H NMR (MeOD-d_3, 500 MHz): δ 10.73 (**d**, dd, J_1 = 5.5 Hz, J_2 = 1.5 Hz, 1H), 10.02 (**f**, dd, J_1 = 8.0 Hz, J_2 = 1.5 Hz, 1H), 9.16 (**g**, s, 1H), 9.16 (**c**, dd, J_1 = 8.0 Hz, J_2 = 1.5 Hz, 1H), 9.11 (**3**, s, 2H), 9.00 (**l**, s, 1H), 8.94 (**3′**, d, J = 8.5 Hz, 2H), 8.54 (**4′**, d, J = 8.5 Hz, 2H), 8.43 (**e**, dd, J_1 = 8.0 Hz, J_2 = 5.5 Hz, 1H), 8.30 (**h**, **k**, m, 2H), 8.27 (**5′**, dd, J_1 = 8.0 Hz, J_2 = 2.0 Hz, 2H), 7.99 (**7′**, dd, J_1 = 4.5 Hz, J_2 = 2.0 Hz, 2H), 7.89 (**a**, dd, J_1 = 5.5 Hz, J_2 = 1.5 Hz, 1H), 7.71 (**i**, **j**, m, 2H), 7.32 (**6′**, dd, J_1 = 8.0 Hz, J_2 = 4.5 Hz, 2H), 7.30 (**b**, dd, J_1 = 8.0 Hz, J_2 = 5.5 Hz, 1H), 1.80 (**4-tBu**, s, 9H).

*Hydrogens from **tpbn***: All hydrogen signals from the chromophoric ligand **tpbn** (**3**, **3′**, **4′**, **5′**, **6′** and **7′**) integrate as 2 hydrogens each, since **tpbn** is positioned symmetrically relative to the other parts of the complex. As the only singlet (*s*) among **tpbn** hydrogens, **3** was assigned as a *s* at 9.11 ppm. Both **3′** and **4′** were picked out as doublets (*d*) that only couple with each other (coupling observed at ^{1}H–^{1}H COSY NMR). **3′** was assigned as the more downfield *d* of the two (8.94 ppm) and **4′** as a more upfield *d* of the two (8.54 ppm), based on the assumption that hydrogen **3** (9.11 ppm) and **3′** (8.94 ppm) have similar environments and would be closer by chemical shifts than **3** and **4′**. Among the spin system **5′**-**6′**-**7′** (correlations with each other observed with ^{1}H–^{1}H COSY NMR), all three are *dd* but **6′** is distinguished as a *dd* with largest second *J*-value among the three (7.32 ppm, dd, J_1 = 8.0 Hz, J_2 = 4.5 Hz). **5′** is assigned as a more downfield *dd* at 8.27 ppm ($J_{5'6'}$ = 8.0 Hz, $J_{5'7'}$ = 2.0 Hz), and **7′** is assigned as a more upfield *dd* at 7.99 ppm ($J_{7'6'}$ = 4.5 Hz, $J_{7'5'}$ = 2.0 Hz), based on the observed *J*-values and the assumption that $J_{5'6'} > J_{7'6'}$. The singlet at 1.80 ppm integrates as 9 hydrogens and is assigned to the **4-tBu** group.

*Hydrogens from **dppn**:* The negatively-charged **chloride** ligand is occupying the axial position and makes all ^{1}H from PDT ligand **dppn** (**a**, **b**, **c**, **d**, **e**, **f**, **g**, **h**, **i**, **j**, **k**, **l**) magnetically inequivalent, with one side of **dppn** facing the same side as **chloride** (**d**, **e**, **f**, **g**, **h**, **i**) and the other pointing away from the **chloride** (**a**, **b**, **c**, **l**, **k**, **j**). Hydrogens **d–f**, which are spatially closest to the **chloride**, are affected by it the most, causing chemical shifts that are significantly more downfield than they would be in the absence of **chloride**. Hydrogen **d** was assigned as the most downfield hydrogen at 10.73 ppm, because of its proximity to the **chloride**. Based on this assignment, J_{de} is 5.5 Hz. Hydrogens **e** and **f** were derived from their coupling to **d**, observed with ^{1}H–^{1}H COSY NMR. Both **e** and **f** appear as doublets of doublets (*dd*), with hydrogen **e** being assigned to the *dd* exhibiting a larger second *J*-value than **f** (**e**, dd, J_{ef} = 8.0 Hz, J_{ed} = 5.5 Hz; **f**, dd, J_{ef} = 8.0 Hz, J_{fd} = 1.5 Hz). With this assignment, J_{ed} = 5.5 Hz which matches the observed J_{de} from the hydrogen **d** assignment. Hydrogen **f** (10.02 ppm) appears more downfield than **e** (8.43 ppm), due to being in the *para*- position relative to the nitrogen that is coordinated to Ru and due to the spatial proximity to the non-coordinated nitrogen on **dppn**. Hydrogen **b** was assigned as the signal that appears very similar to that of hydrogen **e** in terms of multiplicity and *J*-values (both are *dd* with J_1 = 8.0 Hz and J_2 = 5.5 Hz), but **b** (7.30 ppm) is much more upfield than **e** (8.43 ppm) due to the absence of **chloride** near **b**. Hydrogens **a** and **c** were derived from their coupling to **b**, observed by ^{1}H–^{1}H COSY NMR. Both **a** and **c** appear as *dd*, and assignments were made based on the observed *J*-values and the assumption that $J_{ab} < J_{cb}$.

Hence, **a** was assigned as a dd at 7.89 ppm (dd, J_{ab} = 5.5 Hz, J_{ac} = 1.5 Hz) and **c** as a *dd* at 9.16 ppm (J_{cb} = 8.0 Hz, J_{ca} = 1.5 Hz). After hydrogens **a**, **b**, **c**, **d**, **e**, and **f** were assigned, the following trends were observed: hydrogens **b** and **e**, which are in the *meta*-position relative to Ru-coordinated nitrogen, are the most upfield among **a**-**b**-**c** and **d**-**e**-**f**, with **c** and **d** being the most downfield signals in their respective spin systems. In the absence of **chloride** influence, hydrogen **a**, which is in the *ortho*-position, is shielded by Ru (see ref. 1) and appears more upfield than **c**, which is in the *para*-position relative to the coordinating nitrogen and is not shielded by Ru. While **d** is shielded by Ru as much as **a**, spatial proximity to **chloride** affects its chemical shift so that it appears more downfield than **f**. Hydrogens **g** and **l** were assigned as singlets that integrate as 1 hydrogen each, with the assumption that **g** appear slightly more downfield (9.16 ppm) than **l** (9.00 ppm), based on the assumption that hydrogens from the side of **dppn** that is facing **chloride** appear more downfield. Hydrogens on different sides of **dppn** that are further away from **chloride** become more similar by chemical shifts, with **h** and **k** observed very close to each other at 8.30 ppm and **i** & **j** overlapping to form one multiplet at 7.71 ppm.

Complex **2**

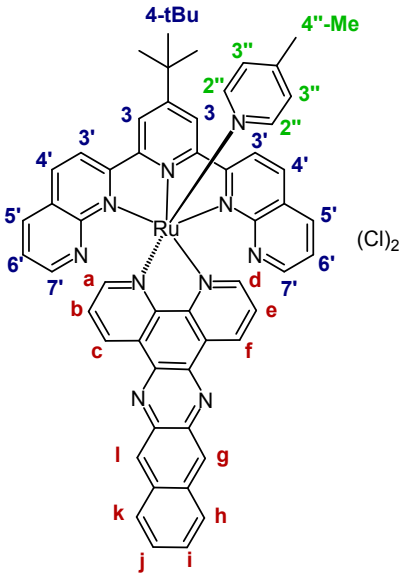

^{1}H NMR (MeOD-d_3, 500 MHz): δ 10.08 (**f**, dd, J_1 = 8.5 Hz, J_2 = 1.5 Hz, 1H), 9.47 (**d**, dd, J_1 = 5.5 Hz, J_2 = 1.5 Hz, 1H), 9.32 (**c**, dd, J_1 = 8.0 Hz, J_2 = 1.0 Hz, 1H), 9.20 (**g**, s, 1H), 9.17 (**3**, s, 2H), 9.05 (**3′**, d, J = 8.5 Hz, 2H), 9.02 (**l**, s, 1H), 8.73 (**4′**, d, J = 8.5 Hz, 2H), 8.43 (**e**, dd, J_1 = 8.5 Hz, J_2 = 5.5 Hz, 1H), 8.37 (**5′**, dd, J_1 = 8.0 Hz, J_2 = 2.0 Hz, 2H), 8.36 (**h**/**k**, d, J = 8.0 Hz, 1H), 8.29 (**h**/**k**, d, J = 8.0 Hz, 1H), 8.13 (**7′**, dd, J_1 = 4.0 Hz, J_2 = 2.0 Hz, 2H), 7.80 (**a**, dd, J_1 = 5.5 Hz, J_2 = 1.0 Hz, 1H), 7.72 (**i**, **j**, m, 2H), 7.65 (**2″**, d, J = 7.0 Hz, 2H), 7.45 (**b**, dd, J_1 = 8.0 Hz, J_2 = 5.5 Hz, 1H), 7.43 (**6′**, dd, J_1 = 8.0 Hz, J_2 = 4.5 Hz, 2H), 7.00 (**3″**, d, J = 6.0 Hz, 2H), 2.25 (**4″-Me**, s, 3H), 1.77 (**4-tBu**, s, 9H).

In complex **2,** all hydrogens follow the same trends as described in the ^{1}H assignments of complex **1**, except for the hydrogens **d** and **f**. In complex **1**, **d** is the most downfield hydrogen, while **f** is the most downfield hydrogen in complex **2**. Once the **chloride** ligand in the axial position is substituted with 4-picoline (**4-pic**), the chemical shift of hydrogen **d** is shifted less downfield, and with the shielding effect of Ru on hydrogen **d** still in place, hydrogen **f** (*para*-position) appears more downfield than hydrogen **d** (*ortho*-position) just like hydrogen **c** (*para*-position) appears more downfield than hydrogen **a** (*ortho*-position). When chemical shifts of hydrogen **f** in complex **1** and hydrogen **f** in complex **2** are compared, they are found to be very similar (10.02 ppm in **1** and 10.08 ppm in **2**), meanwhile the chemical shifts of hydrogen **d** are significantly different (10.73 ppm in **1** and 9.47 ppm in **2**). This confirms the assumption that the chemical shift of hydrogen **d**, which is spatially closest to the axial ligand, is significantly affected by the type of the axial ligand, while hydrogen **f**, which is further away from the axial ligand, is not very affected by the presence of the axial ligand.

In complex **2**, in addition to hydrogens from **tpbn** and ^{1}H from **dppn**, hydrogens from **4-pic** are present: **2″**, **3″**, and **4″-Me**. Both **2″** and **3″** integrate as 2 hydrogens each and were picked out as *d* that only couple with each other (coupling observed at ^{1}H–^{1}H COSY NMR). **2″** was assigned as the more downfield *d* of the two (7.65

ppm) and **3″** as the more upfield *d* of the two (7.00 ppm), based on the assumption that the hydrogen in the *ortho*-position relative to nitrogen (**2″**) appears more downfield. Overall, spin system of **2″**-**3″** resembles spin system **3′**-**4′**, as each appear as a pair of doublets. However, it is characteristic of **4-pic** hydrogens such as **2″** and especially **3″** to appear upfield relative to other pyridyl hydrogens, such as that of **tpbn** and **dppn**, which makes the **2″**-**3″** and **3′**-**4′** spin systems easy to distinguish. The singlet at 2.25 ppm integrates as 3 hydrogens and is assigned to the **4″-Me** group.

Complex **3**

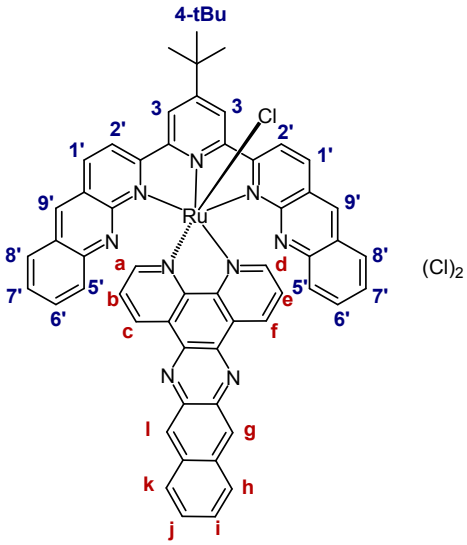

^{1}H NMR (DMSO-d_6, 700 MHz): δ 10.82 (**d**, dd, J_1 = 4.9 Hz, J_2 = 0.7 Hz, 1H), 10.32 (**f**, dd, J_1 = 8.4 Hz, J_2 = 0.7 Hz, 1H), 9.38 (**g**, s, 1H), 9.34 (**3**, s, 2H), 9.22 (**2′**, d, J = 9.1 Hz, 2H), 9.17 (**9′**, s, 2H), 9.05 (**l**, s, 1H), 8.99 (**c**, dd, J_1 = 7.7 Hz, J_2 = 0.7 Hz, 1H), 8.88 (**1′**, d, J = 9.1 Hz, 2H), 8.79 (**e**, dd, J_1 = 8.4 Hz, J_2 = 4.9 Hz, 1H), 8.44 (**h/k**, d, J = 9.1 Hz, 1H), 8.35 (**h/k**, d, J = 7.7 Hz, 1H), 8.06 (**5′**, d, J = 8.4 Hz, 2H), 7.96 (**a**, dd, J_1 = 6.3 Hz, J_2 = 1.4 Hz, 1H), 7.77 (**i/j**, dd, J_1 = 8.4 Hz, J_2 = 7.0 Hz, 1H), 7.73 (**i/j**, dd, J_1 = 7.7 Hz, J_2 = 7.0 Hz, 1H), 7.69 (**7′**, dd, J_1 = 8.4 Hz, J_2 = 7.0 Hz, 2H), 7.50 (**6′**, dd, J_1 = 8.4 Hz, J_2 = 7.0 Hz, 2H), 7.39 (**b**, dd, J_1 = 7.7 Hz, J_2 = 6.3 Hz, 1H), 6.75 (**8′**, d, J = 8.4 Hz, 2H), 1.80 (**4-tBu**, s, 9H).

In complex **3,** all hydrogens from **dppn** follow the same trends as described in the hydrogen assignments of complex **1**. Chromophoric ligand **tpbbn** has hydrogens that are similar to that of the ligand **tpbn,** with a few additional aromatic hydrogens. Hydrogens from **tpbbn** that are similar to the hydrogens from **tpbn** were assigned in a similar manner as described for complex **1** (**3** as a singlet at 9.34 ppm, **2′** and **1′** as a pair of doublets, with **2′** more downfield of the two at 9.22 ppm, and **1′** more upfield of the two at 8.88 ppm). **9′** is assigned to the singlet that integrates as 2 hydrogens (9.17 ppm) and that is not assigned as **3**. Spin system **5′**-**6′**-**7′**-**8′** is identified by correlations observed through ^{1}H–^{1}H COSY NMR. **5′** and **8′** are both doublets with identical *J*-values of 8.4 Hz; **5′** was assigned as the more downfield doublet of the two (8.06 ppm),[12] with **8′** appearing at 6.75 ppm. Hydrogens **6′** and **7′** are both doublets of doublets, and the assignments were made based on the correlations to **5′** and **8′** observed with ^{1}H–^{1}H COSY NMR. **6′** was assigned as the hydrogen at 7.50 ppm (dd, $J_{5'6'}$ = 8.4 Hz, $J_{7'6'}$ = 7.0 Hz), and **7′** was assigned as the hydrogen at 7.69 ppm (dd, $J_{8'7'}$ = 8.4 Hz, $J_{6'7'}$ = 7.0 Hz). The singlet at 1.80 ppm integrates as 9 hydrogens and is assigned to the **4-tBu** group.

Complex **4**

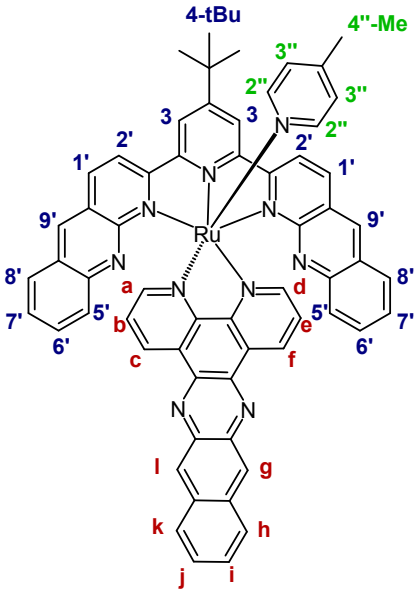

^{1}H NMR (MeOD-d_3, 700 MHz): δ 10.46 (**f**, d, J = 8.4 Hz, 1H), 9.74 (**d**, d, J = 4.9 Hz, 1H), 9.28 (**3**, s, 2H), 9.21 (**c**, d, J = 7.7 Hz, 1H), 9.18 (**g**, s, 1H), 9.13 (**9′**, s, 2H), 9.05 (**2′**, d, J = 8.4 Hz, 2H), 8.93 (**1′**, d, J = 9.1 Hz, 2H), 8.91 (**l**, s, 1H), 8.83 (**e**, dd, J_1 = 8.4 Hz, J_2 = 5.6 Hz, 1H), 8.30 (**h/k**, d, J = 8.4 Hz, 1H), 8.22 (**h/k**, d, J = 7.7 Hz, 1H), 8.02 (**5′**, d, J = 7.7 Hz, 2H), 7.88 (**a**, d, J = 5.6 Hz, 1H), 7.79 (**2″**, d, J = 7.0 Hz, 2H), 7.74 (**7′**, dd, J_1 = 8.4 Hz, J_2 = 7.0 Hz, 2H), 7.67 (**i**, **j**, m, 2H), 7.53 (**6′**, dd, J_1 = 7.7 Hz, J_2 = 7.0 Hz, 2H), 7.43 (**b**, dd, J_1 = 7.7 Hz, J_2 = 5.6 Hz, 1H), 7.01 (**8′**, d, J = 8.4 Hz, 2H), 6.97 (**3″**, d, J = 6.3 Hz, 2H), 2.22 (**4″-Me**, s, 3H), 1.81 (**4-tBu**, s, 9H).

Hydrogens in complex **4** were assigned based off of the ^{1}H assignments for complex **3**, except for the hydrogens **d** and **f**. Like in complex **2**, in complex **4** hydrogen **f** (*para*-position) appears more downfield than hydrogen **d** (*ortho*-position). In complex **4**, in addition to hydrogens from **tpbbn** and **dppn**, hydrogens from **4-pic** are present: **2″**, **3″**, and **4″-Me**. Similar to complex **2**, **2″** was assigned as a doublet at 7.79 ppm and **3″** as a doublet at 6.97 ppm. The singlet at 2.22 ppm integrates as 3 hydrogens and is assigned to the **4″-Me** group.

Complex **5**

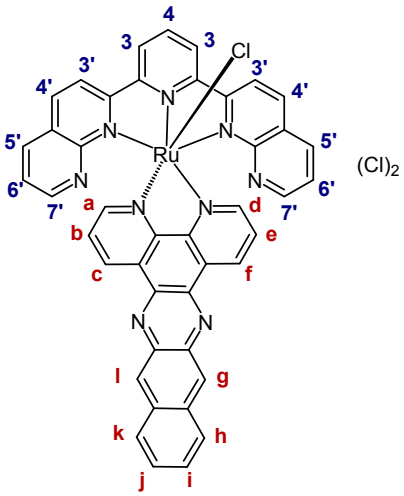

^{1}H NMR (MeOD-d_3, 700 MHz): δ 10.74 (**d**, dd, J_1 = 4.9 Hz, J_2 = 1.4 Hz, 1H), 10.03 (**f**, dd, J_1 = 8.4 Hz, J_2 = 1.4 Hz, 1H), 9.15 (**c**, dd, J_1 = 7.7 Hz, J_2 = 0.7 Hz, 1H), 9.14 (**g**, s, 1H), 9.09 (**3**, d, J = 8.4 Hz, 2H), 8.99 (**l**, s, 1H), 8.81 (**3′**, d, J = 9.1 Hz, 2H), 8.54 (**4′**, d, J = 8.4 Hz, 2H), 8.45 (**e**, dd, J_1 = 8.4 Hz, J_2 = 4.9 Hz, 1H), 8.38 (**4**, t, J =

8.4 Hz, 1H), 8.29 (**h**,**k**, m, 2H), 8.27 (**5′**, dd, J_1 = 7.7 Hz, J_2 = 1.4 Hz, 2H), 8.01 (**7′**, dd, J_1 = 4.9 Hz, J_2 = 1.4 Hz, 2H), 7.87 (**a**, dd, J_1 = 5.6 Hz, J_2 = 0.7 Hz, 1H), 7.69 (**i**, **j**, m, 2H), 7.33 (**6′**, dd, J_1 = 7.7 Hz, J_2 = 4.9 Hz, 2H), 7.27 (**b**, dd, J_1 = 7.7 Hz, J_2 = 5.6 Hz, 1H).

Hydrogens in complex **5** were assigned based off of the ^{1}H assignments for complex **1**. Since the **4-tBu** group is absent in complex **5**, hydrogen **3** that was a singlet in complex **1** appears as the doublet at 9.09 ppm (J = 8.4 Hz), and hydrogen **4** appears as the triplet at 8.38 ppm (J = 8.4 Hz).

Complex **6**

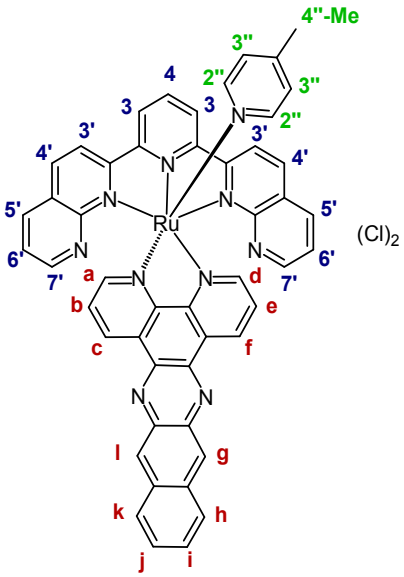

^{1}H NMR (MeOD-d_3, 500 MHz): δ 10.10 (**f**, dd, J_1 = 8.0 Hz, J_2 = 1.0 Hz, 1H), 9.50 (**d**, dd, J_1 = 5.5 Hz, J_2 = 1.5 Hz, 1H), 9.32 (**c**, dd, J_1 = 8.0 Hz, J_2 = 1.0 Hz, 1H), 9.19 (**g**, s, 1H), 9.18 (**3**, d, J = 8.5 Hz, 2H), 9.02 (**l**, s, 1H), 8.91 (**3′**, d, J = 8.5 Hz, 2H), 8.73 (**4′**, d, J = 8.5 Hz, 2H), 8.51 (**4**, t, J = 8.5 Hz, 1H), 8.44 (**e**, dd, J_1 = 8.5 Hz, J_2 = 5.5 Hz, 1H), 8.38 (**5′**, dd, J_1 = 8.5 Hz, J_2 = 2.0 Hz, 2H), 8.36 (**h**/**k**, d, J = 8.0 Hz, 1H), 8.29 (**h**/**k**, d, J = 8.0 Hz, 1H), 8.15 (**7′**, dd, J_1 = 4.5 Hz, J_2 = 2.0 Hz, 2H), 7.81 (**a**, dd, J_1 = 5.5 Hz, J_2 = 1.0 Hz, 1H), 7.72 (**i**, **j**, m, 2H), 7.65 (**2″**, d, J = 6.5 Hz, 2H), 7.44 (**b**, dd, J_1 = 8.0 Hz, J_2 = 5.5 Hz, 1H), 7.44 (**6′**, dd, J_1 = 8.0 Hz, J_2 = 4.0 Hz, 2H), 7.00 (**3″**, d, J = 6.0 Hz, 2H), 2.25 (**4″-Me**, s, 3H).

Hydrogens in complex **6** were assigned based off the ^{1}H assignments of complex **5**, except for the hydrogens **d** and **f**. Like in complex **2**, in complex **6** hydrogen **f** (*para*-position) appears more downfield than hydrogen **d** (*ortho*-position). In complex **6**, in addition to ^{1}H from **dnp** and **dppn**, ^{1}H from **4-pic** are present: **2″**, **3″**, and **4″-Me**. Similar to complex **2**, **2″** was assigned as a doublet at 7.65 ppm and **3″** as a doublet at 7.00 ppm. The singlet at 2.25 ppm integrates as 3 hydrogens and is assigned to the **4″-Me** group.

Complex **7**

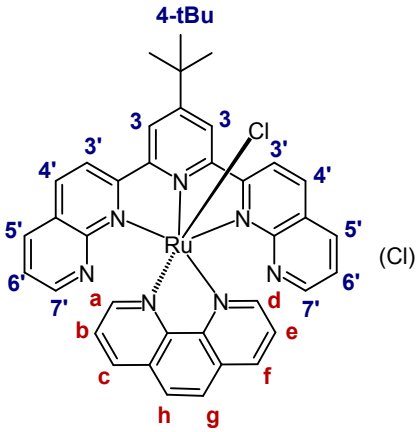

^{1}H NMR (MeOD-d_3, 500 MHz): δ 10.62 (**d**, dd, J_1 = 5.5 Hz, J_2 = 1.5 Hz, 1H), 9.08 (**3**, s, 2H), 8.90 (**3′**, d, J = 8.5 Hz, 2H), 8.89 (**f**, dd, J_1 = 8.0 Hz, J_2 = 1.5 Hz, 1H), 8.49 (**4′**, d, J = 8.5 Hz, 2H), 8.33 (**g**, d, J = 9.0 Hz, 1H), 8.29 (**e**, dd, J_1 = 8.0 Hz, J_2 = 5.5 Hz, 1H), 8.23 (**5′**, dd, J_1 = 8.0 Hz, J_2 = 2.0 Hz, 2H), 8.07 (**c**, dd, J_1 = 8.0 Hz, J_2 = 1.0 Hz, 1H), 7.90 (**h**, d, J = 9.0 Hz, 1H), 7.75 (**7′**, dd, J_1 = 4.5 Hz, J_2 = 2.0 Hz, 2H), 7.73 (**a**, dd, J_1 = 5.5 Hz, J_2 = 1.0 Hz, 1H), 7.31 (**6′**, dd, J_1 = 8.0 Hz, J_2 = 4.0 Hz, 2H), 7.15 (**b**, dd, J_1 = 8.0 Hz, J_2 = 5.5 Hz, 1H), 1.78 (**4-tBu**, s, 9H).

In complex **7**, hydrogens from **tpbn** were assigned based off the ^{1}H assignments of complex **1**. Since **dppn** is replaced with **phen** in complex **7**, there are less magnetically inequivalent hydrogens than in complex **1** (only **a**-**g** in complex **7**, while there are **a**-**l** in complex **1**). Hydrogens **d**-**e**-**f** and **a**-**b**-**c** were assigned following the same strategy as was used for the assignment of hydrogens **d**-**e**-**f** and **a**-**b**-**c** in complex **1**. When chemical shifts of hydrogen **f** in complex **1** and hydrogen **f** in complex **7** are compared, they are found to be quite different (10.02 ppm in **1** and 8.89 ppm in **7**). This outlines the effect of the spatial proximity of the non-coordinated nitrogen from **dppn** on hydrogen **f**, as the proximity to this nitrogen moves chemical shift of **f** downfield. Since **phen** does not have a non-coordinated nitrogen analogous to that of **dppn**, the chemical shift of **f** is moved upfield in complex **7** when compared to chemical shift of **f** in complex **1**. The same effect is responsible for hydrogen **c** being more upfield in complex **7** than in complex **1** (9.16 ppm in **1** and 8.07 ppm in **7**). Hydrogens **h** and **g** form a two-spin system, which is identified by correlations observed with ^{1}H–^{1}H COSY NMR, with **g** assigned as the more downfield of the two (8.33 ppm) and **h** assigned as the more upfield of the two (7.90 ppm) based on the assumption that hydrogens on the side of **phen** that is facing **chloride** appear more downfield.

Complex **8**

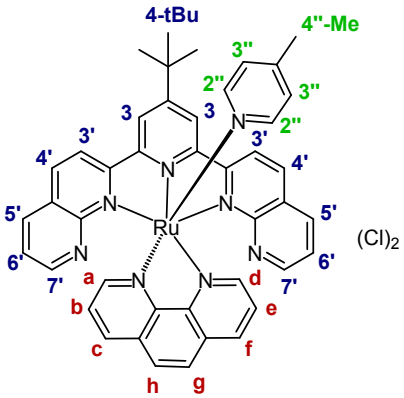

^{1}H NMR (MeOD-d_3, 500 MHz): δ 9.44 (**d**, dd, J_1 = 5.5 Hz, J_2 = 1.5 Hz, 1H), 9.14 (**3**, s, 2H), 9.01 (**3′**, d, J = 8.5 Hz, 2H), 8.94 (**f**, dd, J_1 = 8.5 Hz, J_2 = 1.5 Hz, 1H), 8.68 (**4′**, d, J = 8.5 Hz, 2H), 8.35 (**5′**, dd, J_1 = 8.5 Hz, J_2 = 2.0 Hz, 2H), 8.32 (**g**, d, J = 9.0 Hz, 1H), 8.29 (**e**, dd, J_1 = 8.5 Hz, J_2 = 5.5 Hz, 1H), 8.19 (**c**, dd, J_1 = 8.5 Hz, J_2 = 1.5 Hz, 1H), 7.92 (**h**, d, J = 9.0 Hz, 1H), 7.92 (**7′**, dd, J_1 = 4.5 Hz, J_2 = 2.0 Hz, 2H), 7.67 (**a**, dd, J_1 = 5.5 Hz, J_2 = 1.0

Hz, 1H), 7.66 (**2″**, d, J = 6.5 Hz, 2H), 7.42 (**6′**, dd, J_1 = 8.0 Hz, J_2 = 4.5 Hz, 2H), 7.29 (**b**, dd, J_1 = 8.0 Hz, J_2 = 5.5 Hz, 1H), 6.97 (**3″**, d, J = 6.5 Hz, 2H), 2.23 (**4″-Me**, s, 3H), 1.76 (**4-tBu**, s, 9H).

The hydrogens of complex **8** were assigned following based on the ^{1}H assignments of complex **7**. Unlike what was observed in other complexes containing the **4-pic** axial ligand (complexes **2**, **4**, and **6**), hydrogen **d** is still assigned as the most downfield, not hydrogen **f**. This assignment is based on the observed J-values of coupling with hydrogen **e** and the assumption that $J_{fe} > J_{de}$. Hydrogen **d** is assigned as the doublet of doublets at 9.44 ppm (J_{de} = 5.5 Hz, J_{df} = 1.5 Hz), and hydrogen **f** is assigned as the doublet of doublets at 8.94 ppm (J_{fe} = 8.5 Hz, J_{fd} = 1.5 Hz). When chemical shifts of hydrogen **d** in complex **7** and hydrogen **d** in complex **8** are compared, they are found to be significantly different (10.62 ppm in **7** and 9.44 ppm in **8**), just like in complex **1** *vs* complex **2**. However, even with the upfield shift of hydrogen **d** caused by the absence of **chloride**, hydrogen **d** still stays the most downfield hydrogen in complex **8** because hydrogen **f** from **phen** (~9 ppm) is noticeably more upfield than hydrogen **f** from **dppn** (~10 ppm). In complex **8**, in addition to ^{1}H from **tpbn** and **phen**, ^{1}H from **4-pic** are present: **2″**, **3″**, and **4″-Me**. Similar to complex **2**, **2″** was assigned as a doublet at 7.66 ppm and **3″** as a doublet at 6.97 ppm. The singlet at 2.23 ppm integrates as 3 hydrogens and is assigned to the **4″-Me** group.

Complex **9**

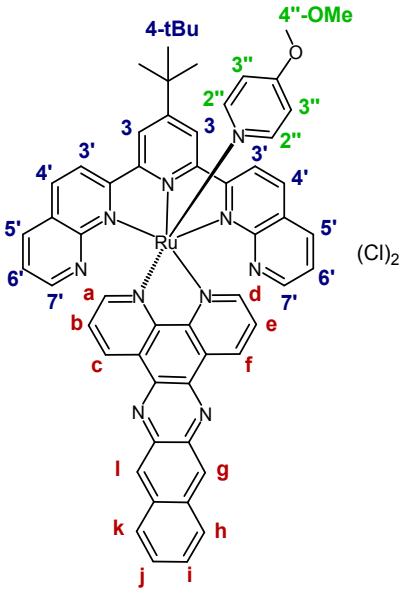

^{1}H NMR (MeOD-d_3, 500 MHz): δ 10.08 (**f**, dd, J_1 = 8.0 Hz, J_2 = 1.0 Hz, 1H), 9.49 (**d**, dd, J_1 = 5.0 Hz, J_2 = 1.0 Hz, 1H), 9.28 (**c**, dd, J_1 = 8.5 Hz, J_2 = 2.0 Hz, 1H), 9.18 (**3**, s, 2H), 9.17 (**g**, s, 1H), 9.06 (**3′**, d, J = 8.5 Hz, 2H), 9.01 (**l**, s, 1H), 8.73 (**4′**, d, J = 8.5 Hz, 2H), 8.44 (**e**, dd, J_1 = 8.0 Hz, J_2 = 5.5 Hz, 1H), 8.37 (**5′**, dd, J_1 = 8.0 Hz, J_2 = 2.0 Hz, 2H), 8.32 (**h**/**k**, d, J = 7.5 Hz, 1H), 8.28 (**h**/**k**, d, J = 8.0 Hz, 1H), 8.14 (**7′**, dd, J_1 = 4.0 Hz, J_2 = 1.5 Hz, 2H), 7.79 (**a**, dd, J_1 = 6.0 Hz, J_2 = 1.5 Hz, 1H), 7.71 (**i**, **j**, m, 2H), 7.56 (**2″**, d, J = 7.5 Hz, 2H), 7.43 (**6′**, **b**, m, 3H), 6.73 (**3″**, d, J = 7.0 Hz, 2H), 3.75 (**4″-OMe**, s, 3H), 1.78 (**4-tBu**, s, 9H).

Hydrogens in complex **9** were assigned based off the ^{1}H assignments of complex **2**, and overall follow the same trend as in complex **2**. As expected, the methyl group signal from the axial ligand **4-mp** in complex **9** (**4″-OMe** at 3.75 ppm) is moved significantly downfield relative to the methyl group signal from the axial ligand **4-pic** in complex **2** (**4″-Me** at 2.25 ppm).

6. ESI⁺ Mass spectra of Ru(II) complexes 1–9

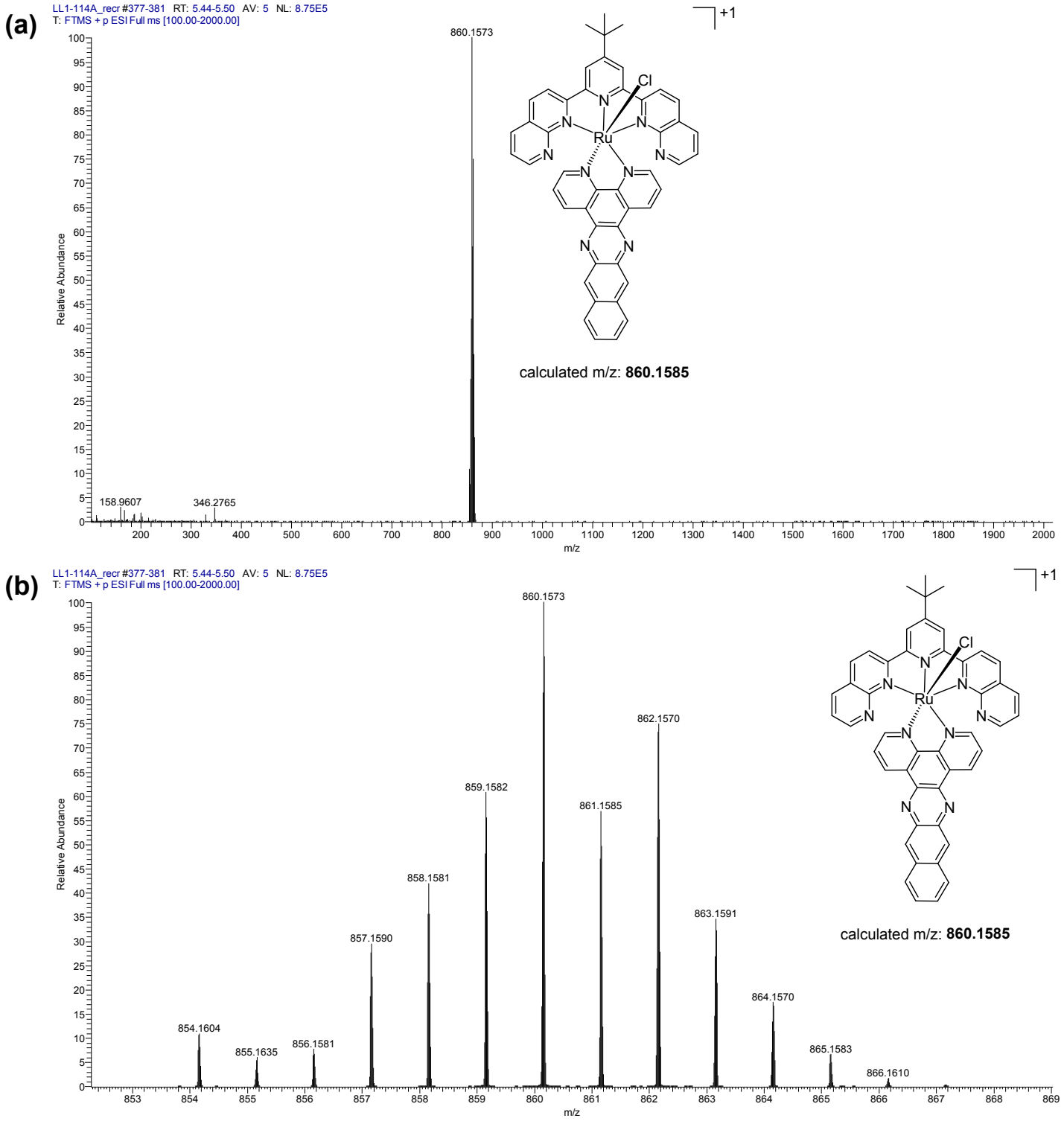

Figure S29. (a) High resolution ESI⁺ mass spectrum for complex **1**. (b) Zoom of 860.1573 peak showing isotopic distribution.

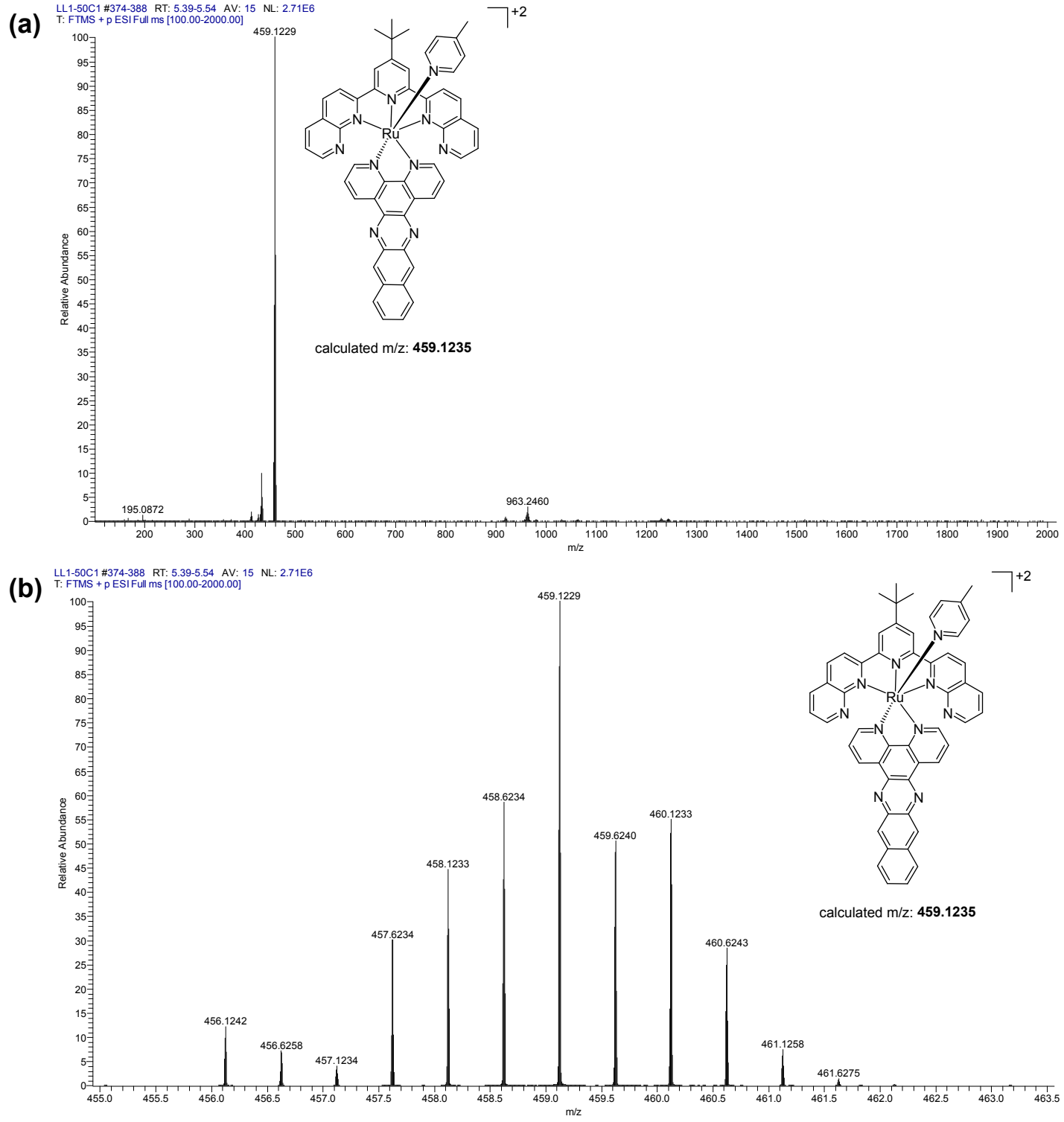

Figure S30. (a) High resolution ESI⁺ mass spectrum for complex **2**. (b) Zoom of 459.1229 peak showing isotopic distribution.

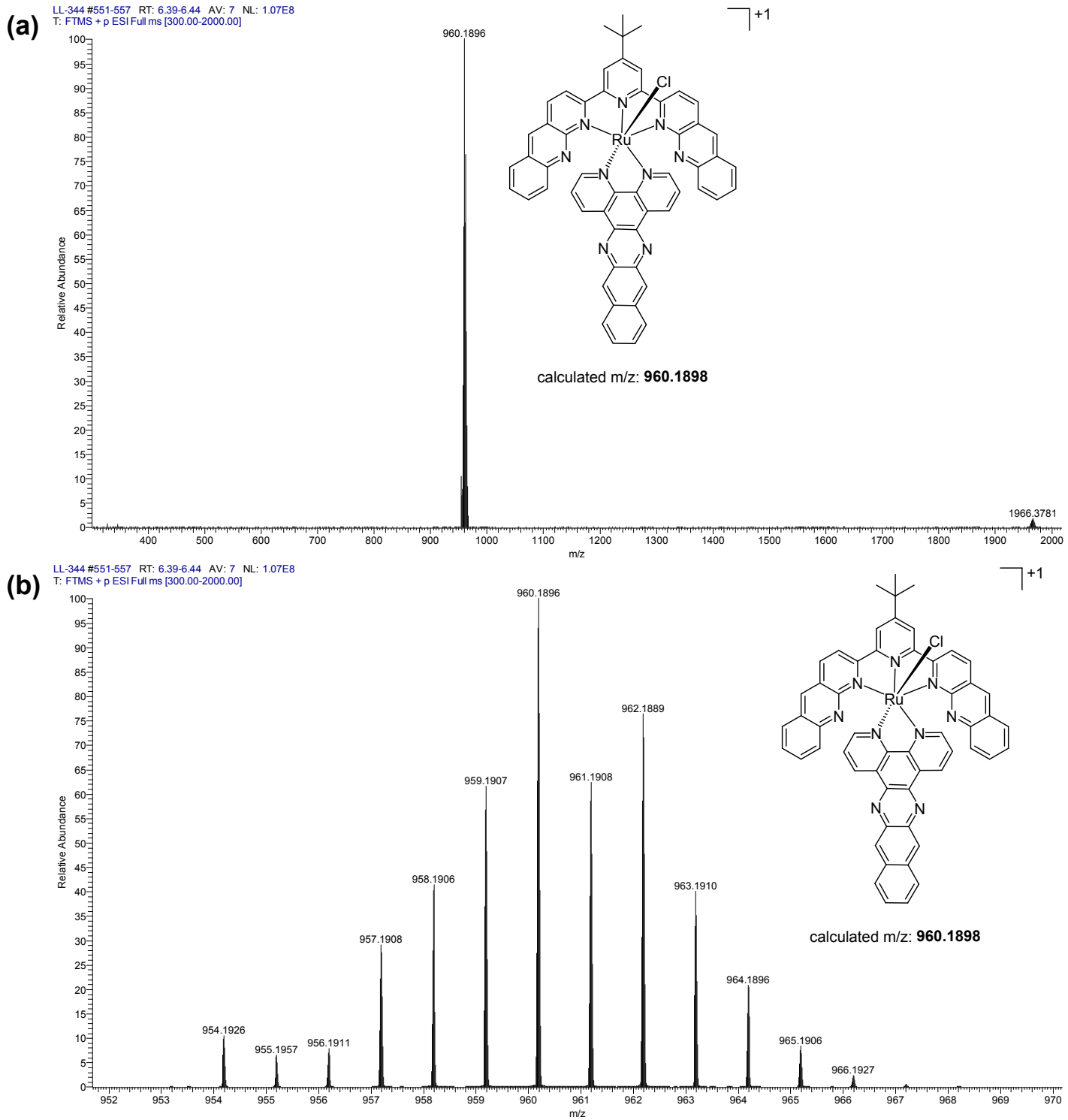

Figure S31. (a) High resolution ESI$^+$ mass spectrum for complex **3**. (b) Zoom of 960.1896 peak showing isotopic distribution

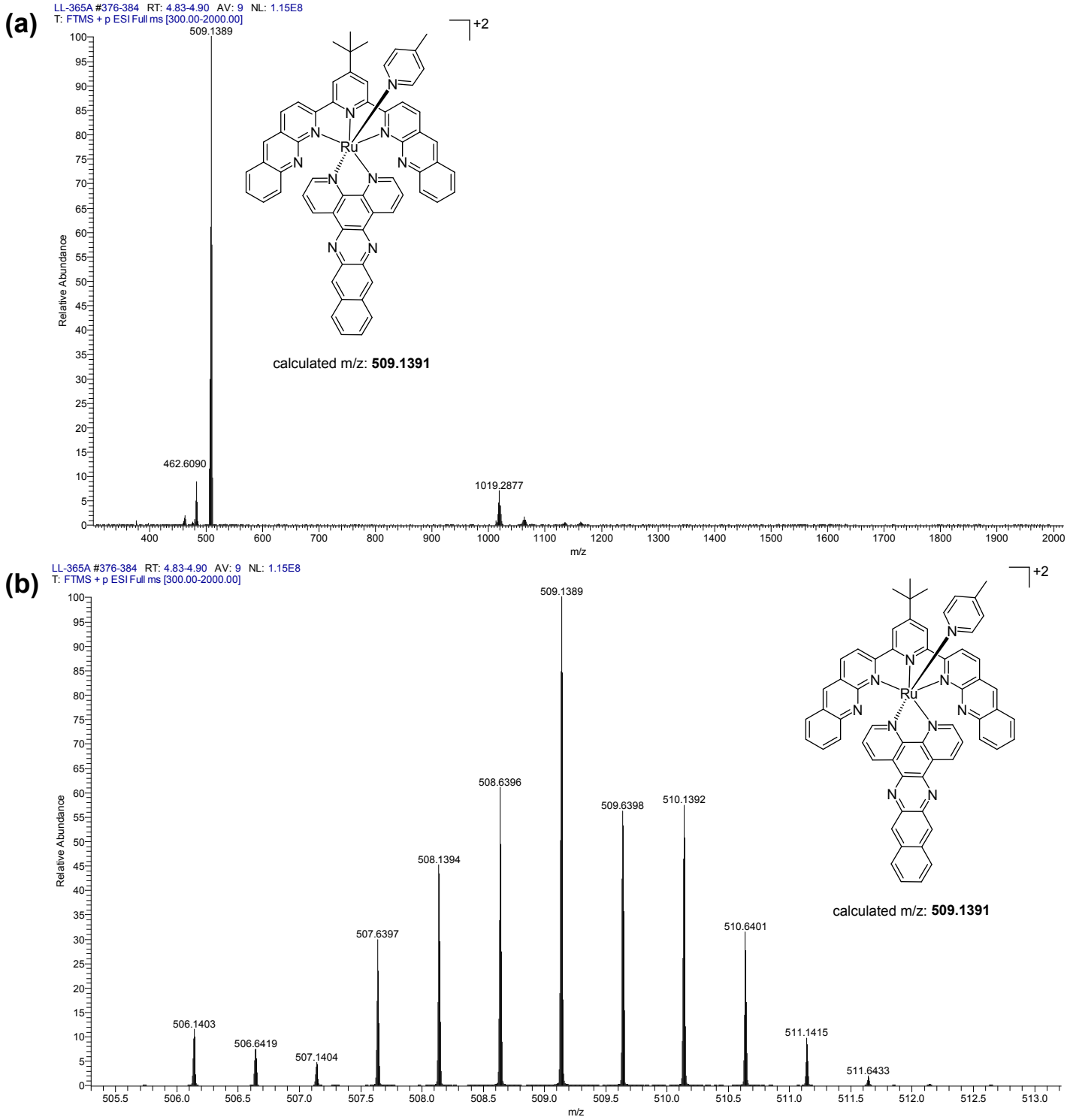

Figure S32. (a) High resolution ESI$^+$ mass spectrum for complex **4**. (b) Zoom of 509.1389 peak showing isotopic distribution.

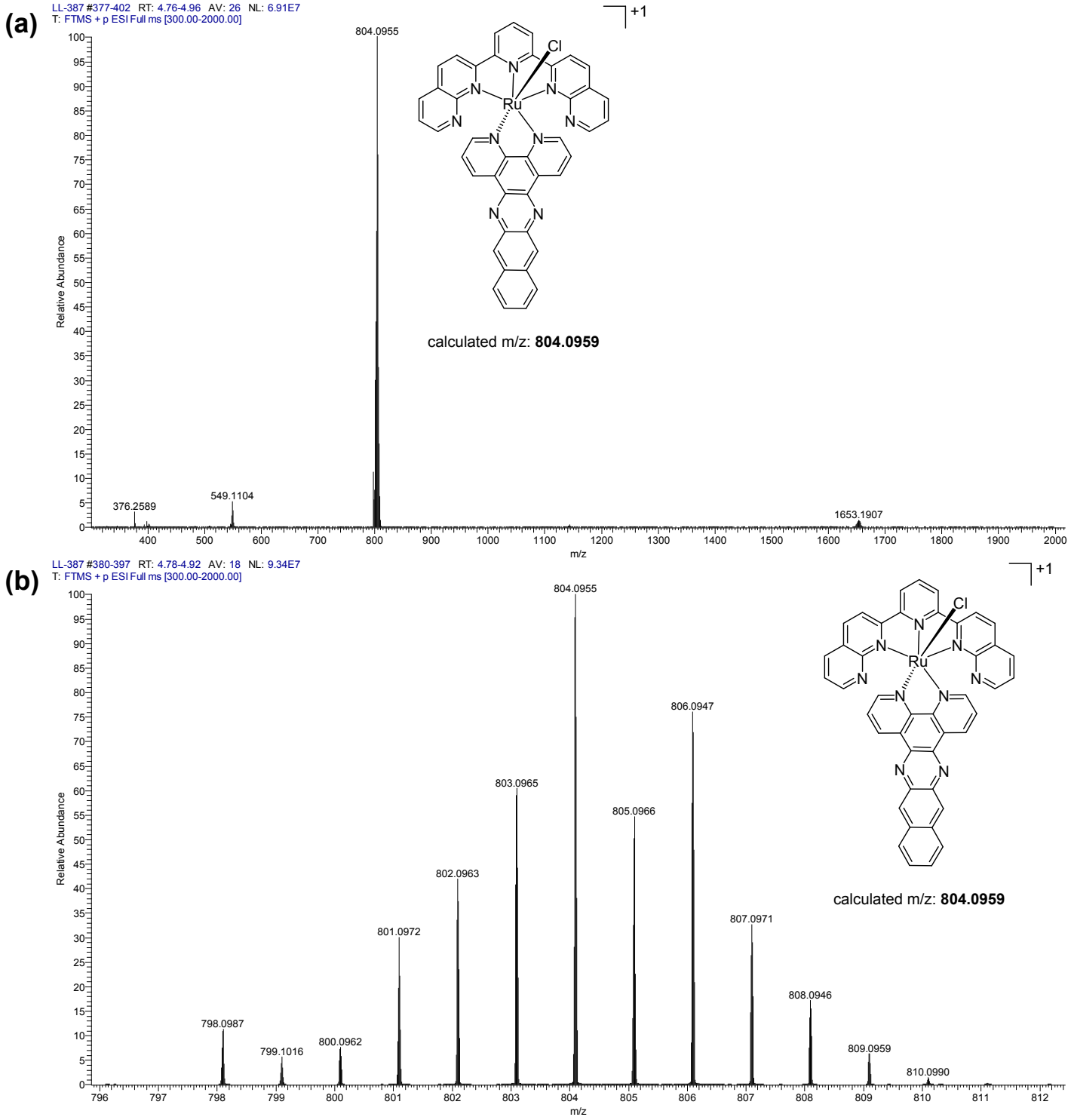

Figure S33. (a) High resolution ESI$^+$ mass spectrum for complex **5**. (b) Zoom of 804.0955 peak showing isotopic distribution.

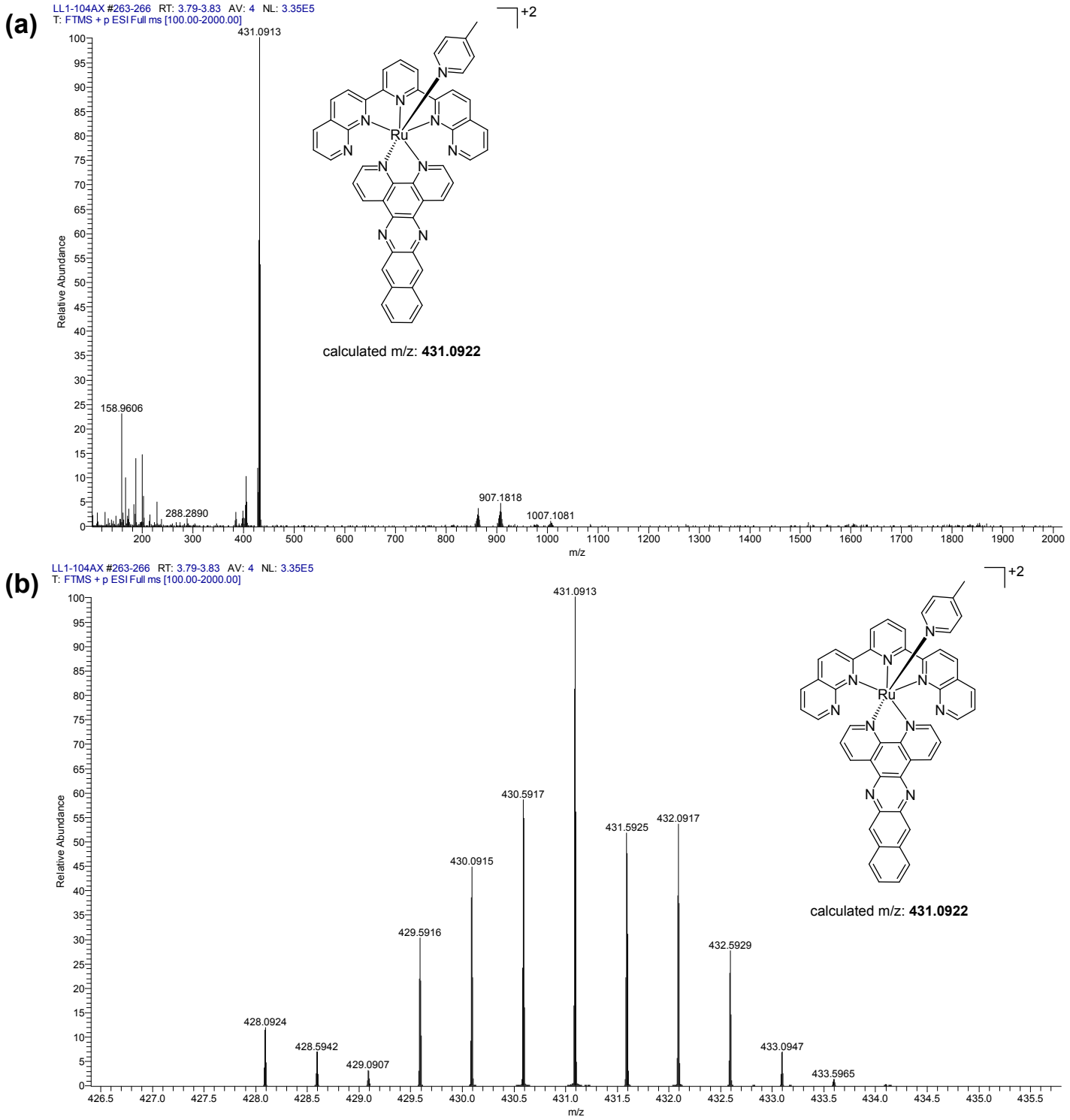

Figure S34. (a) High resolution ESI⁺ mass spectrum for complex **6**. (b) Zoom of 431.0913 peak showing isotopic distribution.

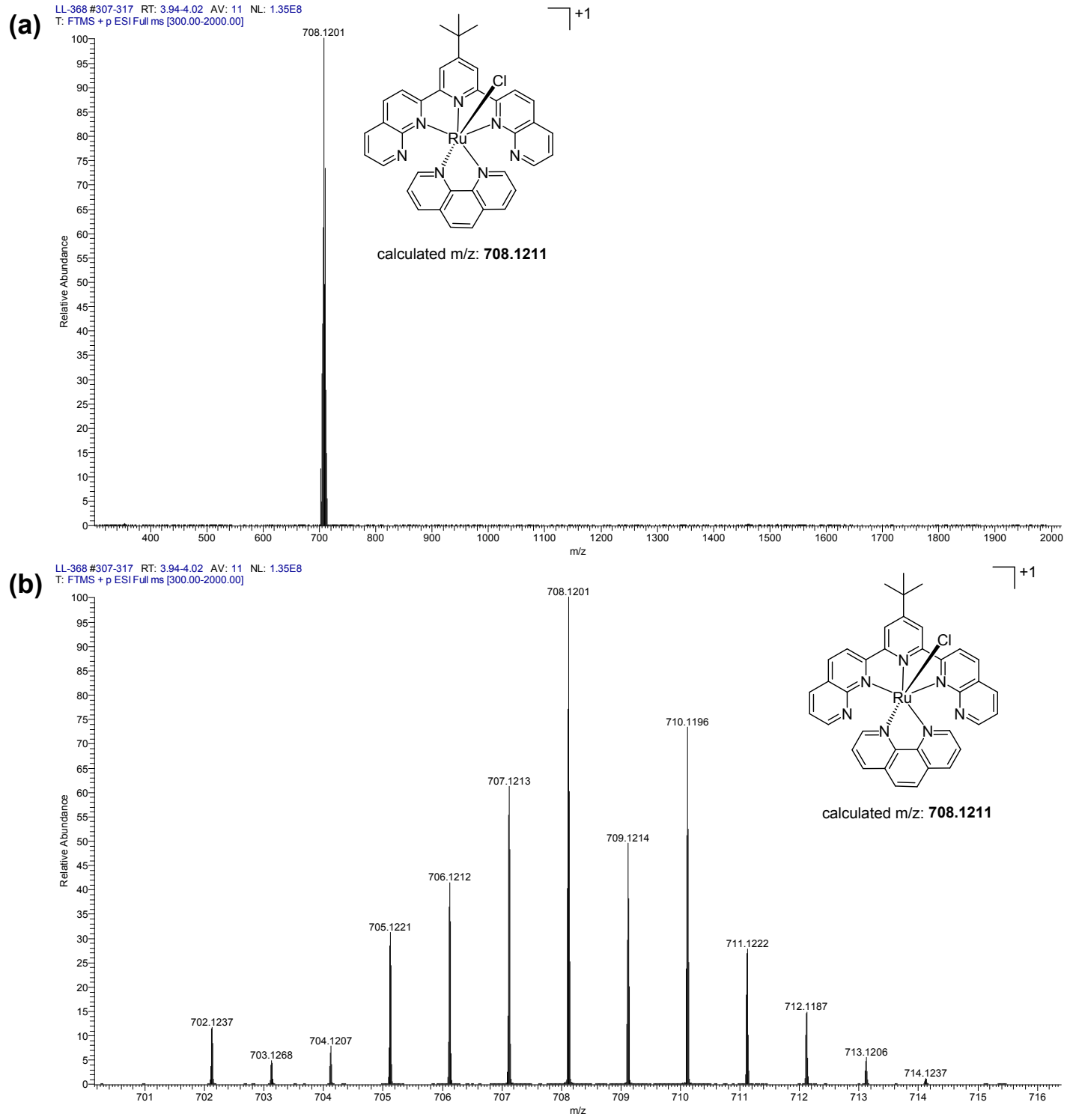

Figure S35. (a) High resolution ESI$^+$ mass spectrum for complex **7**. (b) Zoom of 708.1201 peak showing isotopic distribution.

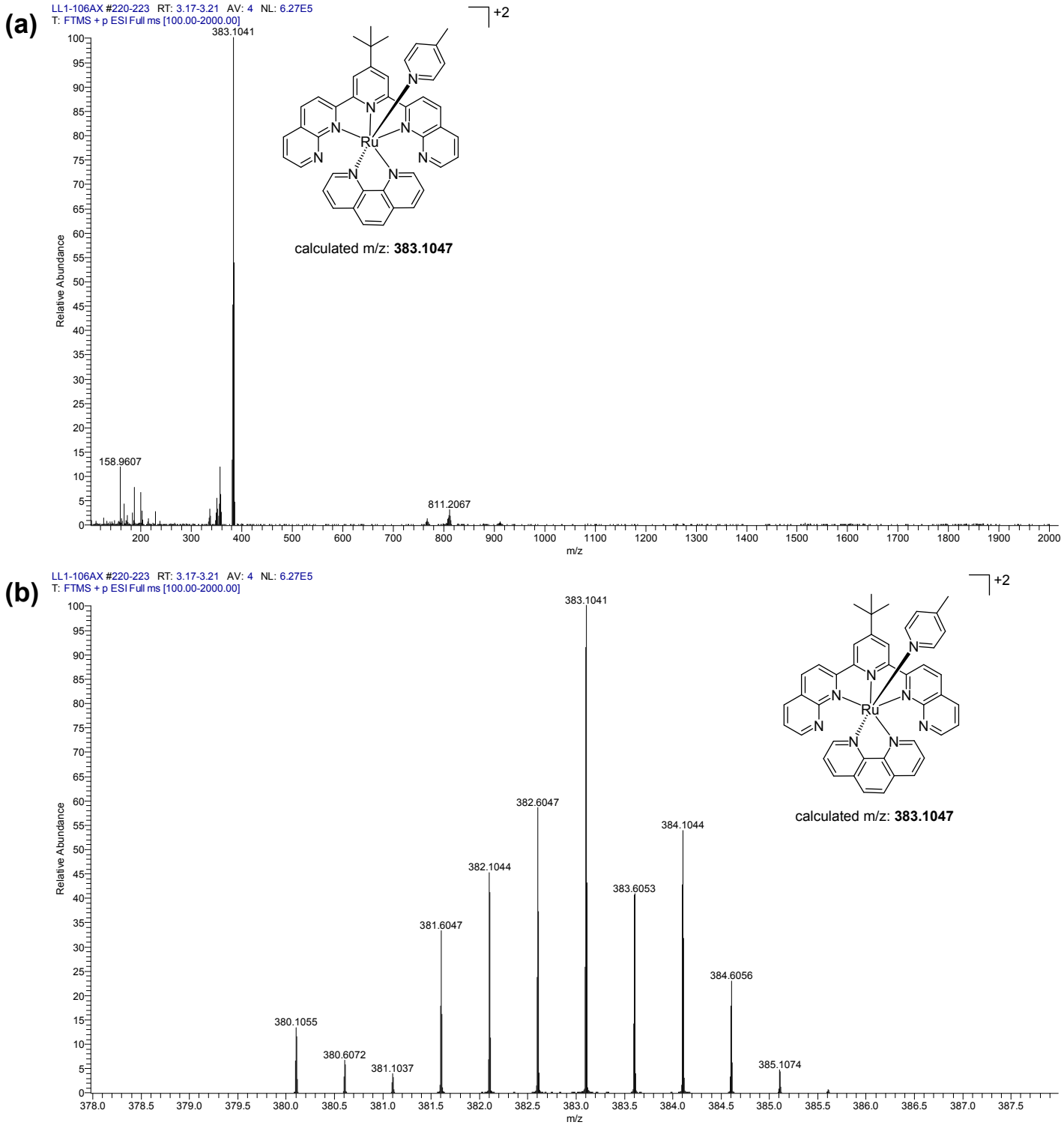

Figure S36. (a) High resolution ESI$^+$ mass spectrum for complex **8**. (b) Zoom of 383.1041 peak showing isotopic distribution.

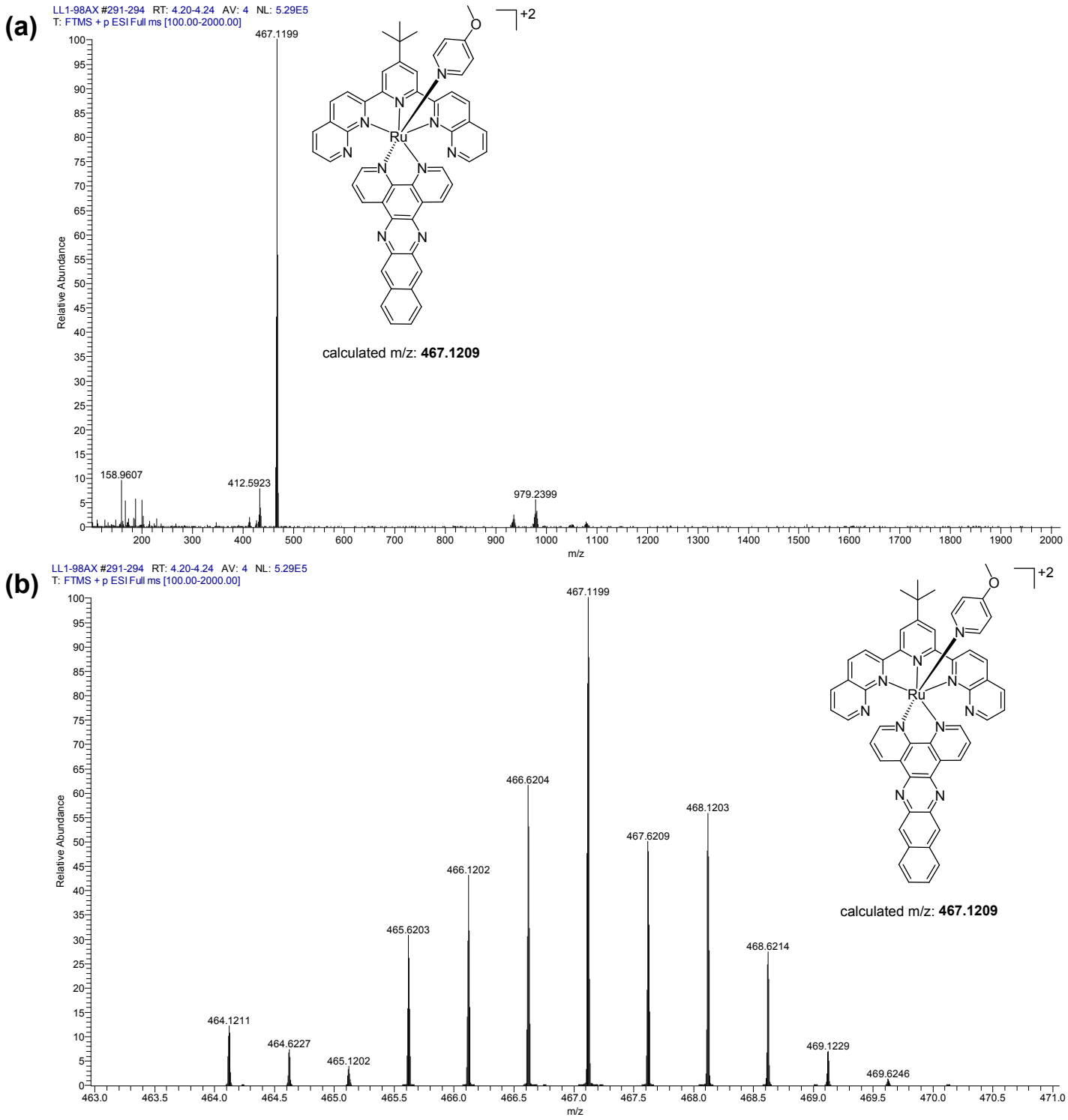

Figure S37. (a) High resolution ESI⁺ mass spectrum for complex **9**. (b) Zoom of 467.1199 peak showing isotopic distribution.

7. HPLC chromatograms of Ru(II) complexes 1–9

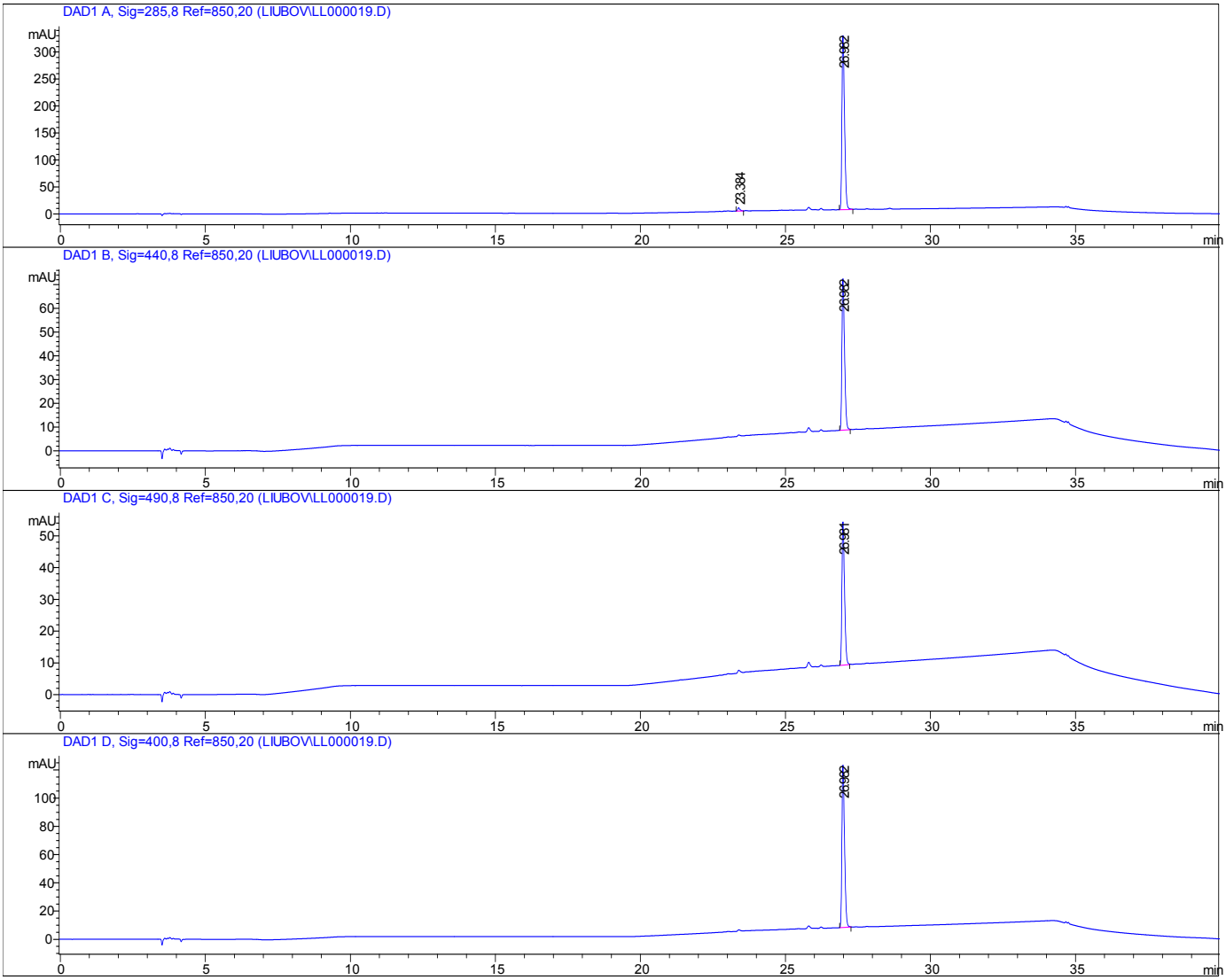

Figure S38. HPLC chromatogram of complex **1** collected at the following wavelengths: 285, 440, 490, 400 nm (98.3% purity by peak area).

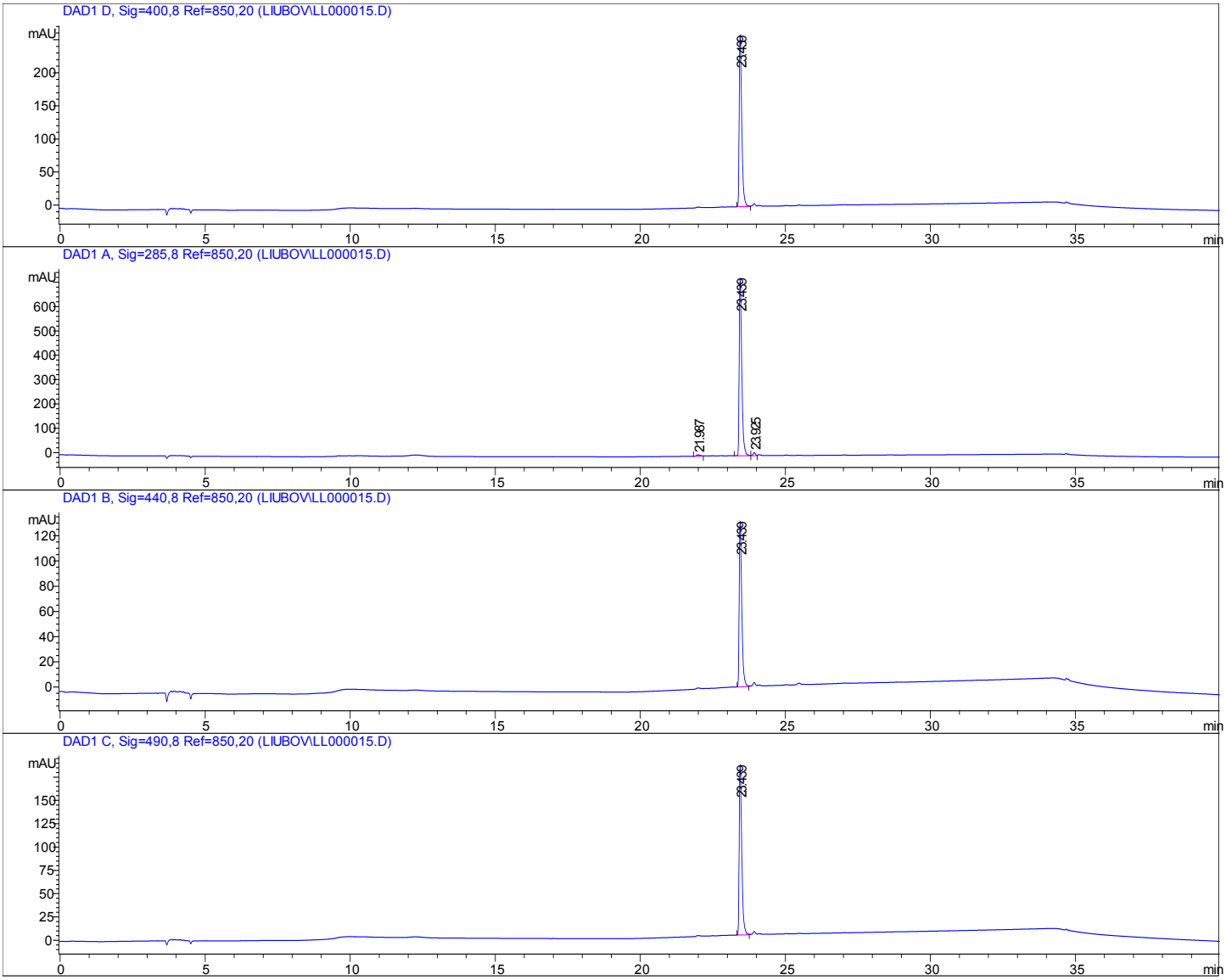

Figure S39. HPLC chromatogram of complex **2** collected at the following wavelengths: 400, 285, 440, 490 nm (97.2% purity by peak area).

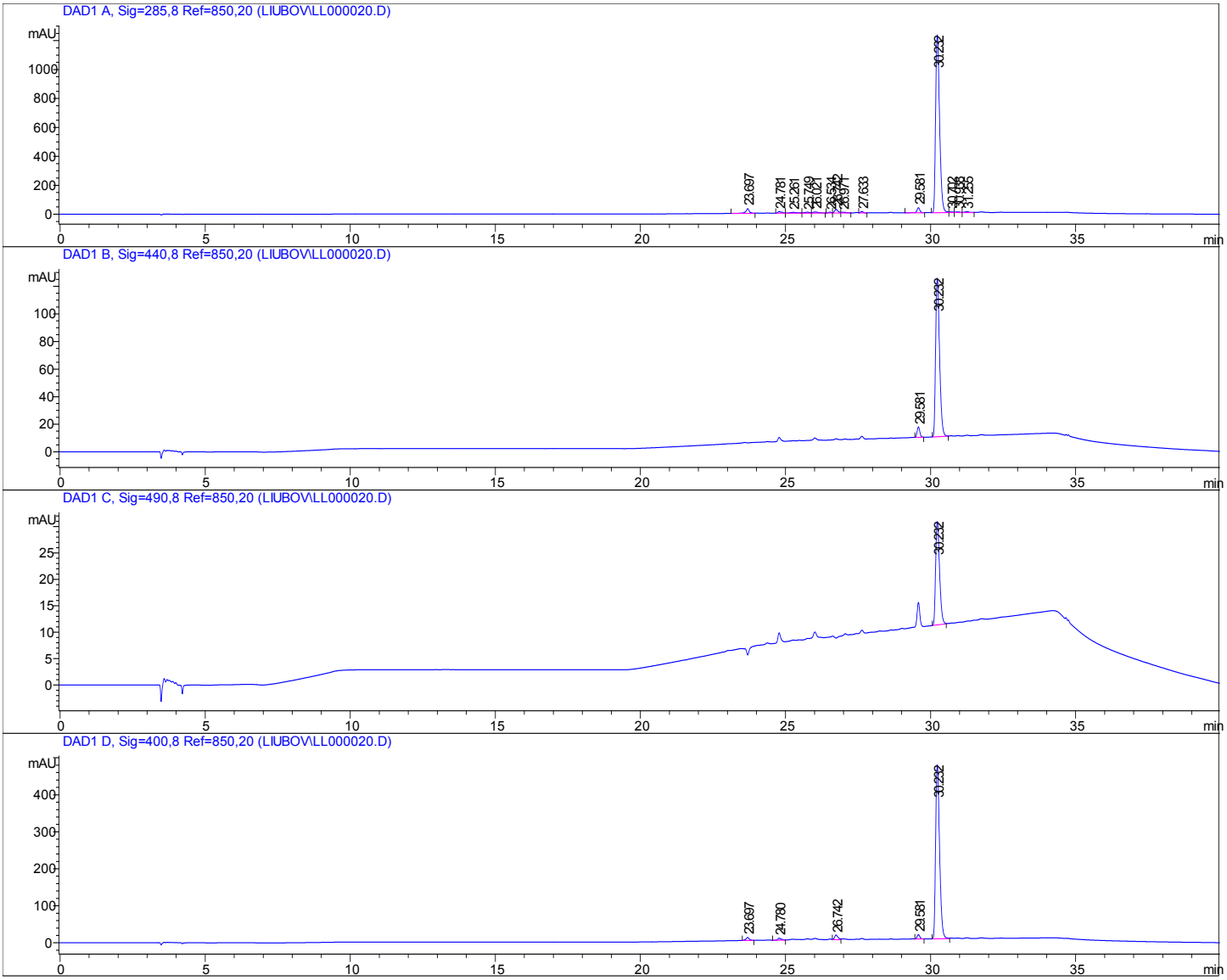

Figure S40. HPLC chromatogram of complex **3** collected at the following wavelengths: 285, 440, 490, 400 nm (94.2% purity by peak area).

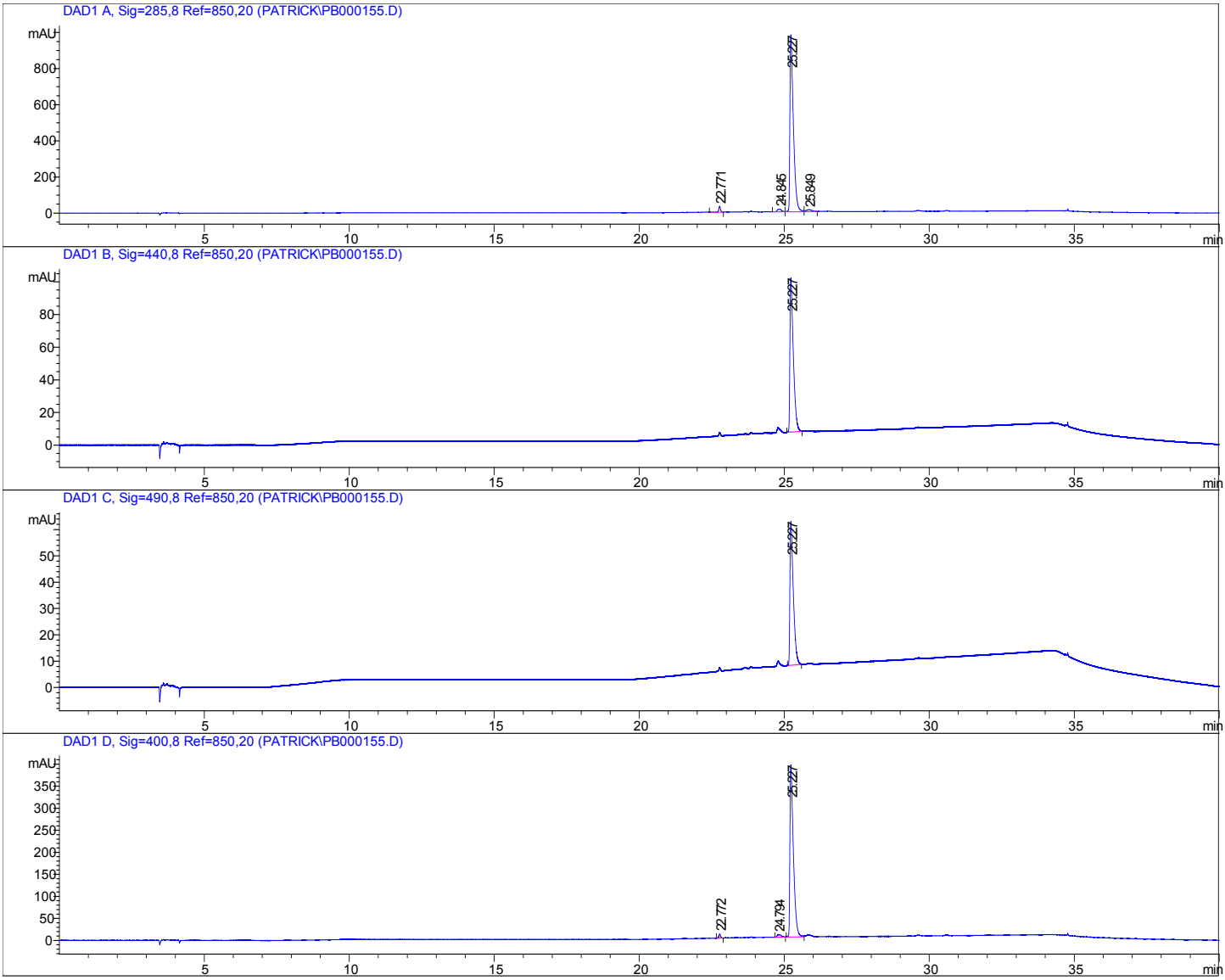

Figure S41. HPLC chromatogram of complex **4** collected at the following wavelengths: 285, 440, 490, 400 nm (94.8% purity by peak area).

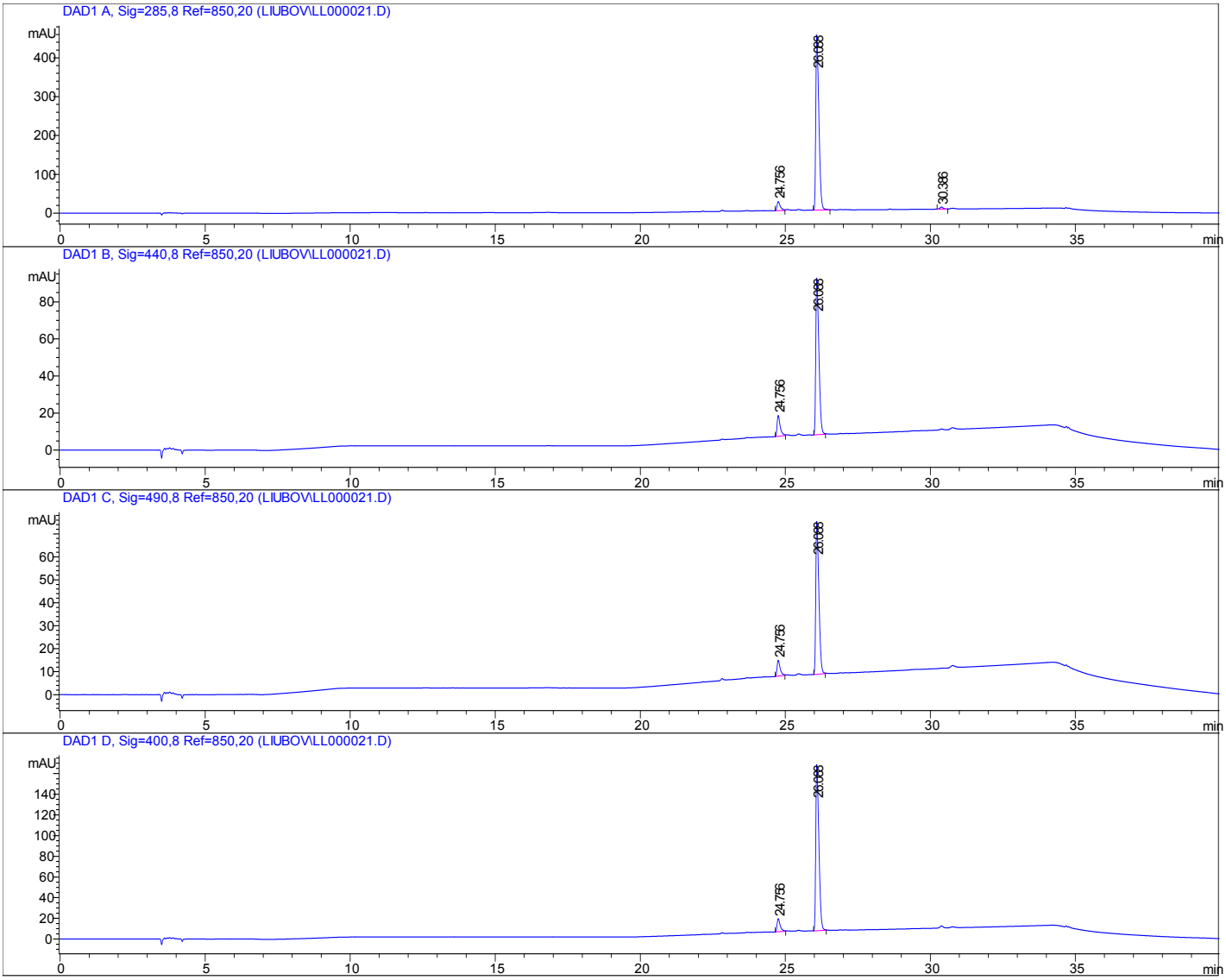

Figure S42. HPLC chromatogram of complex **5** collected at the following wavelengths: 285, 440, 490, 400 nm (88.3% purity by peak area).

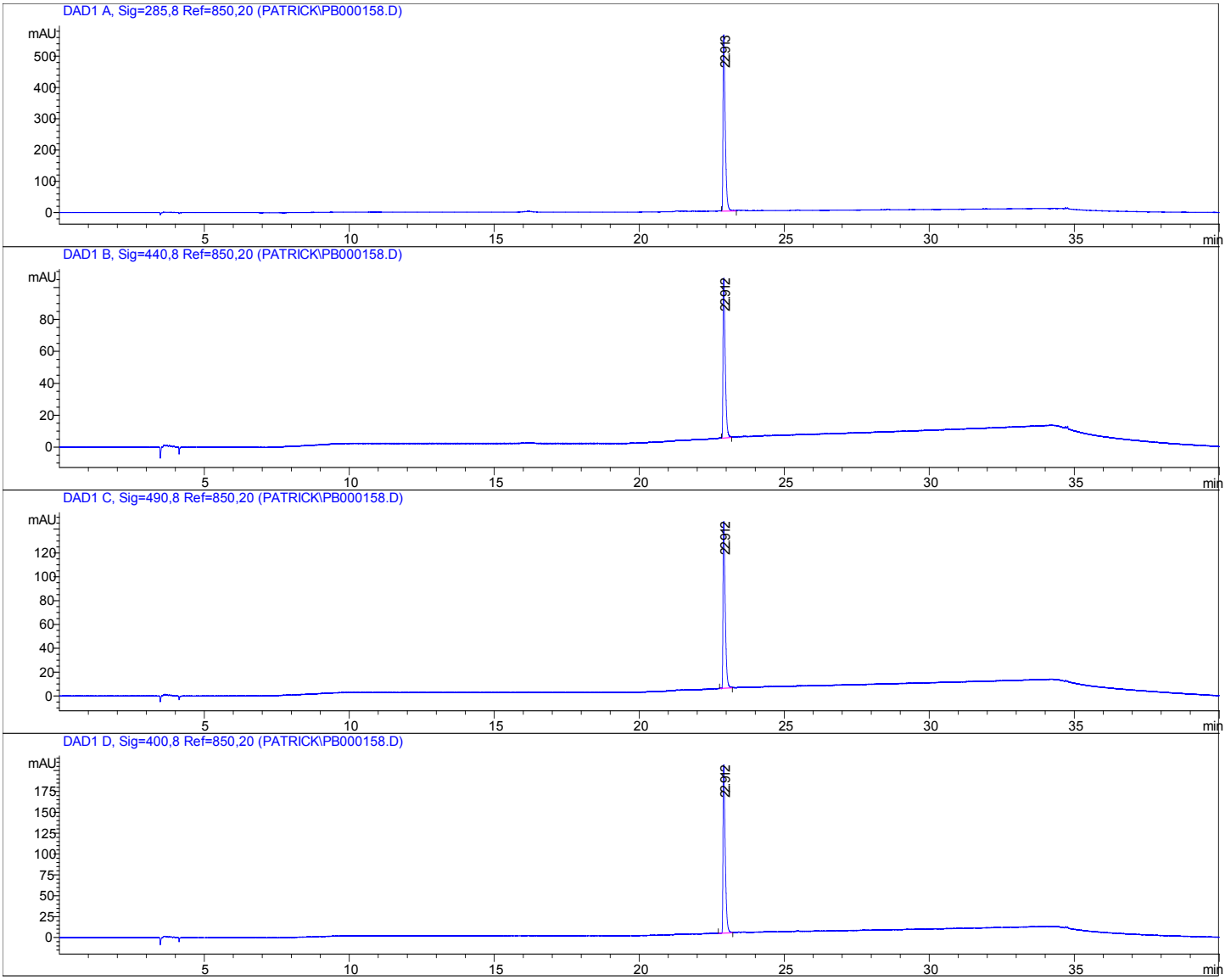

Figure S43. HPLC chromatogram of complex **6** collected at the following wavelengths: 285, 440, 490, 400 nm (100% purity by peak area).

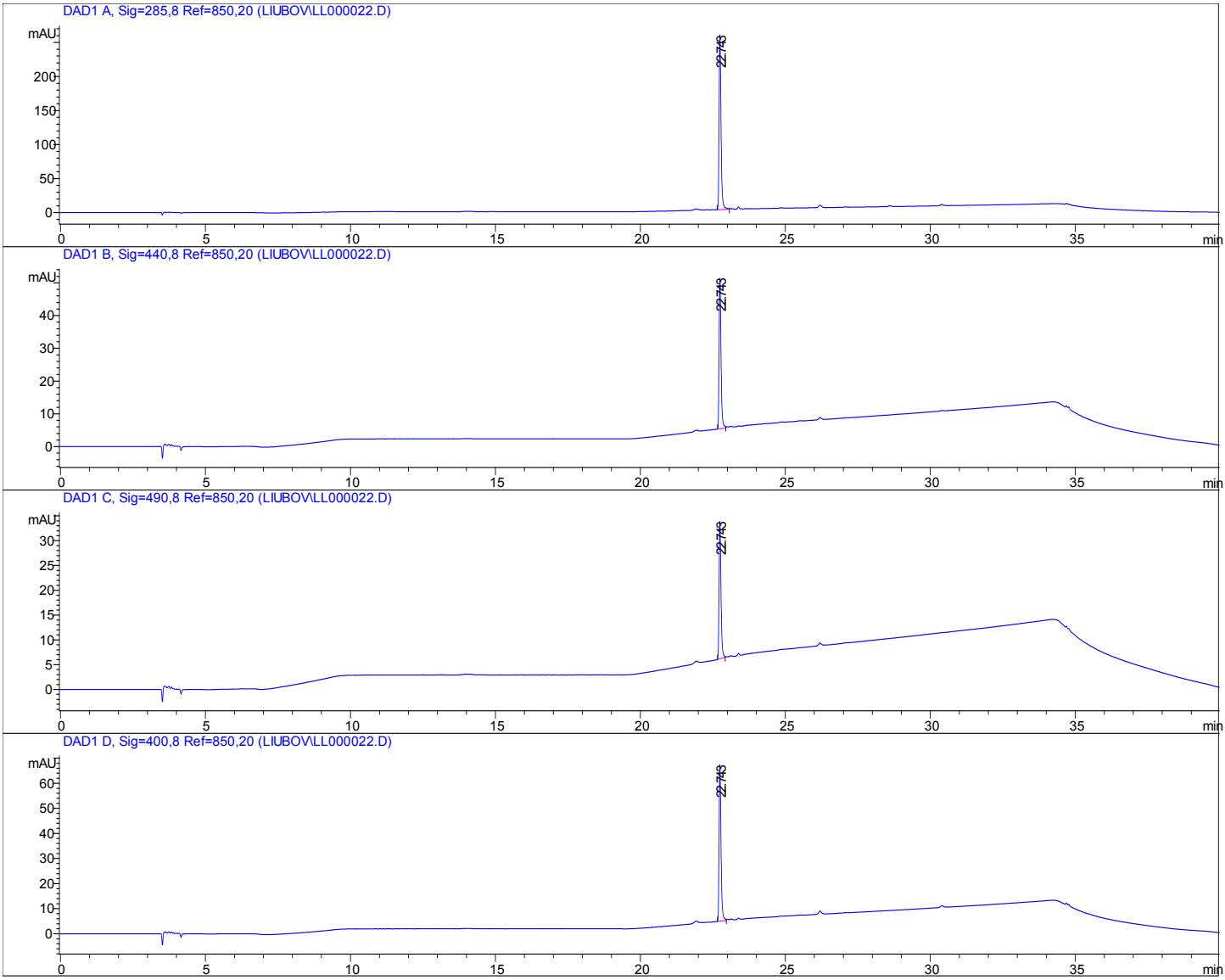

Figure S44. HPLC chromatogram of complex **7** collected at the following wavelengths: 285, 440, 490, 400 nm (100% purity by peak area).

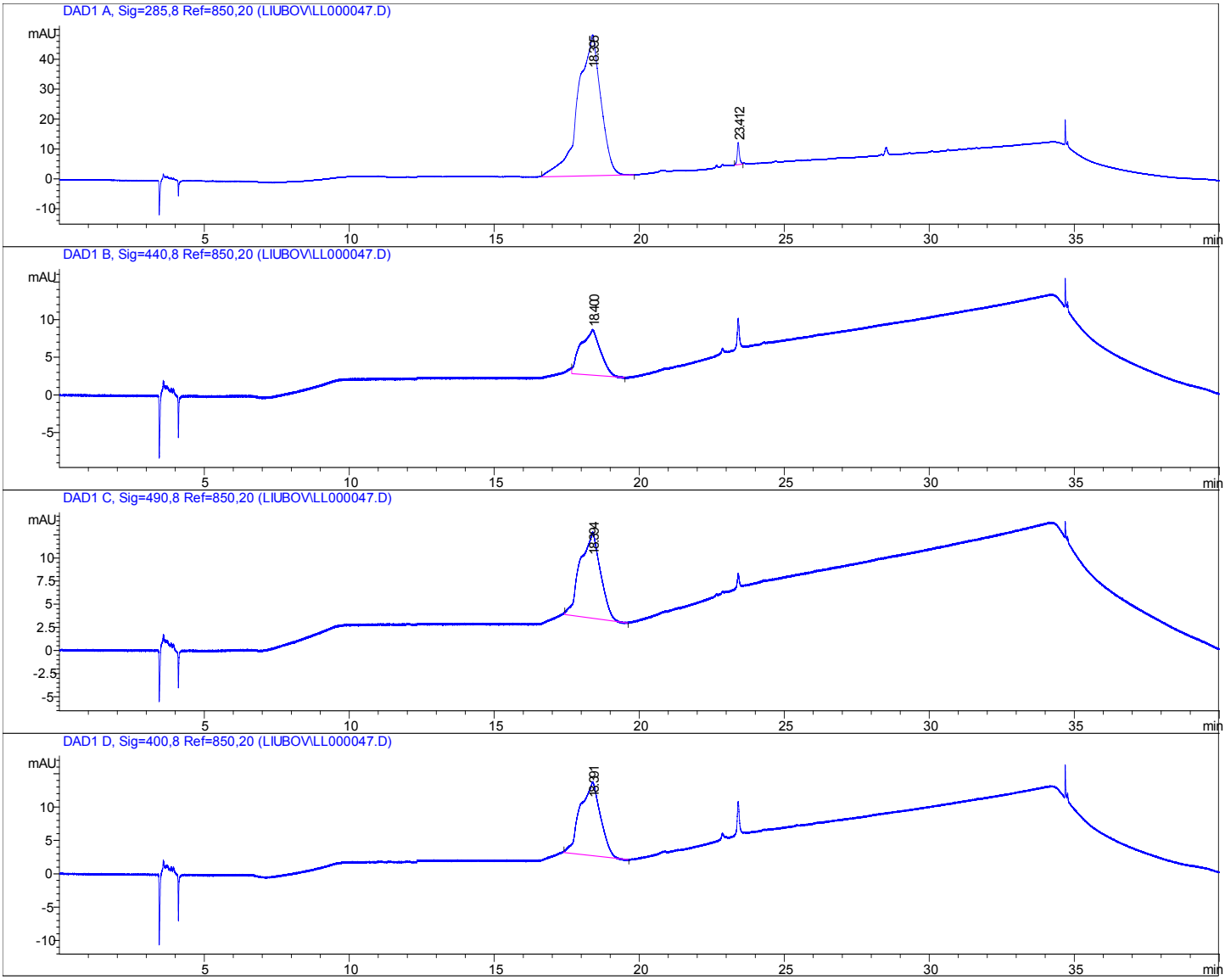

Figure S45. HPLC chromatogram of complex **8** collected at the following wavelengths: 285, 440, 490, 400 nm (98.5% purity by peak area).

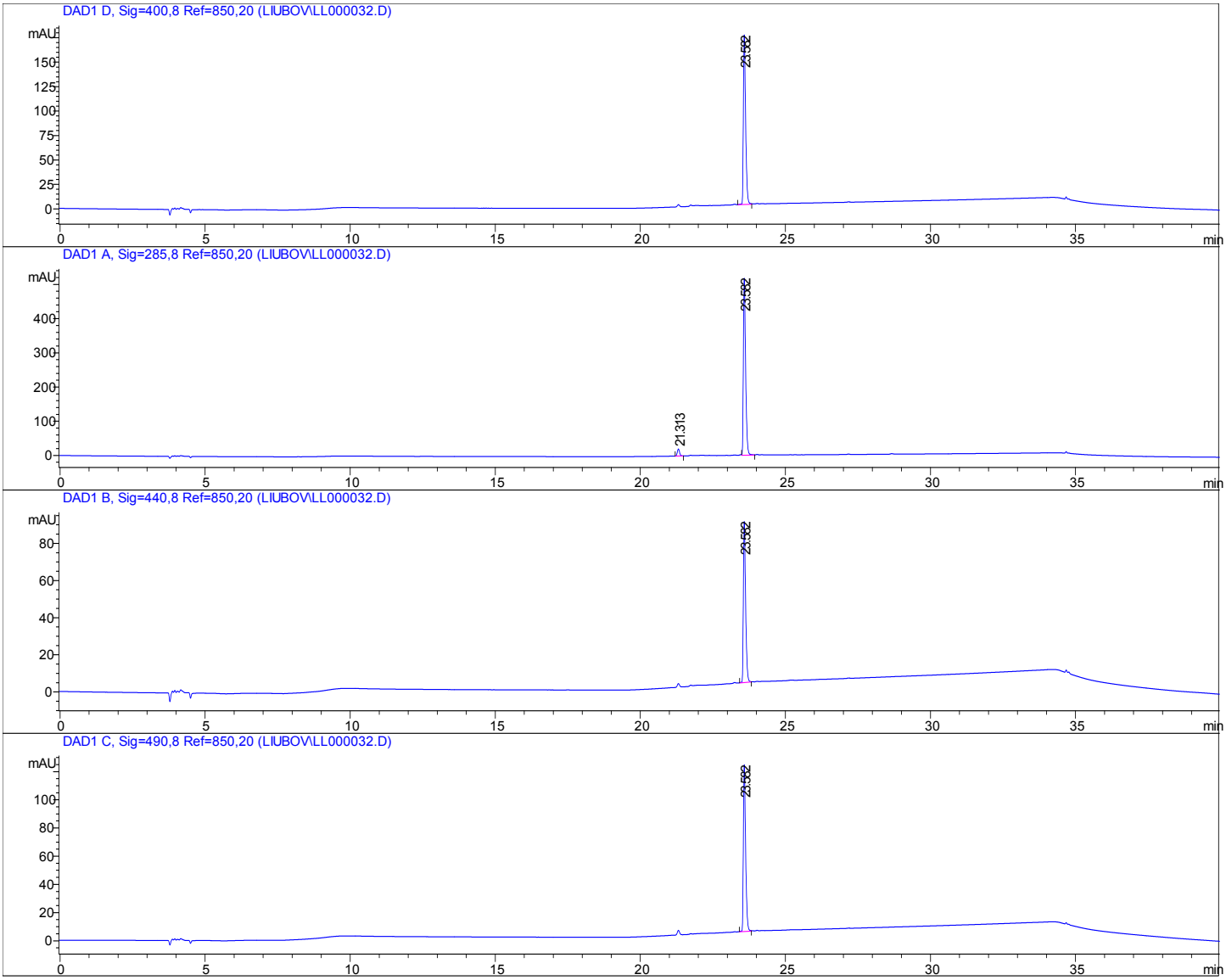

Figure S46. HPLC chromatogram of complex **9** collected at the following wavelengths: 400, 285, 440, 490 nm (96.1% purity by peak area).

8. Photobiology

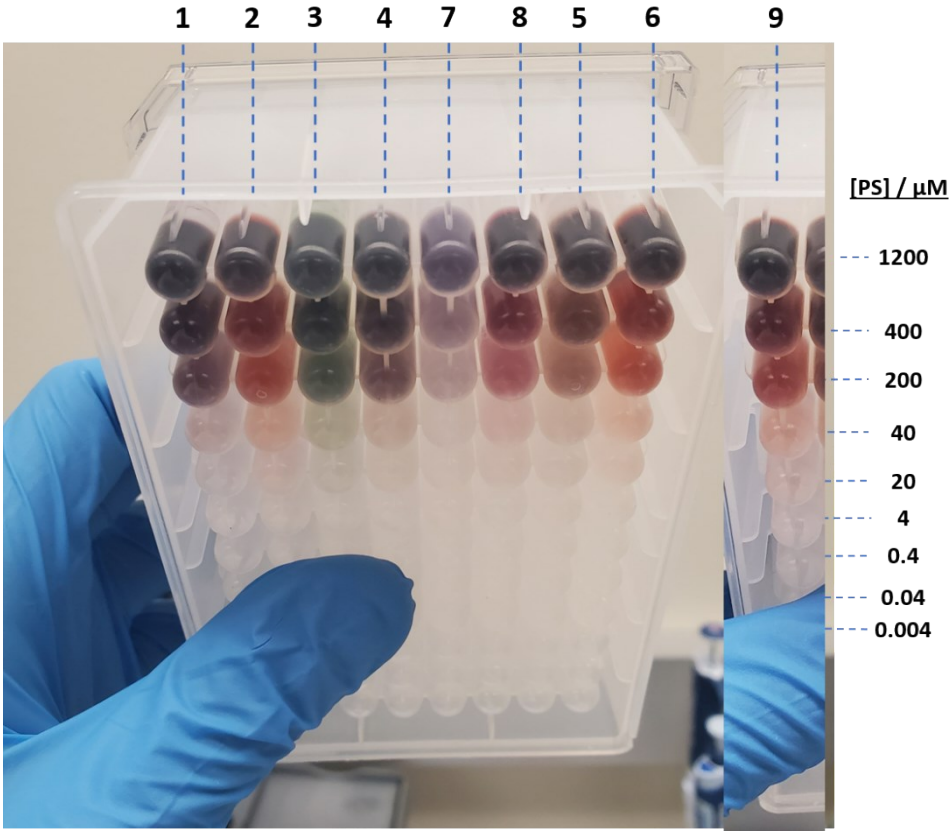

Figure S47. Freshly prepared serial dilutions of compounds **1**–**9** in 1× DPBS.

Table S1. Correlation parameters for Log ($D_{o/w}$) versus Log (Dark EC_{50})

Cell line	A375	B16F10	SKMEL28
Pearson r coefficient	−0.6649	−0.8665	−0.9041
95% CI	−0.9751 to 0.5259	−0.9911 to 0.06677	−0.9937 to -0.1078
R^2	0.4421	0.7509	0.8174
p-value (α=0.05)[a]	0.2208	0.0573	0.0351

Only soluble compounds included. n=5 since compounds **1**,**3**,**5**,**7** precipitated to some extent during experimentation.
[a]two-tailed p-test, p<0.05 = statistically significant

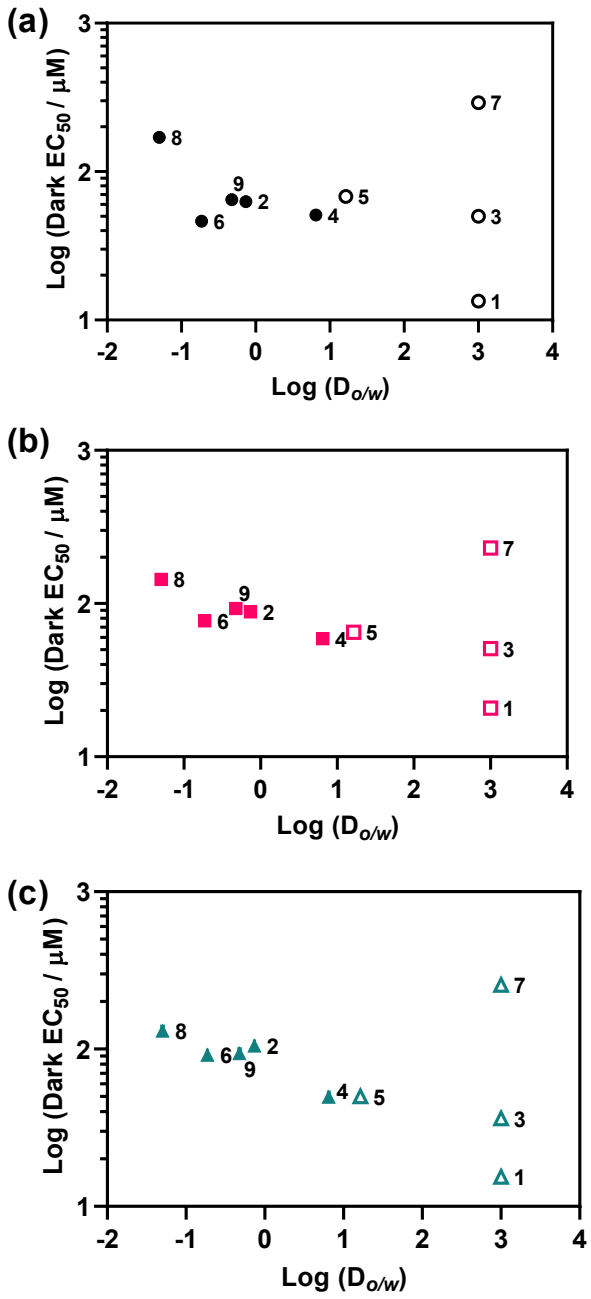

Figure S48. Log-Log scatter plot of distribution coefficient (± SD) versus Dark EC_{50} (± SEM) in (a) A375, (b) B16F10, and (c) SKMEL28 cell lines. Open symbols designate ambiguous Log ($D_{o/w}$) values where precipitation occurred in either the aqueous or organic partitions. Tabulated Log ($D_{o/w}$) are included in Table S2.

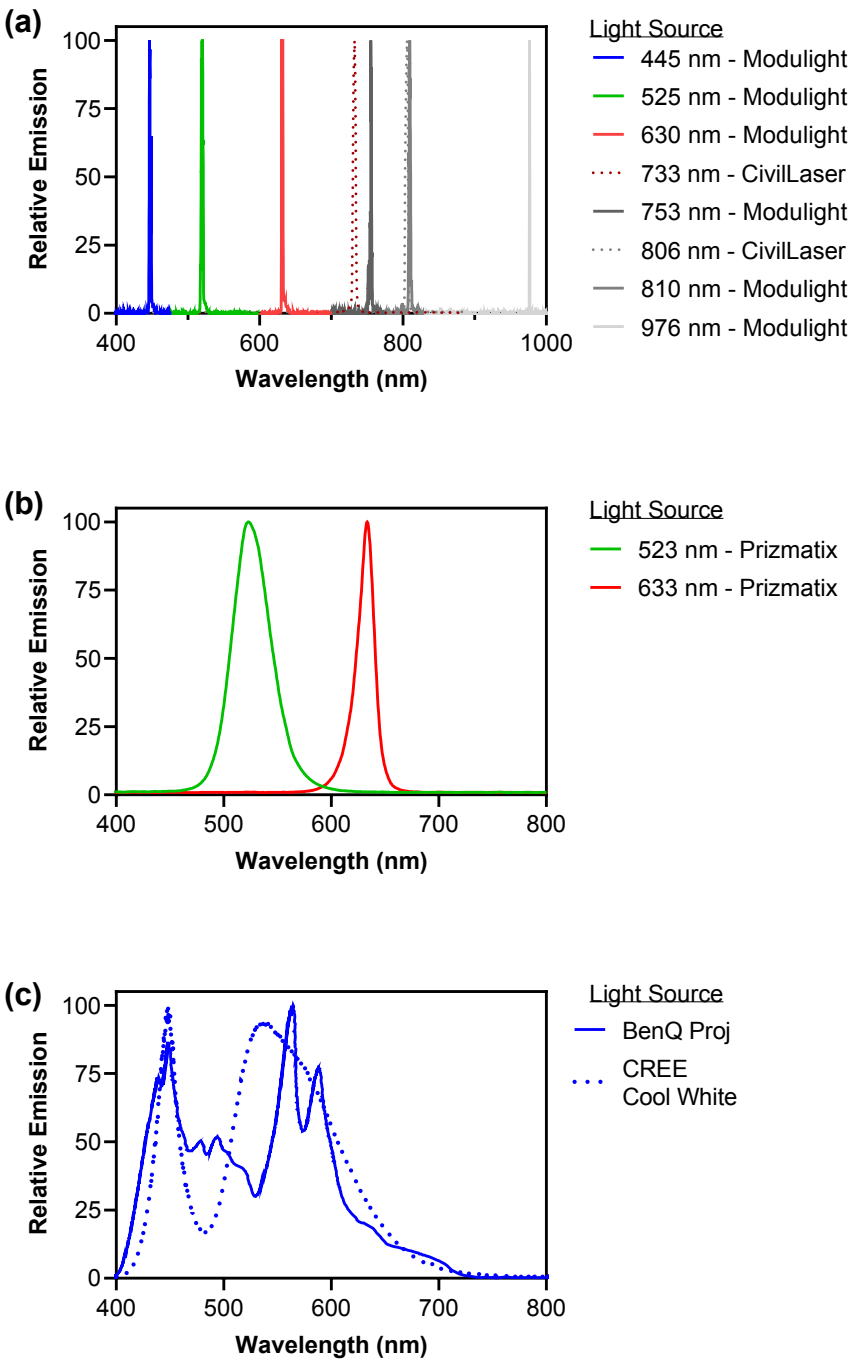

Figure S49. Normalized emission from the light sources used in the photobiological studies: (a) lasers, (b) monochromatic LEDs, and (c) broadband visible projector lamp or broadband visible CREE LEDs.

Table S2. Log distribution coefficient ($LogD_{o/w}$) of **1**–**9** in 1-octanol and PBS (pH=7.4). [a]value not determined due to precipitation.

cmpd	$Log(D_{o/w} \pm SD)$
1	3[a]
2	−0.131 ± 0.009
3	3[a]
4	0.813 ± 0.016
5	1.215 ± 0.055
6	−0.730 ± 0.007
7	3[a]
8	−1.298 ± 0.021
9	−0.32 ± 0.017

Table S3. Comparison of (photo)cytotoxicities in different cell lines across the three laboratories performed by three different researchers.

			EC_{50} ± SEM[1] (μM)			PI[2]	
PS#	Cell Line	Location	Dark[3]	633 nm[4]	Visible[4,5]	633 nm[4]	Visible[4,5]
2	B16F10	UTA	88.2 ± 5.5	1.89 ± 0.03	1.74 ± 0.14	47	51
2	B16F10	Dal	52.3 ± 1.5	1.44 ± 0.04	-	36	-
2	SKMEL28	UTA	105 ± 6	0.798 ± 0.097	0.292 ± 0.016	132	360
2	SKMEL28	AU	70.9 ± 1.9	0.63 ± 0.013	0.329 ± 0.008	113	216
6	B16F10	UTA	77.0 ± 4.3	1.97 ± 0.09	0.940 ± 0.090	39	82
6	B16F10	Dal	63.2 ± 1.0	2.12 ± 0.08	-	30	-
6	SKMEL28	UTA	91.9 ± 5.9	1.37 ± 0.10	0.359 ± 0.026	67	256
6	SKMEL28	AU	79.6 ± 2.5	0.521 ± 0.012	0.333 ± 0.033	153	239
9	B16F10	UTA	92.8 ± 6.0	2.12 ± 0.10	0.87 ± 0.12	44	107
9	B16F10	Dal	29.2 ± 1.6	1.22 ± 0.01	-	24	-
9	SKMEL28	UTA	94.0 ± 7.5	1.52 ± 0.04	0.602 ± n.d.	62	156
9	SKMEL28	AU	56.7 ± 1.5	0.396 ± 0.017	0.286 ± 0.017	143	198

[1]Effective concentration to reduce cell viability to 50% (EC_{50}) and standard error of the mean (SEM), [2]phototherapeutic index (PI) provides the ratio of dark (sham) to light treatment, [3]dark treatment or absence of light during treatment, [4]light treatment uses 20–30 mW cm^{-2} and 100 J cm^{-2}, [5]cool white visible (400–700 nm), [6]n.d. = not determined due to a steep hill slope, "-" = treatment not performed.

Table S4. Comparison of (photo)cytotoxicities of **1**–**9** under four different conditions in female melanoma A375 cells at UTA.

cmpd	EC_{50} ± SEM (μM)					PI			
	Dark[3]	733 nm[4]	633 nm[5]	523 nm[5]	Visible[5,6]	733 nm[4]	633 nm[4]	523 nm[5]	Visible[5,6]
1	13.4 ± 0.4	5.35 ± 0.09	4.78 ± 0.05	4.87 ± 0.08	1.94 ± 0.08	3	3	3	7
2	62.6 ± 0.9	1.77 ± 0.12	1.45 ± 0.02	1.28 ± 0.05	1.21 ± 0.07	35	43	49	52
3	50.0 ± n.d.[7]	49.6 ± n.d.[7]	24.3 ± 1.0	15.6 ± 0.8	1.97 ± 0.22	1	2	3	25
4	51.1 ± n.d.[7]	13.9 ± 2.1	12.7 ± 0.4	12.1 ± 0.3	6.53 ± 0.06	4	4	4	8
5	68.1 ± 2.0	26.4 ± 1.6	20.1 ± 0.8	14.0 ± 0.8	4.87 ± 0.41	3	3	5	14
6	46.3 ± 1.2	1.62 ± 0.12	1.48 ± 0.03	1.10 ± 0.02	1.04 ± 0.07	29	31	42	45
7	292 ± 9	214 ± 6	152 ± 3	170 ± 4	116 ± 4	1	2	2	3
8	170 ± 7	191 ± 7	187 ± 7	198 ± 7	179 ± 15	1	1	1	1
9	64.6 ± 1.0	2.00 ± 0.05	1.59 ± 0.05	1.43 ± 0.03	0.867 ± 0.079	32	41	45	75

[1]Effective concentration to reduce cell viability to 50% (EC_{50}) and standard error of the mean (SEM), [2]phototherapeutic index (PI) provides the ratio of dark (sham) to light treatment, [3]dark treatment or absence of light during treatment, [4]light treatment uses 9 mW cm^{-2} and 100 J cm^{-2}, [5]light treatment uses 20 mW cm^{-2} and 100 J cm^{-2}, [6]cool white visible (400–700 nm), [7]n.d. = not determined due to a steep hill slope.

Table S5. Comparison of (photo)cytotoxicities of **1**–**9** under four different conditions in murine melanoma B16F10 cells at UTA

cmpd	EC_{50} ± SEM (μM)					PI			
	Dark[3]	733 nm[4]	633 nm[5]	523 nm[5]	Visible[5,6]	733 nm[4]	633 nm[4]	523 nm[5]	Visible[5,6]
1	20.8 ± 1.6	5.09 ± 0.07	4.85 ± n.d.[7]	2.17 ± 0.08	1.65 ± 0.05	4	4	10	13
2	88.2 ± 5.5	2.57 ± 0.16	1.89 ± 0.03	1.46 ± 0.09	1.74 ± 0.14	34	47	60	51
3	50.7 ± 1.7	53.4 ± 1.0	49.9 ± n.d.[7]	16.3 ± 1.6	1.92 ± 0.05	1	1	3	26
4	58.8 ± 2.0	15.0 ± 2.0	13.7 ± 0.8	13.7 ± 0.7	6.77 ± 0.15	4	4	4	9
5	65.0 ± 2.5	54.1 ± 1.5	50.3 ± n.d.[7]	27.4 ± 2.4	7.58 ± 0.99	1	1	2	9
6	77.0 ± 4.3	2.14 ± 0.03	1.97 ± 0.09	1.31 ± 0.07	0.939 ± 0.092	36	39	59	82
7	231 ± 9	217 ± 8	166 ± 5	168 ± 4	121 ± 5	1	1	1	2
8	144 ± 4	171 ± 12	176 ± 8	182 ± 9	113 ± 12	1	1	1	1
9	92.8 ± 6.0	2.41 ± 0.04	2.12 ± 0.10	1.47 ± 0.05	0.871 ± 0.115	39	44	63	107

[1]Effective concentration to reduce cell viability to 50% (EC_{50}) and standard error of the mean (SEM), [2]phototherapeutic index (PI) provides the ratio of dark (sham) to light treatment, [3]dark treatment or absence of light during treatment, [4]light treatment uses 9 mW cm^{-2} and 100 J cm^{-2}, [5]light treatment uses 20 mW cm^{-2} and 100 J cm^{-2}, [6]cool white visible (400–700 nm), [7]n.d. = not determined due to a steep hill slope.

Table S6. Comparison of (photo)cytotoxicities of **1**–**9** under four different conditions in male melanoma SKMEL28 cells at UTA

cmpd	EC_{50} ± SEM (μM)					PI			
	Dark[3]	733 nm[4]	633 nm[5]	523 nm[5]	Visible[5,6]	733 nm[4]	633 nm[4]	523 nm[5]	Visible[5,6]
1	15.4 ± 1.1	1.83 ± 0.07	1.43 ± 0.11	1.02 ± 0.23	0.702 ± n.d.[7]	8	11	15	22
2	105 ± 6	1.56 ± 0.04	0.798 ± 0.097	0.424 ± 0.073	0.292 ± 0.016	67	132	248	360
3	36.2 ± 3.0	49.5 ± n.d.[7]	16.2 ± 1.2	13.7 ± 0.5	1.14 ± n.d.[7]	1	2	3	32
4	49.7 ± n.d.[7]	12.6 ± 2.5	7.61 ± 0.06	5.95 ± 0.22	3.29 ± 0.16	4	7	8	15
5	50.0 ± 3.3	16.0 ± 1.1	14.9 ± 0.9	6.09 ± 0.28	1.27 ± 0.21	3	3	8	39
6	91.9 ± 5.9	1.29 ± 0.18	1.37 ± 0.10	0.407 ± 0.084	0.359 ± 0.026	71	67	226	256
7	256 ± 8	167 ± 6	127 ± 7	122 ± 6	67.3 ± 1.7	2	2	2	4
8	131 ± 3	112 ± 5	96.8 ± 4.3	61.5 ± 1.3	41.7 ± n.d.[7]	1	1	2	3
9	94.0 ± 7.5	1.56 ± 0.18	1.52 ± 0.04	0.720 ± n.d.[7]	0.602 ± n.d.[7]	60	62	131	156

[1]Effective concentration to reduce cell viability to 50% (EC_{50}) and standard error of the mean (SEM), [2]phototherapeutic index (PI) provides the ratio of dark (sham) to light treatment, [3]dark treatment or absence of light during treatment, [4]light treatment uses 9 mW cm^{-2} and 100 J cm^{-2}, [5]light treatment uses 20 mW cm^{-2} and 100 J cm^{-2}, [6]cool white visible (400–700 nm), [7]n.d. = not determined due to a steep hill slope.

Table S7. Comparison of leads **1**, **6**, and **9** for (photo)cytotoxicity in normoxia vs. hypoxia in 96-well plates

			EC_{50} ± SEM[1] (μM)			PI[2]	
cmpd	Cell Line	Oxygen %	Dark[3]	633 nm[4]	Visible[4,5]	633 nm[4]	Visible[4,5]
2	SKMEL28	18.5	63.3 ± 1.4	0.520 ± 0.015	0.543 ± 0.009	122	116
6	SKMEL28	18.5	69.4 ± 0.6	0.605 ± 0.021	0.595 ± 0.005	115	117
9	SKMEL28	18.5	103 ± 3	0.654 ± 0.013	0.591 ± 0.006	157	174
R_1[6]	SKMEL28	18.5	135 ± 5	0.612 ± 0.014	0.083 ± 0.001	221	1631
2	SKMEL28	1	42.0 ± 1.1	21.4 ± 2.3	37.6 ± 1.9	2	1
6	SKMEL28	1	67.9 ± 0.8	67.1 ± 2.2	78.2 ± 0.9	1	1
9	SKMEL28	1	90.9 ± 2.0	33.4 ± 5.8	71.0 ± 3.5	3	1
R_1[6]	SKMEL28	1	136 ± 3	133 ± 6	117 ± 2	1	1

[1]Effective concentration to reduce cell viability to 50% (EC_{50}) and standard error of the mean (SEM), [2]phototherapeutic index (PI) provides the ratio of dark (sham) to light treatment, [3]dark treatment or absence of light during treatment, [4]light treatment uses 20–30 mW cm^{-2} and 100 J cm^{-2},[5]cool white broadband visible source (400–700 nm), [6]reference R_1 = oxygen sensitive PDT agent $[Ru(bpy)_2(dppn)]Cl_2$.

Table S8. Correlation parameters for Log (Φ_{Δ}) versus Log (PI)

Cell line	A375	B16F10	SKMEL28
Pearson r coefficient	0.9540	0.9860	0.9773
95% CI	0.7910 to 0.9905	0.9327 to 0.9972	0.8923 to 0.9954
R^2	0.9101	0.9723	0.9551
p-value (α=0.05)[a]	<0.0001	<0.0001	<0.0001

[a]two-tailed p-test, p<0.05 = statistically significant

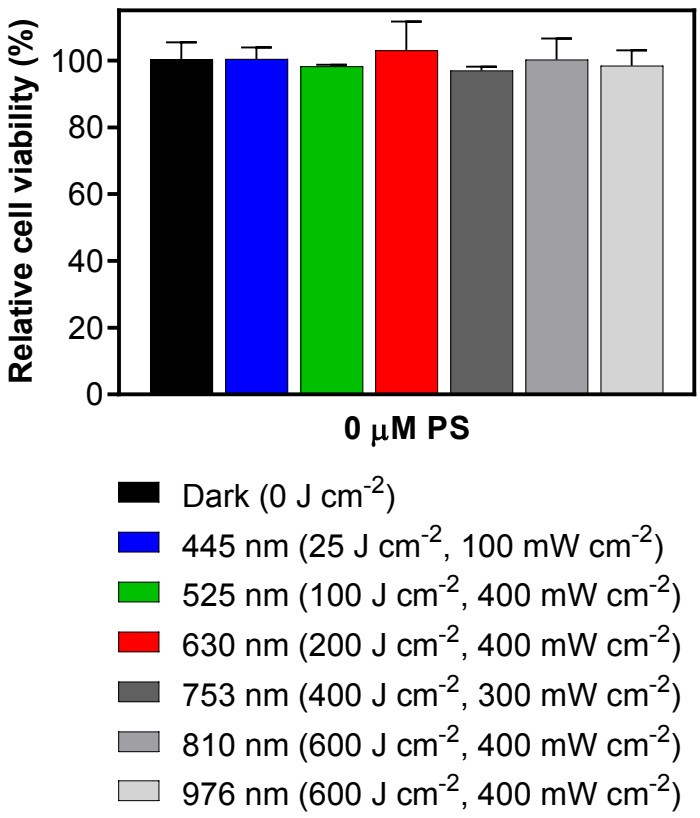

Figure S50. Light controls on ML8500 with SKMEL28 cells at tested treatments with higher fluence and wavelength included for 753, 810, and 976 nm.

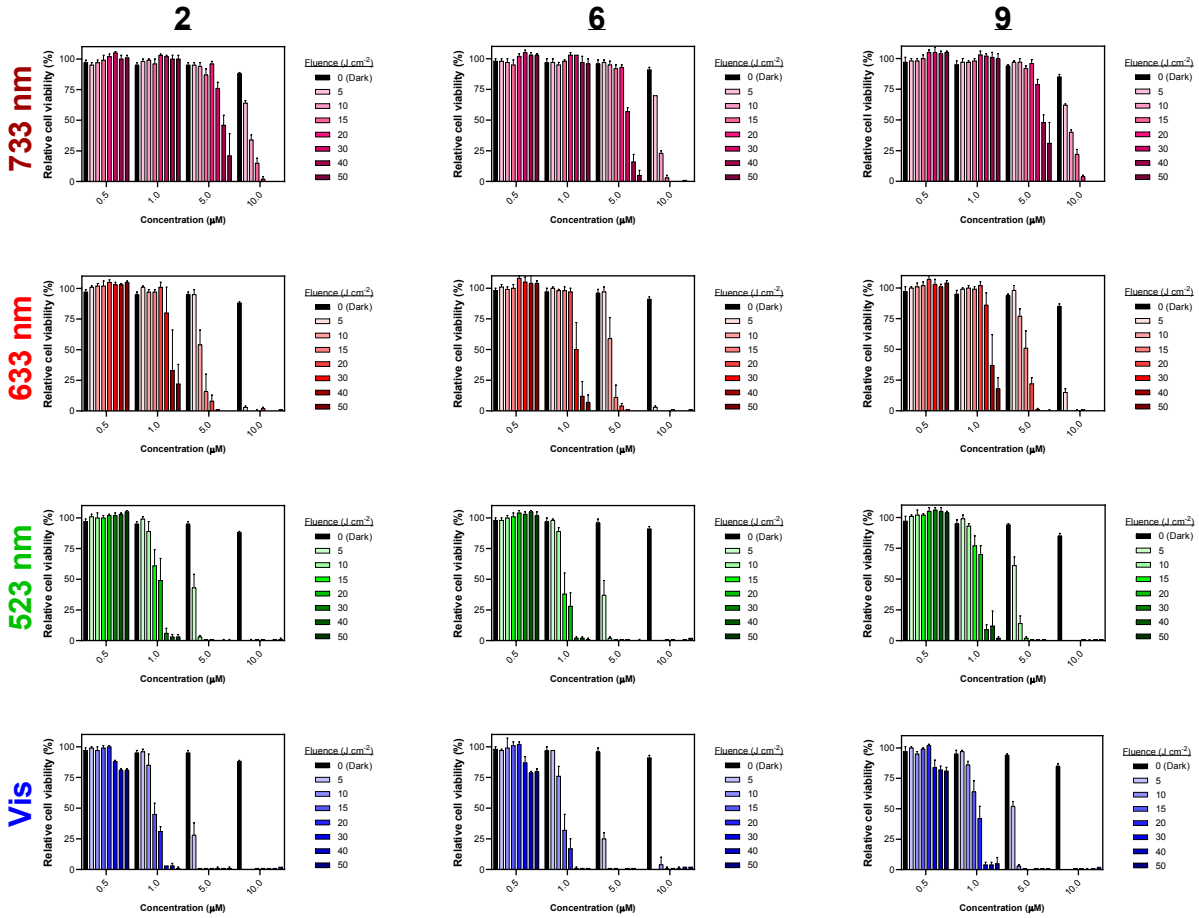

Figure S51. Fluence dependence (± SD) of compounds (left) **2**, (middle) **6**, and (right) **9** against SKMEL28 cells with row-wise 733 nm, 633 nm, 523 nm, and cool white vis treatments at 10 mW cm^{-2} and fluences ranging from 0–50 J cm^{-2}.

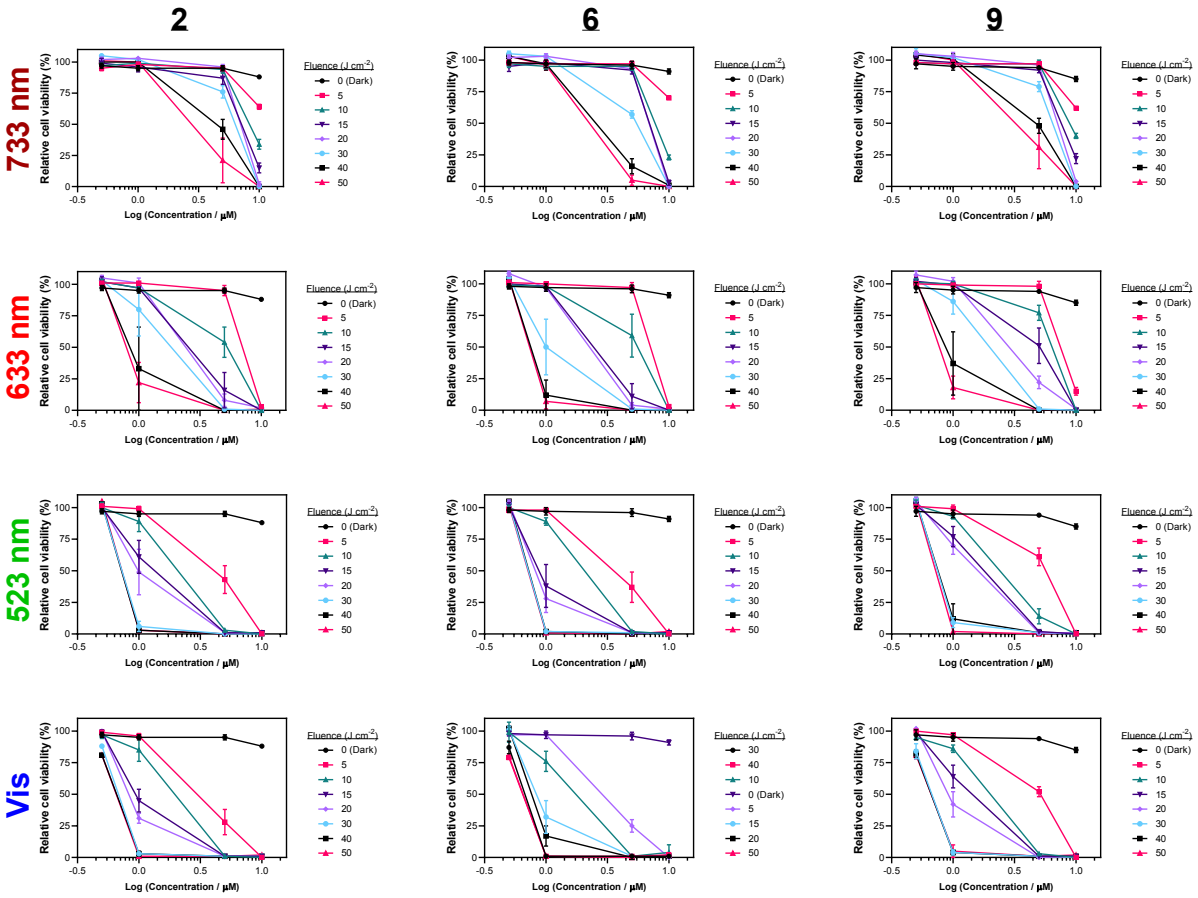

Figure S52. Alternate plotting for the fluence dependence (± SD) of compounds (left) **2**, (middle) **6**, and (right) **9** against SKMEL28 cells with row-wise 733 nm, 633 nm, 523 nm, and cool white vis treatments at 10 mW cm^{-2} and fluences ranging from 0–50 J cm^{-2}.

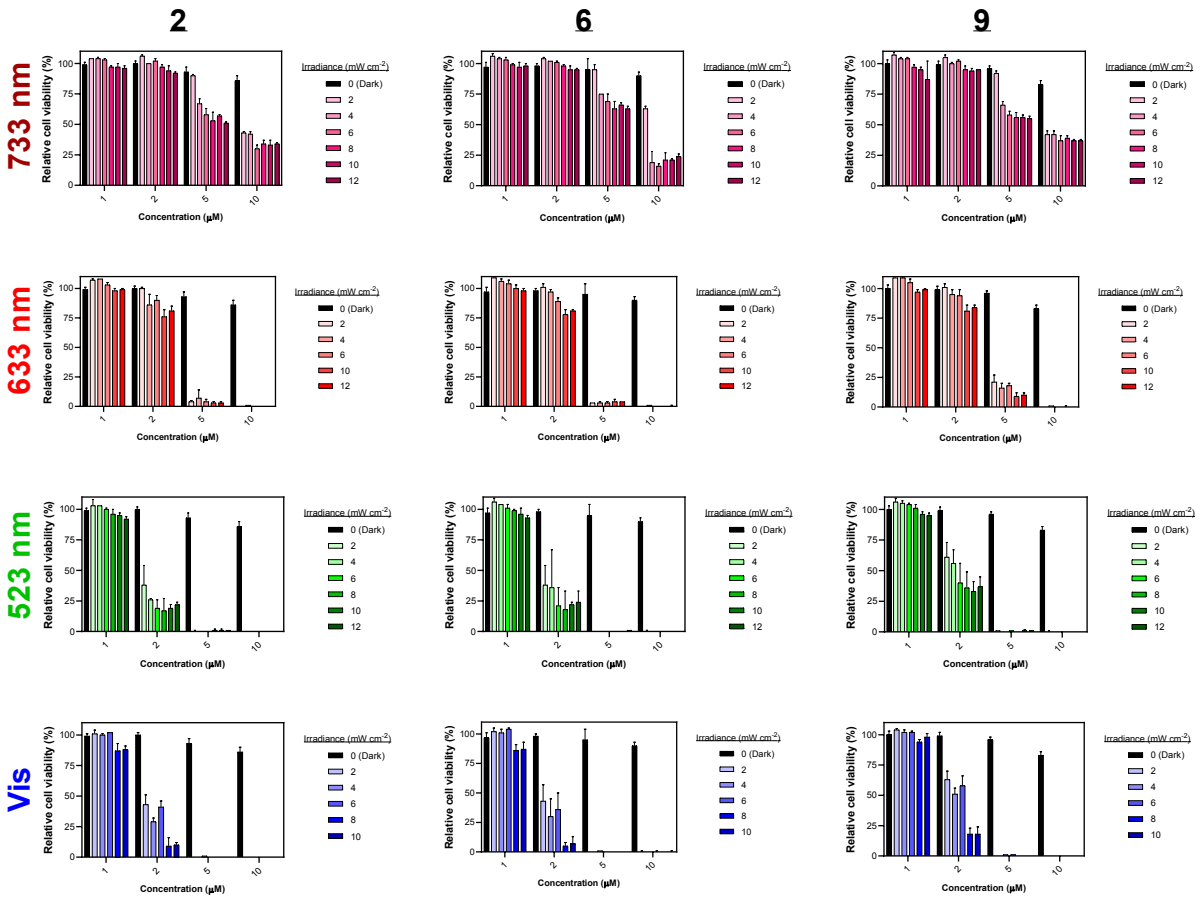

Figure S53. Irradiance dependence (± SD) of compounds (left) **2**, (middle) **6**, and (right) **9** against SKMEL28 cells with row-wise 733 nm, 633 nm, 523 nm, and cool white vis treatments at 10 J cm^{-2} (0 J cm^{-2}, Dark) and irradiances ranging from 2–10 mW cm^{-2}.

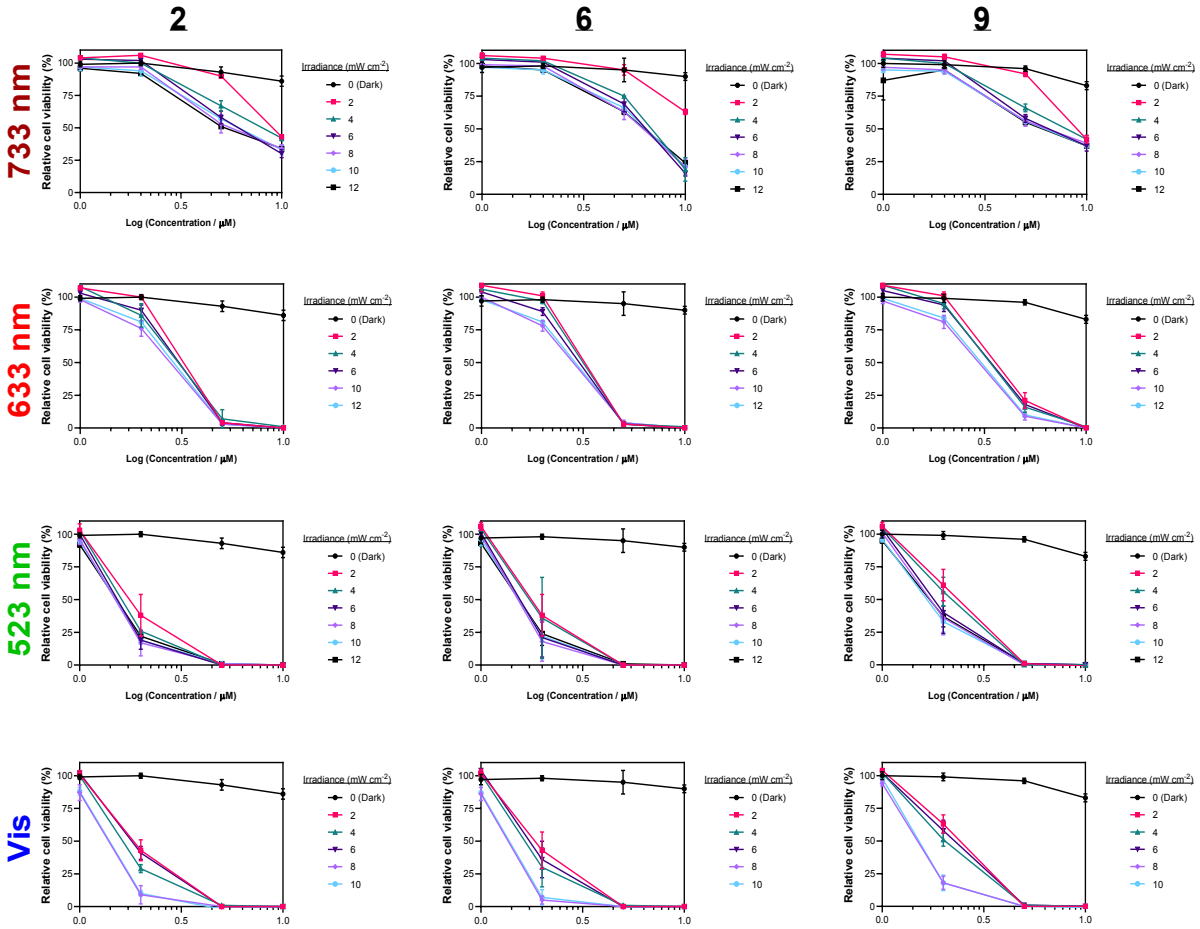

Figure S54. Alternate plotting for the irradiance dependence (± SD) of compounds (left) **2**, (middle) **6**, and (right) **9** against SKMEL28 cells with row-wise 733 nm, 633 nm, 523 nm, and cool white vis treatments at 10 J cm^{-2} (0 J $cm^{-}2$, Dark) and irradiances ranging from 2–10 mW cm^{-2}.

9. References

(1) Roque, J.; Havrylyuk, D.; Barrett, P. C.; Sainuddin, T.; McCain, J.; Colón, K.; Sparks, W. T.; Bradner, E.; Monro, S.; Heidary, D.; Cameron, C. G.; Glazer, E. C.; McFarland, S. A. Strained, Photoejecting Ru(II) Complexes That Are Cytotoxic Under Hypoxic Conditions. *Photochem Photobiol* **2020**, *96* (2), 327–339. https://doi.org/10.1111/php.13174.

(2) DeRosa, M. C.; Crutchley, R. J. Photosensitized Singlet Oxygen and Its Applications. *Coord. Chem. Rev.* **2002**, *233–234*, 351–371. https://doi.org/10.1016/S0010-8545(02)00034-6.

(3) Foxon, S. P.; Metcalfe, C.; Adams, H.; Webb, M.; Thomas, J. A. Electrochemical and Photophysical Properties of DNA Metallo-Intercalators Containing the Ruthenium(II) Tris(1-Pyrazolyl)Methane Unit. *Inorg. Chem.* **2007**, *46*, 409–416. https://doi.org/10.1021/ic0607134.

(4) Monro, S.; Colón, K. L.; Yin, H.; Roque, J.; Konda, P.; Gujar, S.; Thummel, R. P.; Lilge, L.; Cameron, C. G.; McFarland, S. A. Transition Metal Complexes and Photodynamic Therapy from a Tumor-Centered Approach: Challenges, Opportunities, and Highlights from the Development of TLD1433. *Chem. Rev.* **2019**, *119* (2), 797–828. https://doi.org/10.1021/acs.chemrev.8b00211.

(5) R Core Team. *R: A Language and Environment for Statistical Computing*; R Foundation for Statistical Computing: Vienna, Austria, 2020.

(6) Hughes, S. M. Plater: Read, Tidy, and Display Data from Microtiter Plates. *The Journal of Open Source Software* **2016**, *1* (7), 106. https://doi.org/10.21105/joss.00106.

(7) Wickham, H.; François, R.; Henry, L.; Müller, K. *Dplyr: A Grammar of Data Manipulation*; 2020.

(8) Wickham, H.; Bryan, J. *Readxl: Read Excel Files*; 2019.

(9) Schauberger, P.; Walker, A. *Openxlsx: Read, Write and Edit Xlsx Files*; 2019.

(10) Wickham, H.; Henry, L. *Tidyr: Tidy Messy Data*; 2020.

(11) Pazderski, L.; Pawlak, T.; Sitkowski, J.; Kozerski, L.; Szłyk, E. ^{1}H NMR Assignment Corrections and ^{1}H, ^{13}C, ^{15}N NMR Coordination Shifts Structural Correlations in Fe(II), Ru(II) and Os(II) Cationic Complexes with 2,2′-Bipyridine and 1,10-Phenanthroline. *Magn. Reson. Chem.* **2010**, *48*, 450–457. https://doi.org/10.1002/mrc.2600.

(12) Haberdar, R. The Synthesis and Study of 4-Aza-Acridine Type Ligands and Their Ru(II) Complexes, University of Houston, Houston, TX, 2012.

(13) Mcfarland, S.; Lifshits, L. M.; Roque, J. A.; Cole, H. D.; Thummel, R. P.; Cameron, C. G. NIR-absorbing Ru(II) Complexes Containing A-Oligothiophenes for Applications in Photodynamic Therapy. *ChemBioChem* **2020**, cbic.202000419. https://doi.org/10.1002/cbic.202000419.